

Superheated and Dissipative Landau-Ginzburg Systems

Andrew J. Dolgert
Springfield, Virginia

B.A. Williams College, 1992

A Dissertation presented to the Graduate Faculty of the
University of Virginia in Candidacy for the Degree of Doctor of
Philosophy

Department of Physics

University of Virginia
May, 1999

© Copyright by
Andrew J. Dolgert
All Rights Reserved
May, 1999

Acknowledgements

An enormous number of people helped me complete this dissertation. When Alan Dorsey accepted me as an advisee, he said he would be happy to have a collaborator. He, himself, has always been an excellent collaborator, choosing projects thoughtfully, shaping them into coherence, and deciding when they were done. John Di Bartolo worked on the first half of them with me. Tom Blum worked on the second half as did Dr. Michael Fowler, who has been my patient advisor since Dr. Dorsey's departure. When I needed to talk with someone about a sticky point, there were always willing professors around the department including Dr. Vittorio Celli, Dr. Bascom Deaver, Dr. Paul Fendley, Dr. Hank Thacker, and especially Dr. Eugene Kolomeisky.

Thanks Mom and Dad. This would not have happened without Aunt Tish's love and support. Lastly, dear Warren has been the best friend anyone could imagine, and that surely must count as a helpful gift towards finishing this dissertation.

NSF Grant DMR 96-28926 funded one Summer's research, and Dr. Lou Bloomfield lent me 64 MB of memory and a Barracuda.

Abstract

We study two superconducting systems using the Landau-Ginzburg equations. The first is a superconducting half-space with an applied magnetic field parallel to the surface. We calculate the maximum applied field that still supports superconductivity in the material by solving the Landau-Ginzburg equations analytically in asymptotic regimes of the Landau-Ginzburg parameter, κ . These results are then checked against numerical studies.

The other system is a thin, current-carrying strip. Here we do the first systematic study of nucleation of superconductivity in a normal strip and of the motion of a normal-superconducting interface in the presence of a current. This dissipative system requires solving the time-dependent Landau-Ginzburg equations analytically and numerically.

Contents

1	Introduction—Landau-Ginzburg Equations	2
1.1	Thermodynamic Free Energy	2
1.2	Landau-Ginzburg Free Energy	3
1.3	Time-dependent Landau-Ginzburg Equations	5
1.4	Dimensionless Form of Landau-Ginzburg Equations	8
2	Superheating of Superconductors	11
2.1	Introduction	11
2.1.1	The Physical System	11
2.1.2	A Rough Estimate	13
2.1.3	Formulation of the Problem	14
2.1.4	Previous Work	15
2.1.5	Boundary Layer Method for a Converging Channel	17
2.2	Asymptotic Expansions for Small- κ	20
2.3	Stability Analysis of the Solutions	28
2.3.1	Derivation of Equations	28
2.3.2	One-dimensional Perturbations	32
2.3.3	Two-dimensional perturbations	34
2.3.4	Large- κ two-dimensional Stability	38
2.4	Numerical methods	38
2.5	Discussion	40
3	Phase Transition in a Current-carrying Wire	41
3.1	Introduction	41
3.2	The Physical System	42
3.3	Models for Phase Transition in a Wire	46
3.3.1	The TDGL Equations	46
3.3.2	Generalized TDGL Equations	48
3.3.3	Heat Equations	49
3.4	Nucleation of the Superconducting Phase from the Normal Phase	49
3.4.1	Numerical Results	50
3.4.2	Analysis in the $J \rightarrow 0$ Limit	50
3.5	Stationary Interfaces	53
3.5.1	Numerical Methods and Results	53
3.5.2	Asymptotic Analysis of the Interface Solutions: preliminaries	55
3.5.3	Asymptotic Behavior of the Stall Current as $u \rightarrow \infty$	56
3.5.4	Asymptotic Behavior of the Stall Current as $u \rightarrow 0$	59
3.6	Moving Interfaces	62
3.7	Summary and Remarks	65

A Detailed Derivation of the TDGL	66
A.1 Derive TDGL from Landau-Ginzburg Free Energy	66
A.2 Find Dimensionless Variables	68
B Likharev's Equations as an Active Kinetic Equation	70
C Amplitude of the Critical Nuclei in the $J \rightarrow 0$ Limit	72

List of Figures

1.1	Free Energy Diagram of Second-order Phase Transition	4
1.2	The Landau-Ginzburg Energy Mexican Hat	5
2.1	Superconducting Sphere in a Magnetic Field	12
2.2	Cahn-Hilliard Estimate of Nucleus Growth	13
2.3	Converging Channels	18
2.4	Stream Velocity for $Re=43$	19
2.5	Stream Velocity for $Re=9$	21
2.6	Comparison of Superheating Field with Expansions	26
2.7	Order Parameter for $\kappa = 0.1$	27
2.8	Order Parameter for $\kappa = 0.5$	28
2.9	Uniform Solution of the Order Parameter at $\kappa = 0.5$	29
2.10	Dependence of Stability Eigenvalue on Order Parameter	34
2.11	Dependence of Order Parameter on Applied Field	35
2.12	Two-dimensional Stability Eigenvalues	37
2.13	Asymptotic Dependence of Large- κ Superheating Field	38
3.1	Sketch of a Phase-Slip Center	43
3.2	Forked Ascension in Wire CVC	44
3.3	Switching Wave in a Resistive System	45
3.4	Response of a Microbridge to a Current Pulse	47
3.5	Bump Solution for $u = 5.79$, $J = 0.2$	51
3.6	Maximum Amplitude of Bumps at $u = 5.79$	51
3.7	Bump Profiles as J approaches J^*	52
3.8	Stationary Normal-superconducting Interface for Large u	54
3.9	Stationary Normal-superconducting Interface for $u = 1.04$	54
3.10	Asymptotic Dependence of Stall Current	58
3.11	Asymptotics for Small- u Analysis	62
3.12	Asymptotics for Large- u Kinetic Coefficient	63
3.13	Velocity of the Front Versus Current for $u = 5.79$	64
3.14	Velocity as $J \rightarrow J_c$ as a Function of u	65

List of Tables

1.1	Dimensionless TDGL Rescalings	9
2.1	Coherence Lengths and Penetration Depths for Some Materials	12
2.2	Integration Constants for Small- κ Asymptotics	25
3.1	Simple Stability Diagram of a Current-carrying Wire	42
3.2	Primary Results for the Chapter	43
3.3	Numerical Results for Stall Current and Kinetic Coefficient	58

Chapter 1

Introduction—Landau-Ginzburg Equations

We are going to examine superconductors in large applied fields that push them to the verge of nonequilibrium or out of equilibrium. We are interested in the nonlinear dynamics at a mesoscopic level. The mechanisms of superconductivity are not intrinsic to this study. Of more interest is how we can describe balances among populations of superconducting and normal electrons or the magnetic field and the Meissner effect.

We study two systems with phase boundaries. One is the critical field of a first-order phase transition, the other the progression of a phase transition in time. One first analyzes such systems in the bulk by looking at free energies and possibilities of metastable states, but studying spatial variations in the applied fields and responses of the metallic states yields valuable insight into how systems either maintain equilibrium or temper their tendency to collapse.

The Landau-Ginzburg (GL) equations will be our model for these systems. It is a venerable mean-field theory which continues to provide insight into the actual behavior of metals. These equations describe general phase-transitions in terms of spatially-dependent variables. The Landau-Ginzburg equations describe very nonlinear, and hence complex, systems with little price in terms of calculating specific material parameters.¹

The Landau-Ginzburg equations, as we work with them, are coupled nonlinear differential equations. All of the new research in this dissertation deals directly with those differential equations. The focus of the work, therefore, is essentially mathematical and of interest in its own right. All of it, however, is introduced, executed, and summarized in light of the physical content. In fact, we begin this introduction to the Landau-Ginzburg equations with a description of the free energy.

1.1 Thermodynamic Free Energy

It can be shown from thermodynamic arguments that the transition of a metal from normal to superconducting is first order if the system is in an applied magnetic field. When the metal is normal, the magnetic field penetrates the sample. The Gibbs free energy is the free energy of the metal plus that of the magnetic field

$$G_n = F_n + \frac{H^2}{8\pi}. \quad (1.1)$$

¹The recent tendency in literature to use the name Landau-Ginzburg equations rather than the traditional Ginzburg-Landau equations seems to indicate an interest in ascribing primacy to Landau. In either case, it has been nearly impossible to avoid abbreviating the name with either GL or TDGL (for time-dependent Landau-Ginzburg equations.)

When the system becomes superconducting, it expels the magnetic field. The additional work required to expel the field is equal to the original field energy [23]

$$G_s = F_s + \frac{H^2}{4\pi}. \quad (1.2)$$

Here, F_s is the free energy of the metal in the superconducting state. The latent heat of transition from normal to superconducting is thus

$$L = T(S_n - S_s) = -\frac{T}{4\pi} H \frac{dH}{dT}. \quad (1.3)$$

Type-i metals abruptly expel applied magnetic fields at a critical field or temperature so that dH/dT is nonzero for all applied fields. This is a first-order phase transition that will exhibit hysteresis. When there is no applied field, the transition is second-order.

We want to look at the mechanics of the first-order phase transition on a mesoscopic scale with the Landau-Ginzburg equations. The Landau-Ginzburg free energy permits spatial variations in the free energy difference between the normal and superconducting states, $G_n - G_s$, so that we can find what spatial distributions minimize the free energy.

1.2 Landau-Ginzburg Free Energy

In this section, we write down the free energy of a superconductor and derive Landau-Ginzburg differential equations describing its phases. This derivation is well documented in several works [23, 71]. Our goal here is to demonstrate physical meanings of the nondimensionalized forms used in the rest of the work. The Landau-Ginzburg equations are derived from a free energy postulated to be valid near phase transitions from a less ordered phase to a more ordered one. While the form of the free energy near a phase transition is general, we will examine these equations solely in the context of the transition from superconducting to normal.

We are going to look at a phase transition from a higher temperature, disordered state to a lower temperature state with more order and less symmetry. Above an onset temperature called the critical temperature, T_c , the system has one available state. Below that temperature, the superconducting state with lower free energy becomes accessible as shown in Figure 1.1.² If we can find how the Free Energy of the system depends on its superconducting state, then standard thermodynamic arguments will tell us when and how the system is superconducting. We measure how superconducting the system is with an order parameter, $\psi = |\psi|e^{i\theta}$. When the order parameter is zero, the system is normal. When the order parameter is nonzero, the system is superconducting. The density of superconducting electrons is associated with the norm of the order parameter, $n_s \propto |\psi|^2$.

The most significant independent variables are the temperature and order parameter. Because the order parameter is small at the onset of the phase transition, we want to write the free energy density as a series in the order parameter

$$f = f_n + a\psi + b\psi^2 + c\psi^3 + d\psi^4 + \dots \quad (1.4)$$

where the total free energy is the free energy of the normal state plus an excess due to superconductivity. The system, thus the order parameter, will minimize the free energy. Because the order parameter, ψ , is complex (isomorphic to the SO(2) symmetry group), the lowest order invariants are $|\psi|^2$ and $|\psi|^4$. No first

²The Free Energy decreases with increasing temperature as seen from the thermodynamic relation $S = -\left(\frac{\partial A}{\partial T}\right)_V$, where A is the Helmholtz Free Energy.

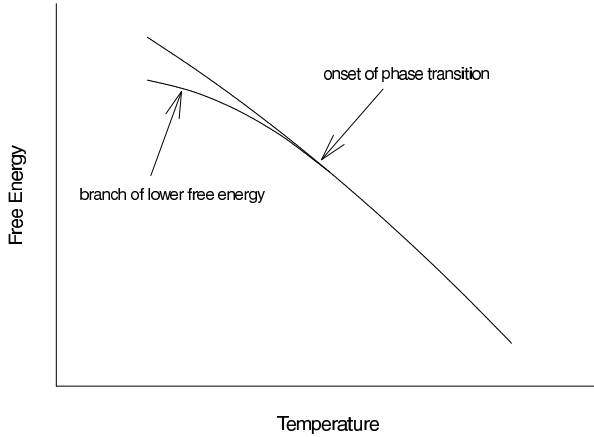


Figure 1.1: This figure shows the free energy of the normal and superconducting phases as a function of temperature. Below the critical temperature, T_c , the system undergoes a second-order phase change to the superconducting phase.

or third-order terms can appear in the free energy. The correct form, to fourth order, is

$$f = f_n + \alpha(T)|\psi|^2 + \frac{\beta(T)}{2}|\psi|^4. \quad (1.5)$$

The coefficients α and β are constants at a given temperature and depend on the system. There can be a free energy minimum for a nonzero order parameter only if $\alpha < 0$ and $\beta > 0$. In this case, the free energy as a function of order parameter is as shown in Figure 1.2, and the equilibrium state is $\psi = \sqrt{-\alpha/\beta}$. The parameters, α and β , depend on temperature, and they define a maximum value of the order parameter so that it varies between $\psi = 0$ and $\psi = \sqrt{-\alpha/\beta}$. Equation 1.5 is *the* Landau-Ginzburg equation because it contains the the basic physics of a bulk system.

Describing a system with any spatial variation requires modifications to the Landau-Ginzburg free energy above to account for the energy cost of bending the order parameter. The lowest order derivative of the order parameter gives us

$$f = f_n + \alpha|\psi|^2 + \frac{\beta}{2}|\psi|^4 + \frac{1}{2m}|\hbar\nabla\psi|^2. \quad (1.6)$$

Lastly, if the metal is in an applied magnetic field, \mathbf{H} , we can include the vector potential, \mathbf{A} , of the magnetic induction, $\mathbf{B} = \nabla \times \mathbf{A}$, gauge-invariantly to find Ginzburg and Landau's expansion of the free energy density

$$f = f_n + \alpha|\psi|^2 + \frac{\beta}{2}|\psi|^4 + \frac{|\mathbf{H}|^2}{8\pi} + \frac{1}{2m} \left| \left(-i\hbar\nabla - \frac{e\mathbf{A}}{c} \right) \psi \right|^2. \quad (1.7)$$

f_n is the free energy of the normal phase. The second to last term is just the energy of the magnetic field and last term a familiar representation of kinetic energy, here the kinetic energy of superconducting charge carriers.

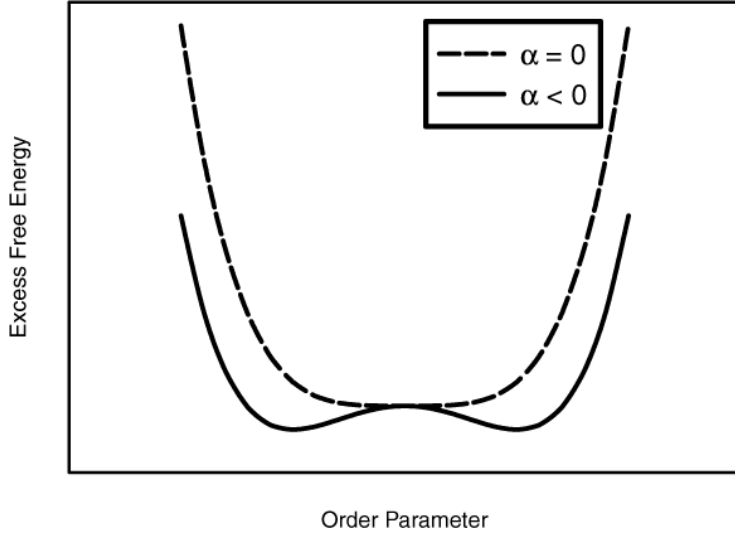


Figure 1.2: For lower temperatures where $\alpha < 0$, the free energy finds its minimum at a nonzero order parameter. At higher temperatures, $\alpha = 0$, and the normal state is most stable.

1.3 Time-dependent Landau-Ginzburg Equations

Because we want to look at a metal at constant temperature, we switch to the Gibbs free energy density. The Gibbs free energy is generally used for chemical systems and includes the work required to expel the magnetic field from the sample. That energy is of the form $U = \frac{1}{8\pi} \int \mathbf{B} \cdot \mathbf{H}$

$$g = f - \frac{\mathbf{B} \cdot \mathbf{H}}{4\pi}. \quad (1.8)$$

The total Gibbs free energy for the sample, integrated over all space, is then

$$G = \int d^3x \left\{ f_n + \alpha|\psi|^2 + \frac{\beta}{2}|\psi|^4 + \frac{|\mathbf{H}|^2}{8\pi} + \frac{1}{2m} \left| \left(-i\hbar\nabla - \frac{e\mathbf{A}}{c} \right) \psi \right|^2 - \frac{\mathbf{B} \cdot \mathbf{H}}{4\pi} \right\}. \quad (1.9)$$

The state variables, (ψ, \mathbf{A}) , will minimize the free energy in steady state. The minimization conditions can be written as functional derivatives

$$\frac{\delta G}{\delta\psi} = 0 \quad \text{and} \quad \frac{\delta G}{\delta\mathbf{A}} = 0. \quad (1.10)$$

Equation 1.10 defines the time-independent Ginzburg-Landau equations if G is the GL free energy. If we want to describe nonequilibrium systems, we can construct a relaxational model using the same free energy

$$\frac{\partial\psi}{\partial t} = -\Gamma \frac{\delta G}{\delta\psi^*} \quad \text{and} \quad \frac{\partial\mathbf{A}}{\partial t} = -\Gamma \frac{\delta G}{\delta\mathbf{A}}. \quad (1.11)$$

This form is called the Glauber model or Type A dynamics. The rate of relaxation of the system is controlled by Γ , called an Onsager coefficient. While the order parameter and vector potential are here shown with the same relaxation rate, we will later choose separate constants, Γ , for each.

The Glauber model does not generate entirely general dynamical equations. For instance, important

work on thin superconducting strips uses a model including higher order time derivatives [97]

$$\frac{1}{\Gamma_1} \frac{\partial \psi}{\partial t} + \frac{1}{\Gamma_2} \frac{\partial^2 \psi}{\partial t^2} = -\frac{\delta G}{\delta \psi^*}. \quad (1.12)$$

The second-order derivative in time permits oscillatory, self-driving solutions. Modern field theories typically include a Langevin term describing noise

$$\frac{\partial \psi}{\partial t} = -\Gamma \frac{\delta G}{\delta \psi^*} + \xi. \quad (1.13)$$

The noise term is necessary in order to include thermally-driven transitions explicitly in the theory. Without it, the system would always remain in any metastable state. The pure relaxational dynamics of the Glauber model assume the system will always proceed towards a lower free energy without any self-driving terms or noise.

The plan for the rest of the chapter is first to follow the prescription above to derive a preliminary version of the time-dependent Landau-Ginzburg equation then write down the improved and preferred equations derived by Gorkov and Eliashberg [51]. The point is that, while Gorkov and Eliashberg derived time-dependent Landau-Ginzburg equations from microscopics, the results are only a minor modification of those derived from the simple relaxational dynamics above.

If we compute the two functional derivatives, $\frac{\delta G}{\delta \psi^*}$ and $\frac{\delta G}{\delta \mathbf{A}}$ (Appendix A.1), we find

$$\frac{1}{\Gamma} \frac{\partial \psi}{\partial t} + \alpha \psi + \beta |\psi|^2 \psi + \frac{1}{2m} (-i\hbar \nabla - \frac{e}{c} \mathbf{A})^2 \psi = 0 \quad (1.14)$$

$$\frac{1}{\Gamma} \frac{\partial \mathbf{A}}{\partial t} + \frac{1}{4\pi} \nabla \times (\nabla \times \mathbf{A} - \mathbf{H}) + \frac{e}{2mc} \psi (-i\hbar \nabla + \frac{e}{c} \mathbf{A}) \psi^* + \frac{e}{2mc} \psi^* (i\hbar \nabla + \frac{e}{c} \mathbf{A}) \psi = 0. \quad (1.15)$$

The first equation, describing the motion of the order parameter, is largely described above. We can see in this equation that in the bulk where ψ does not vary, it will have the value $\psi_0 = \sqrt{-\alpha/\beta}$. In the second equation, we can identify first the term $\nabla \times \nabla \times \mathbf{A}$ as the total current generating the local magnetic field. If we notice that a stationary system has $\frac{\partial \mathbf{A}}{\partial t} = 0$, we see the last two terms must constitute the supercurrent. For instance, one of the boundary conditions on this system is that the total current out of the sample be zero, or

$$(i\hbar \nabla + \frac{e}{c} \mathbf{A}) \psi = 0 \quad (1.16)$$

$$\nabla \times \mathbf{A} = \mathbf{H}. \quad (1.17)$$

A more common way to see the second equation written is

$$\frac{1}{\Gamma} \frac{\partial \mathbf{A}}{\partial t} + \frac{1}{4\pi} \nabla \times (\nabla \times \mathbf{A} - \mathbf{H}) - \frac{i\hbar e}{2mc} (\psi \nabla \psi^* - \psi^* \nabla \psi) + \frac{e^2}{mc^2} |\psi|^2 \mathbf{A} = 0. \quad (1.18)$$

The first term, $\frac{\partial \mathbf{A}}{\partial t}$ is related to the total current for a system out of equilibrium. Because it expresses the inertia of the superconducting electrons accelerating in the presence of a current, it is called the kinetic inductance.

The equation as it stands describes only supercurrent in a sample. Since we are also interested in samples with normal current, we should add an electric field somewhere. If we start from simple E&M, we know that the total current is related to the magnetic field by

$$\nabla \times \mathbf{H} = \frac{4\pi}{c} \mathbf{J} = \frac{4\pi}{c} (\mathbf{J}_n + \mathbf{J}_s). \quad (1.19)$$

Distinguishing the current as either normal or superconducting is called the two-fluid model. It implies

there are distinct populations of normal and superconducting electrons. A more current understanding is that the norm of the order parameter represents the proportion of electrons *participating in Cooper pairing*. Comparing Eqn. 1.19 with Eqn. 1.18, we see the supercurrent is

$$\mathbf{J}_s = \frac{ie\hbar}{2m}(\psi \nabla \psi^* - \psi^* \nabla \psi) - \frac{e^2}{mc}|\psi|^2 \mathbf{A}. \quad (1.20)$$

Because the supercurrent does not dissipate energy, the normal current alone is responsible for any electric field. The two-fluid model seems to identify $\Gamma^{-1} \partial \mathbf{A} / \partial t$ with the normal current. That term is not normal current but the kinetic inductance of the superconducting electrons. Accelerating Cooper pairs to an equilibrium superfluid velocity generates an ephemeral voltage in the sample even though there is no dissipation.

If we want to include a normal current in our model, we can look at replacing the kinetic inductance with a traditional term of the form $\mathbf{J}_n = \sigma \mathbf{E}$. Maxwell's Equations tell us we can always express the electric field with a scalar potential ϕ of the form

$$\mathbf{E} + \frac{1}{c} \frac{\partial \mathbf{A}}{\partial t} = -\nabla \phi. \quad (1.21)$$

If we solve that equation for \mathbf{J}_n and substitute it into Eqn. 1.18, we find the kinetic inductance appears naturally as part of the electric field. Assembling the pieces in the form $\mathbf{J}_t = \mathbf{J}_n + \mathbf{J}_s$, we find

$$\frac{c}{4\pi} \nabla \times \nabla \times \mathbf{A} = -\frac{\sigma}{c} \frac{\partial \mathbf{A}}{\partial t} - \sigma \nabla \phi + \frac{i\hbar e}{2m}(\psi \nabla \psi^* - \psi^* \nabla \psi) - \frac{e^2}{mc}|\psi|^2 \mathbf{A} + \frac{c}{4\pi} \nabla \times \mathbf{H} \quad (1.22)$$

In addition, we have found that Maxwell's Equations determine the Onsager Coefficient, Γ for the relaxation equation for the vector potential. While there was a single relaxation constant, Γ , for the time dependence of both the order parameter and magnetic field, we will now set one of them to agree with Maxwell's equations. This is just a likely choice, and those who look to Landau-Ginzburg equations for more precise correspondence with physical values will often reserve the right to vary independently relaxation coefficients for the order parameter and magnetic field.

One can find in the above equation a gauge symmetry whereby the equation is unchanged under transformations of the type

$$\psi \rightarrow \psi e^{\frac{ie}{\hbar c} \chi} \quad \mathbf{A} \rightarrow \mathbf{A} + \nabla \chi \quad \phi \rightarrow \phi - \frac{1}{c} \frac{\partial \chi}{\partial t}. \quad (1.23)$$

In order that both the equation for the magnetic potential and the order parameter be gauge invariant, we should add a gauge-invariant term for ϕ to Eqn. 1.14 to get

$$\frac{1}{\Gamma} \frac{\partial \psi}{\partial t} + \frac{ie}{\hbar \Gamma} \phi + \alpha \psi + \beta |\psi|^2 \psi + \frac{1}{2m}(-i\hbar \nabla - \frac{e}{c} \mathbf{A})^2 \psi = 0. \quad (1.24)$$

Our insertion of an electric field by hand has effectively switched to proper canonical variables. We have been seeking a sensible form similar to that derived from microscopics by Gorkov and Eliashberg [51] and quoted in Du et al. [31]³

$$\hbar \frac{\partial \psi}{\partial t} + ie\Phi\psi - D(\hbar \nabla + ie\mathbf{A})^2 \psi + (\beta |\psi|^2 + \alpha)\psi = 0 \quad (1.25)$$

$$\nu \nabla \times \nabla \times \mathbf{A} = \mathbf{E} + 2\tau \left[|\psi|^2 \mathbf{A} + \frac{i\hbar}{2e}(\psi^* \nabla \psi - \psi \nabla \psi^*) + \nabla \times \mathbf{H} \right]. \quad (1.26)$$

Without defining the constants, we can say that these equations are, term for term, proportional to those

³When quoting this equation, I have switched the gauge field, \mathbf{A} , to match the sign of my definition, $\mathbf{B} = \nabla \times \mathbf{A}$. Du et al. explained the sign changes by switching the sign of the electric field, a choice not generally welcome to physicists.

we have derived. For reasonable choices of constants, they behave like those derived straight from the Landau-Ginzburg free energy.

The derivations of Eqns. 1.24 and 1.22 may have seemed correct enough with respect to Maxwell's Equations that the version of the time-dependent Landau-Ginzburg equations derived by Gorkov and Eliashberg have an unnecessary number of parameters. A quick way to see how we have been duped by treading well-worn paths is to look for a continuity equation for the charge associated with the superconducting current

$$\frac{\partial|\psi|^2}{\partial t} + \nabla \cdot \mathbf{J}_s = 0. \quad (1.27)$$

A note by Neu [81] points out that such a continuity equation exists, but, in our variables, we would need to choose $\Gamma = -ie/\hbar$. That choice of the Onsager coefficient would violate our relaxational dynamics, but it gives the nonlinear Schrödinger equation. In practice, choosing a complex coefficient allows one to study the Hall Effect in superconductors, but we will generally choose Γ such that the time derivative of ψ has no factor in front. The implication is that $|\psi|^2$ is only loosely associated with the density of superconducting electrons. What we have instead is a non-conserved order parameter. Our version of a continuity equation is

$$\frac{1}{\Gamma} \frac{\partial|\psi|^2}{\partial t} + \frac{\hbar^2}{2m} (\nabla^2|\psi|^2 - 2\nabla\psi \cdot \nabla\psi^*) - \frac{2}{c} \mathbf{J} \cdot \mathbf{A} = 0 \quad (1.28)$$

which is more of a balance between energy in the system and dissipation in the current.

1.4 Dimensionless Form of Landau-Ginzburg Equations

It now falls to us to rewrite the Landau-Ginzburg equations in dimensionless form. In the process, we will expose the important length scales in the problem. The two length scales in the system are the magnetic field penetration depth and the superconducting coherence length. The illustrations of length scales from the time-dependent Landau-Ginzburg equations are very simple and are shown here much as they appear in Du, Gunzburger, and Peterson [32].

The magnetic penetration depth, λ , is a measure of how far an applied magnetic field penetrates a sample. If we look at a perfectly conducting sample occupying a halfspace and apply a constant magnetic field, then the time-dependent Landau-Ginzburg equations, Eqns. 1.14 and 1.15, simplify to

$$\frac{c}{4\pi} \nabla \times \nabla \times \mathbf{A} = -\frac{e^2}{mc} \psi_0^2 \mathbf{A}. \quad (1.29)$$

Taking the curl of this equation, we arrive at the London equation,

$$\nabla \times \nabla \times \mathbf{H} + \frac{1}{\lambda^2} \mathbf{H} = 0 \quad (1.30)$$

where the magnetic penetration depth is

$$\lambda = \sqrt{\frac{mc^2}{4\pi e^2 \psi_0^2}}. \quad (1.31)$$

The London equation predates the Landau-Ginzburg equations. It says that a magnetic field applied to the surface will have a decay length of λ .

We can make a similar calculation for the coherence length. If we imagine a metal normal to the left, superconducting to the right, then the order parameter has to rise from $\psi = 0$ to $\psi = \sqrt{-\alpha/\beta}$. The

$$\begin{aligned}
\lambda &= \left(\frac{mc^2}{4\pi e^2 |\psi_0|^2} \right)^{1/2} & \xi &= \left(-\frac{\hbar^2}{2m\alpha} \right)^{1/2} & H_c &= \left(\frac{4\pi\alpha^2}{\beta} \right)^{1/2} \\
\kappa &= \frac{\lambda}{\xi} = \sqrt{\frac{\beta}{2\pi}} \frac{mc}{e\hbar} & \psi_0 &= \sqrt{-\alpha/\beta} & x &= \lambda x' \\
H &= \sqrt{2} H_c H' & \mathbf{j} &= \frac{cH_c}{2\sqrt{2}\pi\lambda} \mathbf{j}' & \mathbf{A} &= \sqrt{2}\lambda H_c \mathbf{A}' \\
g &= \frac{\alpha^2}{\beta} g' & G &= \frac{\alpha^2 \lambda^3}{\beta} G' & t &= \frac{4\pi\sigma\lambda^2}{c^2} t'
\end{aligned}$$

Table 1.1: These are the rescalings of the time-dependent Landau-Ginzburg equations to their standard dimensionless form.

Landau-Ginzburg equations in the absence of magnetic field reduce to

$$\alpha\psi - \beta|\psi|^2\psi - \frac{\hbar^2}{2m}\nabla^2\psi = 0. \quad (1.32)$$

The solution to this equation with the desired boundary conditions is

$$\psi = \sqrt{\frac{-\alpha}{\beta}} \tanh\left(\frac{x - x_0}{\sqrt{2}\xi}\right) \quad (1.33)$$

where

$$\xi = \left(\frac{\hbar^2}{-2m\alpha} \right)^{1/2}. \quad (1.34)$$

We call ξ the coherence length. It is the order parameter's recovery length to perturbations.

Using the length scales shown above, we can (see Appendix A.2) rescale the variables so that only two remain

$$\gamma \left(\frac{\partial\psi}{\partial t} + i\kappa\phi\psi \right) + \psi - |\psi|^2\psi - \left(\frac{i}{\kappa} \nabla + \mathbf{A} \right)^2\psi = 0 \quad (1.35)$$

$$\frac{\partial\mathbf{A}}{\partial t} + \nabla\phi + \nabla \times \nabla \times \mathbf{A} - \frac{i}{2\kappa}(\psi\nabla\psi^* - \psi^*\nabla\psi) + \mathbf{A}|\psi|^2 = 0. \quad (1.36)$$

The switch to dimensionless variables is nicely summarized in Du, Gunzburger, and Peterson [32]. A more complete summary is shown in Table 1.1. The Onsager coefficient has become

$$\gamma = \frac{1}{\alpha\Gamma t_0} \quad (1.37)$$

where t_0 is the rescaling of time shown in Table 1.1, and calculations from BCS theory determine it to be between 0.8 and 1.0 [51]. As you may guess, we'll take it to be unity.

The other parameter is the Ginzburg-Landau parameter,

$$\kappa = \frac{\lambda}{\xi} \quad (1.38)$$

which is a dimensionless parameter characterizing the metal under consideration. In this formulation of the

Landau-Ginzburg equations, it is the only such parameter. A metal with small κ was once called *hard*—it resists penetration by magnetic fields.⁴ Metals with $\kappa < 1/\sqrt{2}$ are called type-i, those with $\kappa > 1/\sqrt{2}$ type-ii.

In these new variables, the current is rescaled so that the nondimensional current

$$\mathbf{J}_s = \frac{i}{2\kappa}(\psi \nabla \psi^* - \psi^* \nabla \psi) - |\psi^2| \mathbf{A}. \quad (1.39)$$

The new boundary conditions are

$$\left(\frac{i}{\kappa} \nabla \psi + \mathbf{A} \psi \right) \cdot \hat{n} = 0 \quad (1.40)$$

$$\nabla \times \mathbf{A} \times \hat{n} = \mathbf{H} \times \hat{n}. \quad (1.41)$$

They still express the requirement that no supercurrent flow out of the sample and that the tangential magnetic field be continuous at the boundary.

These nondimensional TDGL equations, Eqns. 1.35 and 1.36, are also invariant under a gauge transformation,

$$\psi \rightarrow \psi e^{i\kappa\chi}, \quad \mathbf{A} \rightarrow \mathbf{A} + \nabla\chi, \quad \text{and} \quad \phi \rightarrow \phi - \frac{\partial\chi}{\partial t}. \quad (1.42)$$

This indicates that, as written, the equations are not well-posed because they do not have a single set of solutions but a whole family of solutions joined by the function χ . While it is possible to solve the equations analytically for a family of solutions without specifying a specific χ , we will work with specific functions χ , or specific gauges. We will derive those gauges as they apply in later chapters.

We have introduced the Landau-Ginzburg equations from general properties of the free energy and with little reference to the physics of the electronic system of the normal or superconducting metals. The majority of this work will be concerned with the equations themselves. As just shown, the physical system informed the derivation at two points—the choice of $SO(2)$ symmetry in the original free energy and the length scales of the gauge variables, λ , ζ and ϕ . We use those length scales to analyze the superheating of a half-space in the next chapter.

⁴These days *hard* superconductors refer to type-ii superconductors with lots of pinning impurities to hold vortices.

Chapter 2

Superheating of Superconductors

2.1 Introduction

A first analysis of the free energy of a metal examines the properties of a bulk specimen large enough that surface tension associated with edges is negligible. Below a thermodynamic critical field, H_c , a bulk superconductor in equilibrium will be in a Meissner phase. Above that critical field, a type-i superconductor will become normal, allowing magnetic fields to penetrate, and a type-ii superconductor will enter the Abrikosov phase, characterized by the infusion of flux into the sample in the form of discrete vortices.

If, instead of estimating the critical field for a phase transition just by comparing which phase has the least free energy, we, in addition, ask at what applied field flux at the boundary of the sample (with vacuum) can push past through the surface currents, we see that the phase transition is delayed. If one were to begin with a superconducting metal and steadily increase the magnetic field, there would not be a phase transition at H_c but for some higher value we call the superheating field, H_{sh} . (While we are not actually heating the sample, the word “superheating” refers to the similar delay of a phase transition in more familiar systems like water.) For applied magnetic fields well above the critical field, the bulk would prefer to change phases, but the order parameter at the surface decreases from its value in the bulk in order that the metal remain superconducting. On a microscopic scale, the depression of the order parameter is caused when the penetrating magnetic field aligns spins in the Cooper pairs. The phase transition is delayed only when the edges of the sample are considered.

If we want to understand the time-dependent collapse of superconductivity in a superconductor, characterizing the superheated Meissner state will tell us our initial conditions for the collapse. The superheating solutions to our system (described in Eqns. 2.13–2.16) measure energy barriers separating local equilibrium from catastrophic collapse. Scaling solutions for cascading phase transitions often depend on first integrals of initial conditions during a superheated state. We will not be able to produce those scaling solutions, but a later chapter pursues a similar system found more tractable.

The matched asymptotics in this chapter were published in a journal paper [27]. New material appears in the analysis of perturbations on the solutions.

2.1.1 The Physical System

The superheating field is more practically important for quite a few reasons. First, it is one of the most common ways to determine the Landau-Ginzburg parameter of a type-i metal [16]. Second, there have been proposals in the past ten years to use superconducting granules to detect weak electromagnetic elementary particles, including WIMPS and magnetic monopoles [80]. Here, the granules act as bubble chambers, flipping from superconducting to normal when a particle strikes. A review is given in Barone [5].

Both measurements of the Landau-Ginzburg parameter and detectors study small spherical or ellipsoidal particles rather than large slabs of superconductor. Larger samples generally show almost no superheating

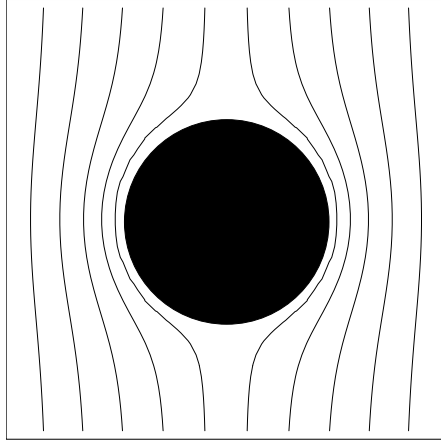


Figure 2.1: A superconducting sphere expels applied magnetic fields. The increased field at the equator is called the demagnetizing field. To order λ/R , the field at the equator is $3/2$ the applied field.

	$\lambda [\text{\AA}]$	$\xi [\text{\AA}]$	κ
Al	500	16000	0.03
Sn	500	2300	0.2
Pb	400	830	0.5

Table 2.1: These are some sample coherence lengths and penetration depths for a few materials [3]. The dimensionless constant $\kappa = \lambda/\zeta$. The coherence length and penetration depth appropriate to the Landau-Ginzburg equations differ slightly from the physical quantities. A good discussion of this is in Feder and McLachlan [35].

due to defects. When early theories predicted almost no superheating [36], experiments on bulk superconductors supported the results [24, 11]. It was then discovered that it is possible to make colloids of very uniform superconducting particles ranging in size from $10\text{--}100\,\mu\text{m}$. Because the defects are smaller than the order parameter coherence length, superheating is near ideal.

When calculating the superheating field of a spherical granule, one needs to account for the demagnetization fields caused by expulsion of flux from the granule. For a spherical grain which is perfectly superconducting, the field at the equator of a grain is three halves the applied magnetic field. Ellipsoidal grains and penetration depths complicate the exact calculation, but the experiment still rests on the physics of a field penetrating the surface of a superconductor.

The master of the superheating field is Hugo Parr. He ascribes his lineage to Feder and McLachalan [35], and in 1979, he published his final paper of a series on the subject [88, 84, 86, 85, 87, 90]. Using small grains of various metals, he found nearly ideal superheating fields in both type-i and type-ii superconducting grains in suspension. While he did not use SQUID techniques common to later studies on granules as detectors, his results showed that the prediction of the large superheating fields for type-i superconductors is accurate to within a percent. He used the granule system to study the temperature dependence of the penetration depth and coherence length in detail. He even noted the recently rediscovered “giant vortex state” of type-ii granules not large enough to contain a single discrete vortex [90, 46].

We want to calculate the superheating field, H_{sh} , as a function of κ , the Landau-Ginzburg parameter. That parameter is the ratio of the coherence length of the Cooper pairs, ξ , to the magnetic field penetration depth, λ . This is known to within 10 % for most superconductors. A few are shown in Table 2.1. We will examine the most basic system we can, a superconducting half space.

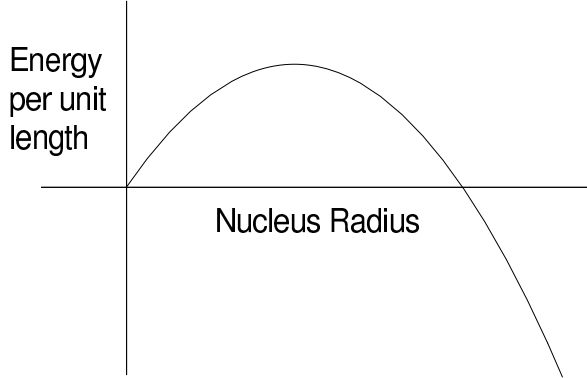


Figure 2.2: A small nucleus of the normal state in a superconductor will have a large positive surface tension. No nucleus can grow unless its size is larger than a critical radius where it is energetically favorable.

2.1.2 A Rough Estimate

If we focus on the first entry of flux into a superconductor, we can think of a small nucleus at the edge of the metal. For a type-II superconductor, the flux will enter as vortices typically much smaller than the penetration depth of the magnetic field. In 1964, Bean and Livingston estimated the critical magnetic field at which flux would enter a type-II superconductor by imagining a small test flux interacting with the unperturbed system [8]. The same picture of a small flux line interacting with a nearly intact superconducting state is still used to refine magnetization curves [17]. For a type-I superconductor, we can model the entry of flux as the nucleus of a phase transition from superconducting to normal. When the critical radius of a nucleus of normal metal becomes as small as the typical perturbation of the system, a phase transition will occur. Our goal is to determine the transition field as a function of the Landau-Ginzburg parameter, κ .

Picture a nucleus of normal metal in a superconducting cylinder. We can look at a two-dimensional slice of an infinite cylinder so that the nucleus has an energy per unit length determined by the competition between volume energy and surface tension. Surface energy per unit volume depends on the difference between the applied magnetic field and the critical field

$$\frac{E}{\text{unit volume}} = -\frac{H_0^2 - H_c^2}{4\pi}. \quad (2.1)$$

The applied field is assumed to be larger than the critical field for superheating. The energy cost of an interface between normal and superconducting regions is the surface tension. We can write a nondimensional form of the surface tension

$$\sigma_{\text{ns}} = \frac{H_c^2}{4\pi} \bar{\sigma}_{\text{ns}}, \quad (2.2)$$

where Osborn and Dorsey [82] determined that, for asymptotically small κ , $\bar{\sigma}_{\text{ns}}$ is

$$\bar{\sigma}_{\text{ns}} = \frac{0.943}{\kappa} - \frac{0.880}{\kappa^{1/2}}. \quad (2.3)$$

From the competition between the surface and bulk energies, we can write the total energy of a nucleus of normal metal

$$\frac{E}{\text{length}} = -\frac{H_0^2 - H_c^2}{4\pi} \pi r^2 + \frac{H_c^2 \lambda}{4\pi} \bar{\sigma}_{\text{ns}} 2\pi r. \quad (2.4)$$

The radius at which this energy becomes negative is the critical radius for nucleus growth.

A graph of the energy dependence is shown in Fig. 2.2. Smaller nuclei have a large ratio of surface to volume, so the positive surface tension makes them shrink. Nuclei large enough for the negative bulk energy to become dominant have radii larger than the critical radius

$$r_c = \frac{2H_c^2 \lambda \bar{\sigma}_{\text{ns}}}{H_0^2 - H_c^2}. \quad (2.5)$$

We can estimate that a phase transition must occur when the critical radius of the nucleus is about the same size as the penetration depth

$$\frac{2H_c^2 \lambda \bar{\sigma}_{\text{ns}}}{H_0^2 - H_c^2} \approx \lambda \quad (2.6)$$

Solving this for the applied field where the system must collapse, we find

$$H_0^2 = H_c^2(1 + 2\bar{\sigma}_{\text{ns}}). \quad (2.7)$$

If we insert our asymptotic value for $\bar{\sigma}_{\text{ns}}$, we find

$$H_0/H_c \approx \frac{1.34}{\kappa^{1/2}} - 0.641. \quad (2.8)$$

The factor in front is about twice the value calculated later, but the order of the first term is correct. The superheating field of a type-i superconductor will diverge as $\kappa \rightarrow 0$ with a power of $\kappa^{-1/2}$ because the positive surface tension diverges as κ^{-1} .

Now we look at a more mathematical approach which accounts for surface currents and magnetic fields using the Landau-Ginzburg equations.

2.1.3 Formulation of the Problem

The bare requirements for a superheating problem are an applied magnetic field and a surface. We will study a superconducting half-space where all space $x > 0$ is filled with metal and all space $x < 0$ is empty with an applied magnetic field \mathbf{H} . This is not a time-dependent problem so we need use only the time-independent Landau-Ginzburg free energy

$$G = \int d^3x \left\{ -|\psi|^2 + \frac{1}{2}|\psi|^4 + (\nabla \times \mathbf{A})^2 - 2\nabla \times \mathbf{A} \cdot \mathbf{H} + \left| \left(\frac{1}{\kappa} \nabla + i\mathbf{A} \right) \psi \right|^2 \right\}. \quad (2.9)$$

where κ is the GL parameter, ψ is the amplitude of the superconducting order parameter, \mathbf{A} is the vector potential ($\mathbf{B} = \nabla \times \mathbf{A}$), and \mathbf{H} is the magnetic field applied to the side of the sample. The lengths are in units of the penetration depth λ and fields are in units of $\sqrt{2}H_c$. While supercurrents shield the metal from applied magnetic fields, they are not dissipative so we don't need to include any terms related to the electric field in order to model this system.

The nondimensional free energy is invariant under a local linear transformation of the form

$$\psi \rightarrow \psi e^{i\kappa x} \quad \text{and} \quad \mathbf{A} \rightarrow \mathbf{A} + \nabla \chi. \quad (2.10)$$

The gauge transformation amounts to an extra degree of freedom. It is called local because the transformation depends on coordinates, $\chi = \chi(x)$. While we could, in principle, perform calculations without specifying a gauge, the easy and common practice is to fix the gauge. We fix the gauge by completely specifying a

function χ in terms of observables. In this case, if one writes $\psi = fe^{i\theta}$, we can make ψ real by defining

$$\chi = -\theta/\kappa \quad \Rightarrow \quad \xi = \psi e^{i\theta} = fe^{i\theta}e^{-i\theta} = f. \quad (2.11)$$

The phase of ψ is eliminated without any loss of generality. The transformed free energy is

$$G = \int d^3x \left\{ \frac{1}{\kappa^2} \nabla^2 f + \mathbf{Q}^2 f^2 - f^2 + \frac{1}{2} f^4 + (\nabla \times \mathbf{Q})^2 - 2(\nabla \times \mathbf{Q}) \cdot \mathbf{H} \right\}. \quad (2.12)$$

where $f = |\psi|$ is the amplitude of the superconducting order parameter and \mathbf{Q} is the gauge-invariant vector potential. Having transformed the free energy, we take the functional derivative in order to get the equilibrium equation

$$\frac{1}{\kappa^2} \nabla^2 f - f \mathbf{Q}^2 + f - f^3 = 0 \quad (2.13)$$

$$\nabla \times \nabla \times \mathbf{Q} + f^2 \mathbf{Q} = 0 \quad (2.14)$$

with boundary conditions

$$\nabla f \cdot \hat{n} = 0 \quad (2.15)$$

$$(\nabla \times \mathbf{Q} - \mathbf{H}) \times \hat{n} = 0. \quad (2.16)$$

If we think of a classical mechanical system where $x \rightarrow t$, these would be equations of motion for a particle in a potential. Eq. 2.14 describes the currents in the system in the form

$$\mathbf{J}_{\text{total}} - \mathbf{J}_{\text{superconducting}} = 0 \quad (2.17)$$

because there is no normal current. Furthermore, the divergence of Eq. 2.14 demonstrates explicitly that the supercurrent is zero.

Now we further restrict our treatment to a single dimension by treating independent variables as constant in directions parallel to the surface. Since our sample is a halfspace $x > 0$, we apply a magnetic field parallel to the surface by specifying $\mathbf{H} = h_a \hat{z}$. We represent that magnetic field with a vector potential $\mathbf{Q} = (0, q(x), 0)$. All spatial variations are in the \hat{x} direction so that the resulting equations are

$$\frac{1}{\kappa^2} f'' - q^2 f + f - f^3 = 0, \quad (2.18)$$

$$q'' - f^2 q = 0, \quad (2.19)$$

$$h = q'. \quad (2.20)$$

where primes denote derivatives with respect to x . These much simplified equations will suffice us the whole of the derivation of the superheating until we need to examine its stability.

2.1.4 Previous Work

The Landau-Ginzburg equations have been used to study the superheating field since their inception. All work done with them has been approximate because these are coupled nonlinear equations and intractable for this application. All approaches focused either on large or small asymptotics in κ . We will look at both, discussing in greater detail the work on small κ .

In 1950, Ginzburg and Landau [71] wrote Eqns. 2.18 and 2.19 in order to find the effect of a magnetic field applied parallel to a superconductor. Assuming the order parameter varied only a little for a hard superconductor (small κ), they wrote $f = f + \tilde{f}$ where $f = 1$ was the bulk solution and $\tilde{f} < 0$ showed the depression of superconductivity at the boundary. Second-order terms, \tilde{f}^2 and $q\tilde{f}$, were negligible. The

resulting equations were

$$\frac{1}{\kappa^2} \tilde{f}'' - 2\tilde{f} - q^2 = 0 \quad (2.21)$$

$$q'' = q. \quad (2.22)$$

Solving these is straightforward, and the approximate order parameter is

$$f = 1 + \frac{\kappa H^2}{\sqrt{2}(2 - \kappa^2)} \left(\frac{\kappa}{\sqrt{2}} e^{-2x} - e^{-\sqrt{2}\kappa x} \right) \quad (2.23)$$

While they did not further investigate the superheating field, the above equation did establish that the order parameter at the surface responds to applied magnetic fields according to κH^2 . Note also that our dimensionless units measure distance in terms of the magnetic penetration depth so that this first approximation shows $q \propto e^{-x}$.

In 1958, Ginzburg [48] estimated the superheating field for large and small κ . For $\kappa \rightarrow \infty$, he solved the Landau-Ginzburg equations exactly to find $H_{sh} = 1/\sqrt{2}$ (Recall the field is normalized to $\sqrt{2}H_c$). He did not examine the stability of that solution to discover the physical superheating field is actually lower.

For small κ , however, Ginzburg made fruitful conjectures from scaling arguments: “From [Eq. 2.23], and from an analysis of [Eqs. 2.18 and 2.19] with the introduction of variables $\zeta = \sqrt{\kappa}x$, $\chi = f/\sqrt{\kappa}$ and $b = \sqrt{\kappa}q$, it can be inferred that, for $\sqrt{\kappa} \ll 1$, $H_{sh} = \text{const}/\sqrt{\kappa}$.” How do we explain these choices?

We want to isolate and solve the relevant parts of the coupled nonlinear differential equations. Here, the relevant parts are those concerning the magnetic field. For hard superconductors, the order parameter will remain nearly constant while the magnetic field dies off quickly. We also have the sense that the superheating field for a hard superconductor is large. A good first step would be to rescale the vector potential so that it is closer to being $\mathcal{O}(1)$. Given choices like $b = \kappa q$ or $b = \sqrt{\kappa}q$, one might look at κH^2 in Eqn. 2.23 and choose the latter so that κH^2 would become the $\mathcal{O}(1)$ $(\nabla \times b)^2$ in the new variables. There is also a mathematical expression for our expectation that the order parameter remain steady while the vector potential varies. We simply change the length scale of the problem so that the vector potential looks more like a perturbation. With units in terms of the penetration depth, we have $q \propto e^{-x}$. We can use units $\zeta = \sqrt{\kappa}x$ so that ζ remains $\mathcal{O}(1)$ when x is large. We now have the following set of equations

$$\frac{1}{\kappa} f'' - \frac{1}{\kappa} b^2 f + f - f^3 = 0 \quad (2.24)$$

$$\kappa b'' - f^2 b = 0. \quad (2.25)$$

Since we claim it is the behavior of the vector potential that describes this problem, we want to include the second equation. We can do that by rescaling $\sqrt{\kappa}\chi = f$ with the effect

$$\frac{1}{\kappa} \chi'' - \frac{1}{\kappa} b^2 \chi + \chi - \kappa \chi^3 = 0 \quad (2.26)$$

$$b'' - \chi^2 b = 0. \quad (2.27)$$

From here, one can do series solutions for χ and b in κ . The zeroth order solution is that $\chi = 1/\sqrt{\kappa}$. Just from the zeroth order solution, we can look at Eqn. 2.27 to find $b = -Ce^{-\zeta/\kappa} = -Ce^{-x}$ so that, $q = b/\sqrt{\kappa} = -(C/\sqrt{\kappa})e^{-x}$. Our rescalings along the way sought to ensure that all proportionality constants were $\mathcal{O}(1)$. We conclude, therefore, that $H = \text{const}/\sqrt{\kappa}$. Ginzburg determined that constant numerically to find

$$H_{sh} = \frac{0.89}{\sqrt{\kappa}} H_c. \quad (2.28)$$

The Orsay Group on Superconductivity [53] (including de Gennes), in 1966, took a similar physical

approach with a different mathematical technique. Rather than look at scaling, they used a variational argument. The basis is that the magnetic field goes rapidly to zero while the order parameter takes its time. The order parameter is calculated in the absence of the applied field

$$\frac{1}{\kappa^2} f'' = f(f^2 - 1). \quad (2.29)$$

The vector potential is calculated for a fixed order parameter so that

$$q = q(0)e^{-f(0)x}. \quad (2.30)$$

Then they put these estimates into the free energy and concentrate, as did Ginzburg, on the terms involving q , q' , and f' . Terms in f are dropped. They vary the free energy with respect to $f(0)$ to find what $f(0)$ gives a free energy minimum. The result is a nontrivial estimation of the applied field in terms of $f(0)$

$$H^2 = \frac{2\sqrt{2}}{\kappa} f^2(0)(1 - f^2(0)). \quad (2.31)$$

The applied field always reaches its maximum for $f(0) = 1/\sqrt{2}$ where

$$H_{sh} = 2^{-1/4} \kappa^{-1/2} H_c. \quad (2.32)$$

This exact analytical coefficient is the same as that derived later in this chapter, but the eponymous Ginzburg would cite our paper from 1996 [27] in his 1998 work on the thermoelectric effect [49]. We can see in Eqn. 2.31 (plotted in Fig. 2.11 on page 35) that the superheating field occurs where $\frac{\partial H}{\partial f(0)} = 0$. It is also apparent that the order parameter at the surface is nonzero at the maximum applied field.

More recently, Hugo Parr [87] combined intuitive rescalings and a variational approach to derive the next term in the superheating field.

$$H_{sh} = 2^{-1/4} \kappa^{-1/2} \left(1 + \frac{15\sqrt{2}}{32} \kappa \right) H_c \quad (2.33)$$

The techniques are not significantly different from those above. The reasons for his rescaling are not clear and the calculation for the second term is very complicated. His work is important because the addition of the second term brings the asymptotics quite close to the full solution of the Landau-Ginzburg equations as shown in Fig. 2.6 on page 26. This permitted him to make practical verifications of the estimated superheating field.

Our contribution to the examination of the superheating field is two-fold. First, we determine the superheating field to greater precision than previous work. Second, and more importantly, we use a method called matched asymptotics to do that derivation with surety. While matched asymptotics are informed by the physical considerations discussed above—short penetration depth, slow variation of order parameter—the method transforms the problem into linear series solutions which can be integrated mechanically.

2.1.5 Boundary Layer Method for a Converging Channel

The boundary layer method is a standard technique of singular perturbation theory, but it is much less well known than WKB, so we will review it here. An excellent book on the subject is Bender and Orszag [10]. For physicists, a more amusing introduction might be a simpler problem from fluid dynamics.

Landau and Lifshitz [72] derive the exact solution of the equations of motion for a viscous, incompressible solution flowing into a converging channel, but they don't find a closed form solution. We follow their brief derivation enough to make sense of the main differential equation, then use the boundary layer method to find a closed form solution for low viscosity, high Reynolds number fluids. This is a system with a single small length scale, identified by the Reynolds number. It should be good practice for the Landau-Ginzburg

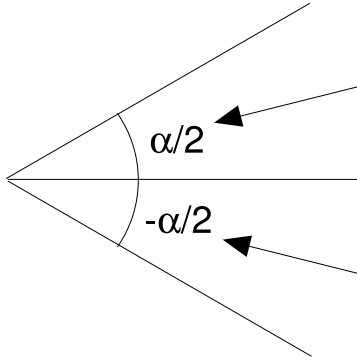


Figure 2.3: Fluid flows into a converging channel and out a pinhole at the vertex.

equations which exhibit two or more length scales in multiple coupled nonlinear equations.

The system geometry is shown in Fig. 2.3. The fluid flows into the channel and out a pinhole. We assume the flow is entirely radial. We could determine the equation of motion for an inviscid liquid just from mass conservation. Given a mass Q of liquid per unit time,

$$Q = \rho \int_{-\alpha/2}^{\alpha/2} vr d\phi. \quad (2.34)$$

For an inviscid liquid, the solution would be

$$Q = \frac{\alpha}{2\pi} \rho v r \quad \Rightarrow \quad v = \frac{2\pi Q}{\rho \alpha r}. \quad (2.35)$$

In order to include viscosity, we will use radial coordinates where the Navier-Stokes equations are

$$v \frac{\partial v}{\partial r} = -\frac{1}{\rho} \frac{\partial p}{\partial r} + \nu \left(\frac{\partial^2 v}{\partial r^2} + \frac{1}{r^2} \frac{\partial^2 v}{\partial \phi^2} + \frac{1}{r} \frac{\partial v}{\partial r} - \frac{v}{r^2} \right) \quad (2.36)$$

$$-\frac{1}{\rho r} \frac{\partial p}{\partial \phi} + \frac{2\nu}{r^2} \frac{\partial v}{\partial \phi} = 0 \quad (2.37)$$

$$\frac{\partial(rv)}{\partial r} = 0. \quad (2.38)$$

These equations are still supplemented by the mass conservation equation, Eq. 2.34. Because of the last equation, Eq. 2.38, we know $v \propto 1/r$, so we change variables to

$$u(\phi) = \frac{rv}{6\nu}. \quad (2.39)$$

Substituting u in Eq. 2.37, we can integrate to find the pressure

$$\frac{1}{\rho} (p - p_{\text{wall}}) = \frac{12\nu^2}{r^2} u. \quad (2.40)$$

Substituting the pressure into Eq. 2.36, we find

$$\frac{\partial^2 u}{\partial \phi^2} + 4u + 6u^2 = \frac{r^3}{6\rho\nu} \frac{\partial p_{\text{wall}}}{\partial r}. \quad (2.41)$$

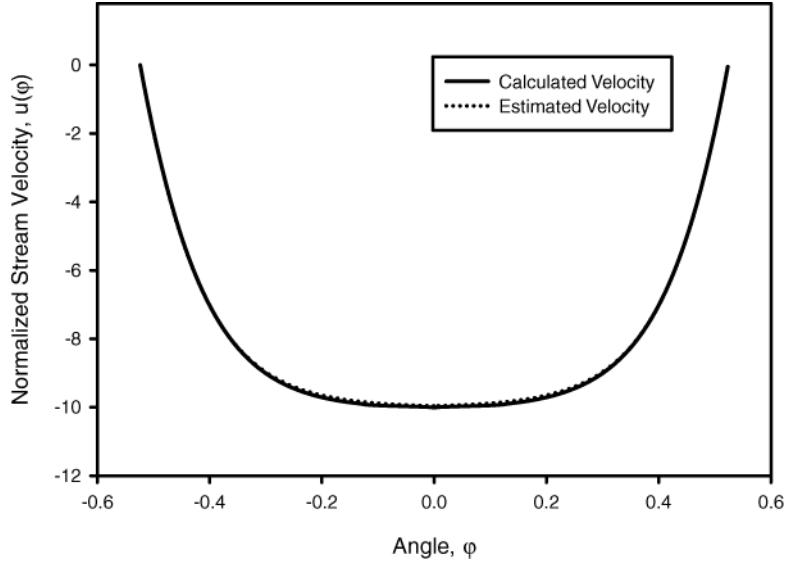


Figure 2.4: Fluid flow is uniform in the center of the channel. It drops to zero only near the sides. The region affected by viscosity is $\mathcal{O}(1/\sqrt{Re})$. The estimated stream velocity for a large Reynolds number, $Re = 43$, is a very good approximation of the exact solution.

Noticing that the left-hand side depends only on ϕ and the right-hand side only on r , we assign each to a constant, $2c$, and arrive at the main differential equation for this system

$$u'' + 4u + 6u^2 = 2c. \quad (2.42)$$

Here, u depends only on ϕ and c is a constant of integration.

Landau and Lifshitz express Eq. 2.42 in integral form and discuss the nature of the solutions. We will examine the case where the viscosity, ν , is small, or Reynolds number, $Re = |Q|/\rho\nu$, is large. Here we expect that, through most of the channel, the liquid will move with nearly the same velocity as the inviscid case, Eq. 2.35. Near the sides, however, the velocity at the walls must drop to zero. The affected region in the channel will be $\mathcal{O}(1/\sqrt{Re})$. The affected region is our boundary layer. We can rewrite the differential equation in different variables to see why there is a boundary layer.

First, note that the constant, c is $\mathcal{O}(Re^2)$. This could be proven by estimating p_{wall} from Bernoulli's Equation. We also know from Eq. 2.35 that the maximum u is less than

$$u_m = \frac{Q\pi}{3\nu\rho\alpha r} = -Re \frac{\pi}{3\alpha r}. \quad (2.43)$$

That tells us that u is $\mathcal{O}(Re)$. Let's first write the main differential equation in terms of $\mathcal{O}(1)$ variables. Substitute $U = u/Re$ and $C = c/Re^2$ to find

$$\frac{1}{Re}U'' + \frac{4}{Re}U + 6U^2 = 2C. \quad (2.44)$$

It is customary to write the small parameter as $\epsilon = 1/Re$

$$\epsilon U'' + 4\epsilon U + 6U^2 = 2C. \quad (2.45)$$

While this equation applies in the center of the channel, it is our *outer equation* because it describes the region far from the boundary layer. For flows near the center, U'' is small so we don't expect it to be

important. We will need to rescale in order to look at flows near the side. We can use a simple series solution to solve the outer equation. Substituting the series

$$U = U_0 + \epsilon U_1 + \epsilon^2 U_2 + \dots \quad (2.46)$$

$$C = C_0 + \epsilon C_1 + \epsilon^2 C_2 + \dots \quad (2.47)$$

we find

$$6U_0^2 = 2C_0. \quad (2.48)$$

The solution is $U_0 = \sqrt{C_0/3}$ in the center. We can write down the next order differential equation, too

$$U_0'' + 4U_0 + 12U_0 U_1 = 2C_1 \quad \Rightarrow \quad U_1 = \frac{C_1}{6U_0} - \frac{1}{3}. \quad (2.49)$$

We determine constants, C_0 and C_1 from matching the solution near the boundary. A nice side effect of the series solutions is that each succeeding order is always a linear differential equation.

Near the boundary, we expect the second derivative of U to be important. We express this by rescaling the ϕ -coordinate, $\Phi = \phi/\sqrt{\epsilon}$.

$$\frac{\partial^2 U}{\partial \Phi^2} + 4\epsilon U + 6U^2 = C. \quad (2.50)$$

We have the option of rescaling U , in addition. While we expect U is smaller near the boundary, rescaling $U \rightarrow \sqrt{\epsilon}U$ would give us $U'' = C$ which could not fulfill boundary conditions. We usually seek rescalings where more than one term is of the highest order of ϵ because you usually need two or more terms to find a non-trivial solution. Scaling variables such that nontrivial solutions exist is called the *principle of dominant balance*. Currently U'' is balanced against $6U^2 - C$ which seems like it could fulfill boundary conditions non-trivially. If we substitute series into this equation, we find

$$U = U_{m0}(-2 + 3 \tanh^2(\pm \sqrt{-3U_0}(\Phi - k))). \quad (2.51)$$

The integration constant, k , is determined from matching to the outer solution.

Now that we have an inner and outer solution, we match them. We do that by writing the inner solution in terms of the outer variables, $\Phi = \phi/\sqrt{\epsilon}$.

$$U = U_{m0}(-2 + 3 \tanh^2(\pm \sqrt{-3U_0}(\epsilon^{-1/2}\phi - k))). \quad (2.52)$$

Now we define the constant k such that $U(-\alpha/2) = 0$. The inner equation is already set to match $U_{\text{outer}} = U_{m0}$. We therefore see the real size of our boundary layer is $1/\sqrt{3|U_0|} = 1/\sqrt{3|u_0|\text{Re}}$.

The solution for the boundary layer meets the boundary condition, $u = 0$, at the side of the channel and meets the solution to the inner equation as $\phi \rightarrow \infty$. The outer solution would not, by itself, be capable of fulfilling the boundary conditions at the walls, but it does match to the inner solution near the walls. The solutions of the superconducting half-space will have the same property. Inner and outer solutions together form a uniform solution to the system.

2.2 Asymptotic Expansions for Small- κ

In this section we will develop an asymptotic expansion for the superheating field for small- κ , using the method of matched asymptotic expansions [10, 105]. For small- κ the longer length scale is the coherence length ξ . In order to treat the problem with singular perturbation theory, we need to write it such that the factor in front of the highest order derivative is small. Second order equations with a small parameter

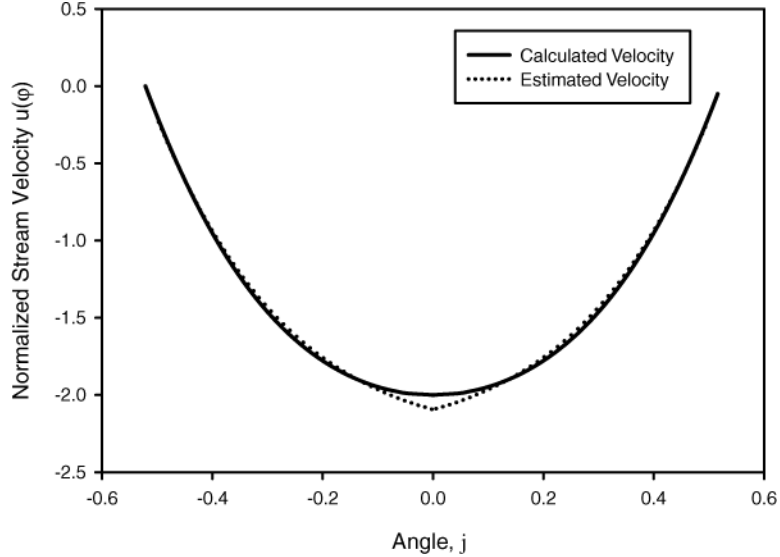


Figure 2.5: The estimated stream velocity for moderately large Reynolds number, $Re = 9$, is a fair approximation of the exact solution.

modifying the highest derivative tend to exhibit rapid behavior near the boundary. In this case, the rapid behavior is the penetration of the magnetic field. That field is the boundary of boundary layer theory, which we use here.

Rescaling x by κ , we introduce a new dimensionless coordinate $x' = \kappa x$ which means we now measure distance using the coherence length. The resulting GL equations in these “outer variables” are

$$f'' - q^2 f + f - f^3 = 0, \quad (2.53)$$

$$\kappa^2 q'' - f^2 q = 0, \quad (2.54)$$

$$h = \kappa q', \quad (2.55)$$

with the primes now denoting differentiations with respect to x' .

Outer solution. In order to obtain the outer solutions expand f , q , and h in powers of κ :

$$f = f_0 + \kappa f_1 + \kappa^2 f_2 + \dots, \quad (2.56)$$

$$q = q_0 + \kappa q_1 + \kappa^2 q_2 + \dots, \quad (2.57)$$

$$h = h_0 + \kappa h_1 + \kappa^2 h_2 + \dots. \quad (2.58)$$

Substituting into Eqs. (2.53)-(2.55), at $O(1)$ we have

$$f_0'' - q_0^2 f_0 + f_0 - f_0^3 = 0, \quad (2.59)$$

$$-f_0^2 q_0 = 0. \quad (2.60)$$

Since we want $f \rightarrow 1$ as $x' \rightarrow \infty$, the only possible solution to Eq. (2.60) is $q_0 = 0$. We can then immediately integrate Eq. (2.59),

$$f_0(x') = \tanh\left(\frac{x' + x_0}{\sqrt{2}}\right), \quad (2.61)$$

with $x_0 = x_0(\kappa)$ an arbitrary constant.¹ To $O(\kappa)$, the outer equations are

$$f_1'' - 2q_0 f_0 q_1 - q_0^2 f_1 + f_1 - 3f_0^2 f_1 = 0, \quad (2.62)$$

$$-f_0^2 q_1 - 2f_0 q_0 f_1 = 0, \quad (2.63)$$

$$h_0 = 0. \quad (2.64)$$

Once again, the only solution to Eq. (2.63) is $q_1 = 0$; substituting this into Eq. (2.62), we find $f_1 = C_1 f_0'$, with C_1 a constant:

$$f_1 = \frac{C_1}{\sqrt{2}} \operatorname{sech}^2 \left(\frac{x' + x_0}{\sqrt{2}} \right). \quad (2.65)$$

We can continue in this manner; at every order $q_n = 0$, $h_n = 0$, and $f_n = C_n f_0^{(n)}$, with the C_n 's constants which are determined by matching onto the inner solution.

Inner solution. The outer solution breaks down within a boundary layer of $O(\kappa)$ near the surface. This suggests introducing a rescaled inner coordinate $X = x'/\kappa$, so that $X = O(1)$ within the boundary layer. It is also possible to rescale f and q , with the hope that this will lead to a tractable inner problem. Such a rescaling must lead to a successful matching of the inner and outer solutions; i.e., the inner solutions as $X \rightarrow \infty$ must match onto the outer solutions as $x' \rightarrow 0$. Since $f_0(0) = \tanh(x_0/\sqrt{2})$, then assuming that $x_0 \neq 0$ we have $f_0(0) = O(1)$, indicating that the order parameter should not be rescaled in the inner region; therefore we set $f(x') = F(X)$ in the inner region. However, from the outer solution for the vector potential we see that the only constraint on $q(X)$ in the inner region is that $q(X) \rightarrow 0$ as $X \rightarrow \infty$ (presumably exponentially). Therefore, we are free to rescale q by κ in the inner region, hopefully in a way which simplifies the inner equations. One possibility is $q(x') = \kappa^{-\alpha} Q(X)$; substituting this into the GL equations, Eqs. (2.53)-(2.55), we see that unless 2α is an integer, fractional powers of κ will be introduced into the inner equations, contradicting our expansion of f and q in integer powers of κ in the outer region. Therefore, the simplest assumption is that $\alpha = 1/2$, leading to the following choice for the inner variables:

$$x' = \kappa X, \quad f(x') = F(X), \quad q(x') = \kappa^{-1/2} Q(X), \quad h(x') = H(X). \quad (2.66)$$

In these variables Eqs. (2.53)-(2.55) become

$$F'' - \kappa Q^2 F + \kappa^2 (F - F^3) = 0, \quad (2.67)$$

$$Q'' - F^2 Q = 0, \quad (2.68)$$

$$\kappa^{1/2} H = Q', \quad (2.69)$$

where now the primes denote differentiation with respect to X . The boundary conditions are

$$F'(0) = 0, \quad H(0) = H_a. \quad (2.70)$$

The next step is to expand the inner solutions in powers of κ :

$$F = F_0 + \kappa F_1 + \kappa^2 F_2 + \dots, \quad (2.71)$$

$$Q = Q_0 + \kappa Q_1 + \kappa^2 Q_2 + \dots, \quad (2.72)$$

$$H = \kappa^{-1/2} H_0 + \kappa^{1/2} H_1 + \dots. \quad (2.73)$$

Note that there is no term of $O(1)$ in the expansion for H , since we would be unable to match such a term

¹Because x_0 depends on κ , it should also be expanded in series. For the orders of terms used in the following derivation, the differences are negligible. A letter from the Bolley *et al.* [13] pointed out the difficulty which was painstakingly recalculated and corrected by John Di Bartolo in an erratum [28]. The affected terms are of high enough order that they show up here only in Table 2.2 and Eq. 2.94.

to the outer solution. Using the boundary condition $H(0) = H_a$ leads to

$$H_a = \kappa^{-1/2} H_0(0) + \kappa^{1/2} H_1(0) + \dots \quad (2.74)$$

Substituting these expansions into Eqs. (2.67)-(2.69), at $O(1)$ we obtain

$$F_0'' = 0, \quad Q_0'' - F_0^2 Q_0 = 0, \quad H_0 = Q_0'. \quad (2.75)$$

Solving these equations subject to the boundary conditions (2.70) (we also need $Q_0 \rightarrow 0$ as $x \rightarrow \infty$ in order to match onto the outer solution), we obtain

$$F_0(X) = A_0, \quad Q_0(X) = B_0 e^{-A_0 X}, \quad H_0(0) = -A_0 B_0, \quad (2.76)$$

with A_0 and B_0 constants. In what follows we will assign $F_n(0) = A_n$ and $Q_n(0) = B_n$ for notational simplicity. The $O(\kappa)$ equations are

$$F_1'' = Q_0^2 F_0, \quad Q_1'' - F_0^2 Q_1 = 2F_0 Q_0 F_1, \quad H_1 = Q_1'. \quad (2.77)$$

Solving with the boundary condition $F_1'(0) = 0$, we obtain

$$F_1(X) = A_1 + \frac{B_0^2}{4A_0} [2A_0 X + e^{-2A_0 X} - 1], \quad (2.78)$$

$$Q_1(X) = e^{-A_0 X} \left\{ B_1 - \frac{B_0^3}{16A_0^2} \left[1 - e^{-2A_0 X} + 16 \frac{A_0^2 A_1}{B_0^2} X + 4A_0^2 X^2 \right] \right\}, \quad (2.79)$$

$$H_1(0) = -\frac{1}{8} \frac{B_0^3}{A_0} - A_0 B_1 - A_1 B_0. \quad (2.80)$$

Finally, to $O(\kappa^2)$ we have for F_2

$$F_2'' = -F_0 + F_0^3 + 2Q_0 Q_1 F_0 + Q_0^2 F_1, \quad (2.81)$$

the solution of which (with $F_2'(0) = 0$) is

$$\begin{aligned} F_2(X) = & \frac{17}{128} \frac{B_0^4}{A_0^3} + \frac{1}{4} \frac{B_0^2 A_1}{A_0^2} - \frac{1}{2} \frac{B_0 B_1}{A_0} + A_2 + \left(B_0 B_1 - \frac{3}{32} \frac{B_0^4}{A_0^2} \right) X - \frac{1}{2} A_0 (1 - A_0^2) X^2 \\ & + \left[\frac{1}{2} \frac{B_0 B_1}{A_0} - \frac{1}{4} \frac{B_0^2 A_1}{A_0^2} - \frac{5}{32} \frac{B_0^4}{A_0^3} - \left(\frac{1}{8} \frac{B_0^4}{A_0^2} + \frac{1}{2} \frac{B_0^2 A_1}{A_0} \right) X - \frac{1}{8} \frac{B_0^4}{A_0} X^2 \right] e^{-2A_0 X} \\ & + \frac{3}{128} \frac{B_0^4}{A_0^3} e^{-4A_0 X}. \end{aligned} \quad (2.82)$$

The expression for Q_2 is even more unwieldy, and is not needed in what follows.

Matching. To determine the various integration constants which have been introduced we must match the inner solution to the outer solution. Since the outer solution for q is simply $q = 0$, and all of our inner solutions decay exponentially for large X , the matching is automatically satisfied for q , as well as for the magnetic field h . To match the inner and outer solutions for the order parameter, we are guided by the *van Dyke matching principle* [105], which states that the m term inner expansion of the n term outer solution should match onto the n term outer expansion of the m term inner solution. While the matching principle works for any pair, (m, n) , experience shows which choices yield meaningful results at a particular order of the computation. In our case we will take $m = 3$ and $n = 2$. Therefore, write the two term outer solution $f_0(x') + \kappa f_1(x')$ in terms of the inner variable X , and expand for small κ , keeping the first three terms in

the expansion in powers of κ :

$$\begin{aligned} f_0(\kappa X) + \kappa f_1(\kappa X) &\sim \tanh\left(\frac{x_0}{\sqrt{2}}\right) + \kappa \operatorname{sech}^2\left(\frac{x_0}{\sqrt{2}}\right) \frac{1}{\sqrt{2}} [C_1 + X] \\ &\quad + \kappa^2 \operatorname{sech}^2\left(\frac{x_0}{\sqrt{2}}\right) \tanh\left(\frac{x_0}{\sqrt{2}}\right) \left[-C_1 X - \frac{X^2}{2}\right]. \end{aligned} \quad (2.83)$$

Next, write the three term inner solution $F_0(X) + \kappa F_1(X) + \kappa^2 F_2(X)$ in terms of the outer variable x' , and expand for small κ , this time keeping the first two terms of the expansion:

$$\begin{aligned} F_0(x'/\kappa) + \kappa F_1(x'/\kappa) + \kappa^2 F_2(x'/\kappa) &\sim A_0 + \frac{B_0^2}{2} x' - \frac{1}{2} A_0(1 - A_0^2) x'^2 \\ &\quad + \kappa \left[A_1 - \frac{B_0^2}{4A_0} + \left(B_0 B_1 - \frac{3}{32} \frac{B_0^4}{A_0^2} \right) x' \right]. \end{aligned} \quad (2.84)$$

By writing both expressions in terms of x' , and equating the various coefficients of x' and κ , we see that the expansions do indeed match if we choose

$$A_0 = \tanh\left(\frac{x_0}{\sqrt{2}}\right), \quad (2.85)$$

$$B_0 = -2^{1/4} \operatorname{sech}\left(\frac{x_0}{\sqrt{2}}\right) = -2^{1/4} (1 - A_0^2)^{1/2}, \quad (2.86)$$

$$A_1 = \frac{B_0^2}{4A_0} + \operatorname{sech}^2\left(\frac{x_0}{\sqrt{2}}\right) \frac{C_1}{\sqrt{2}} = \frac{\sqrt{2}}{4} \frac{1 - A_0^2}{A_0} + (1 - A_0^2) \frac{C_1}{\sqrt{2}}, \quad (2.87)$$

$$B_1 = \frac{3}{32} \frac{B_0^3}{A_0^2} - \frac{\sqrt{2} A_0 (1 - A_0^2)}{B_0} \frac{C_1}{\sqrt{2}}. \quad (2.88)$$

Eliminating C_1 ,

$$B_1 = -\frac{\sqrt{2} A_0 A_1}{B_0} + \frac{3}{32} \frac{B_0^3}{A_0^2} + \frac{1}{2} \frac{1 - A_0^2}{B_0}. \quad (2.89)$$

Substituting into our expressions for $H_0(0)$ and $H_1(0)$ from Eqs. (2.76) and (2.80), we obtain

$$H_0(0) = 2^{1/4} A_0 (1 - A_0^2)^{1/2}, \quad (2.90)$$

$$H_1(0) = \frac{2^{3/4} (2A_0^2 + 14)(1 - A_0^2)^{1/2}}{64 A_0} - \frac{2^{1/4} (2A_0^2 - 1)}{(1 - A_0^2)^{1/2}} A_1. \quad (2.91)$$

In order to calculate the superheating field (or, more correctly, the *maximum* superheating field), we need to maximize $H_0(0)$ and $H_1(0)$ with respect to A_0 and A_1 . Maximizing $H_0(0)$ with respect to A_0 , we find that the maximum occurs at $A_0^* = 1/\sqrt{2}$, $B_0^* = -2^{-1/4}$, so that $H_0(0) = 2^{-3/4}$. Substituting this result into $H_1(0)$, we find the surprising result that the coefficient of A_1 is zero, and $H_1(0) = 2^{3/4} 15/64$. Our superheating field is then

$$H_{\text{sh}} = 2^{-3/4} \kappa^{-1/2} \left[1 + \frac{15\sqrt{2}}{32} \kappa + O(\kappa^2) \right]. \quad (2.92)$$

In order to determine A_1 we need to proceed to a higher order calculation. The method is the same as before, although the algebra quickly becomes tedious; we have used the computer algebra systems *Maple V* and *Mathematica* to organize the expansion. The results from a six term inner expansion are summarized

n	A_n	B_n	x_n	$H_n(0)$
0	$2^{-1/2}$	$-2^{-1/4}$	$2^{1/2} \tanh^{-1}(2^{-1/2})$	$2^{-3/4}$
1	$-7/32$	$-(9/16)2^{1/4}$	$-(15/16)2^{1/2}$	$(15/64)2^{3/4}$
2	$(395/2048)2^{1/2}$	$(147/512)$	$429/512$	$-(325/2048)2^{1/4}$
3	?	?	?	$(14191/65539)2^{3/4}$
4	?	?	?	$-(67453267/62914560)2^{1/4}$

Table 2.2: The lower order integration constants are shown in the text. Higher orders required symbolic mathematics software. Miraculous cancellations allowed derivation of the first six terms of the superheating field without knowledge of most third- and fourth-order constants.

in Table 2.2. Including the next order term in the expansion in the superheating field, we have

$$H_{\text{sh}} = 2^{-3/4} \kappa^{-1/2} \left[1 + \frac{15\sqrt{2}}{32} \kappa - \frac{325}{1024} \kappa^2 + O(\kappa^3) \right]. \quad (2.93)$$

The first term is exactly the result obtained by the Orsay group [48, 53], who used a variational argument to obtain their result. The second term is identical to the result obtained by Parr [87]. Parr combined an inspired guess for the behavior of the order parameter near the surface with a variational calculation in order to obtain his result. It is interesting to note that our result for A_1 also agrees with Parr's result. The advantage of the method of matched asymptotic expansions is that we can make this expansion systematic, and therefore in principle carry out this expansion as far as we wish. The third term in Eq. (2.93) is one of the new results of this chapter; the fourth and fifth terms are included in Table 2.2. With the five-term expansion for H_{sh} it is possible to employ resummation techniques to improve the expansion. For instance, the $[2, 2]$ Padé approximant [10] is

$$H_{\text{sh}}^{\text{Padé}} = 2^{-3/4} \kappa^{-1/2} \frac{1 + 4.6825120 \kappa + 3.3478315 \kappa^2}{1 + 4.0195994 \kappa + 1.0005712 \kappa^2}. \quad (2.94)$$

In Fig. 2.6 we compare the numerically calculated superheating field against the one, two, and three term asymptotic expansions. The one term (i.e., the Orsay group) result never seems particularly accurate. There is a marked improvement with the two term expansion, with the three term expansion offering only a modest additional improvement. The $[2, 2]$ Padé approximant agrees with the numerical data to within about 1 % all the way to $\kappa = 1$.

Uniform solutions. From the inner and outer expansions it is possible to construct *uniform* solutions, which are asymptotically correct for all x as $\kappa \rightarrow 0$. To do this we simply add the inner and outer solutions of a given order, which guarantees the correct behavior in the outer region as well as in the boundary layer. However, this would produce a result which was $2f_{\text{match}}$ in the matching region, so we need to subtract f_{match} in order to obtain the correct behavior in this region. As an example, we will construct the 2-term uniform solution for the order parameter. Adding the two-term outer solution, $f_0(x') + \kappa f_1(x')$, to the two-term inner solution, $F_0(X) + \kappa F_1(X)$, subtracting the solution in the matching region, which is $1/\sqrt{2} + (\sqrt{2}/4)\kappa X - (15/32)\kappa$, and writing the entire combination in terms of the original variable x (which is the same as X), we obtain

$$f_{\text{unif},2}(x) = \tanh\left(\frac{\kappa x + x_0}{\sqrt{2}}\right) - \frac{15}{16} \kappa \operatorname{sech}^2\left(\frac{\kappa x + x_0}{\sqrt{2}}\right) + \frac{\kappa}{4} e^{-\sqrt{2}x}. \quad (2.95)$$

As $x \rightarrow \infty$, $f_{\text{unif},2}(x) \rightarrow 1$; also, $f_{\text{unif},2}(0) = 1/\sqrt{2} - (7/32)\kappa$, as we expect. However, $f'_{\text{unif},2}(0) = (15/64)\kappa^2$, so that the zero-derivative boundary condition is only satisfied to $O(\kappa)$.

In Fig. 2.7 and Fig. 2.8 we compare the numerically calculated order parameter and magnetic field with the two term outer solutions and the three term inner solutions. The agreement is quite good for $\kappa = 0.1$,

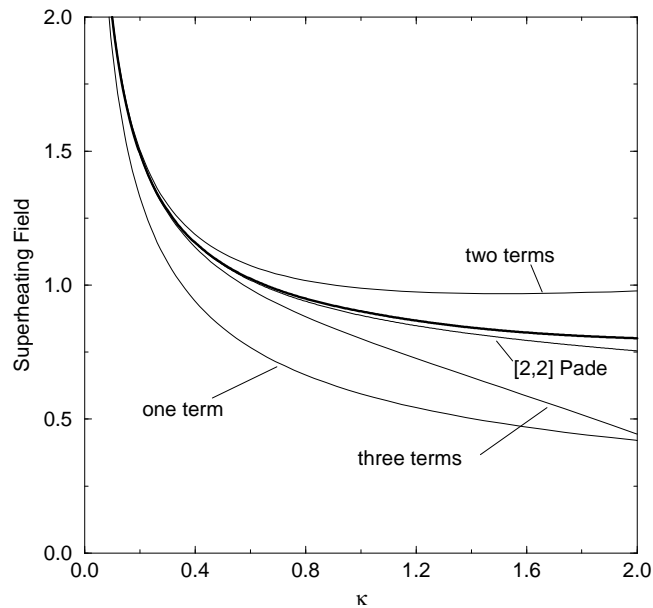


Figure 2.6: A comparison of the numerically calculated superheating field H_{sh} (heavy line) with the three term asymptotic expansion for small- κ , and the $[2, 2]$ Padé approximant. The one-term expansion due to the Orsay group deviates systematically from the calculated superheating field. The two- and three-term expansions provide a marked improvement over the one-term expansion.

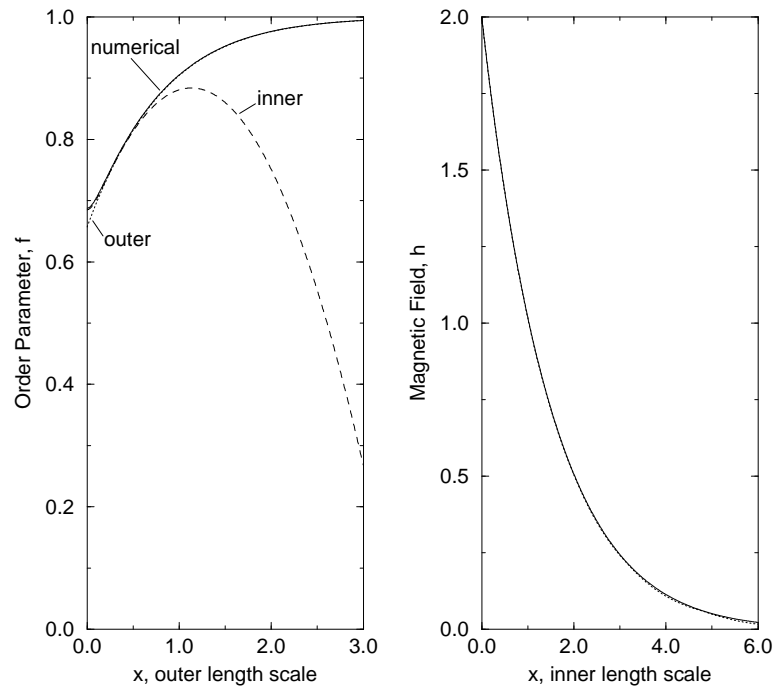
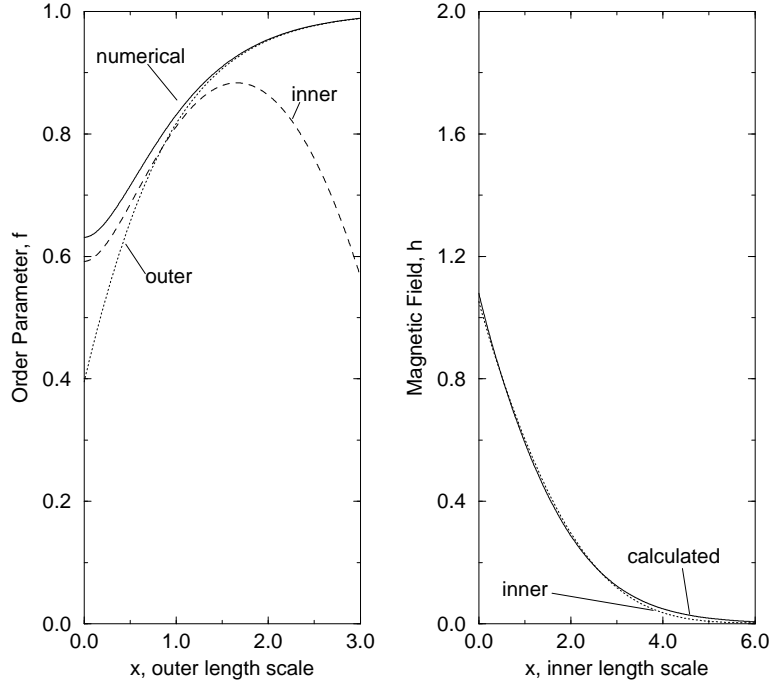


Figure 2.7: A comparison of the three term inner and outer solutions for the order parameter and the magnetic field with the numerical solution for $\kappa = 0.1$. The asymptotic solutions approximate the computed values only in the appropriate regions. The matching region where the inner and outer meet is $O(\kappa)$ as can be estimated from the inner solution for f .

Figure 2.8: The same as Fig. 2.7 for $\kappa = 0.5$.

with deviations appearing at $\kappa = 0.5$. These figures also illustrate the existence of a matching region where the inner and outer solutions overlap; this region grows as $\kappa \rightarrow 0$. Lastly, we show in Fig. 2.9 how the two term uniform expansion constructed earlier supplies a uniform approximation to the order parameter and magnetic field over the whole region.

2.3 Stability Analysis of the Solutions

2.3.1 Derivation of Equations

We test the stability of the solutions by solving the second variation of the free energy to see whether the Landau-Ginzburg solutions sit in a minimum, maximum or saddle point of the free energy. The second variation of the Free Energy can be found any one of a number of ways. The first solution shown is equivalent to using Calculus of Variations and the second is known as a time-dependent formulation.

If we perturb the extremal solution (f, q) of the GL equations by allowing $f(x) \rightarrow f(x) + \tilde{f}(x)$ and $q(x) \rightarrow q(x) + \tilde{q}(x)$, then the second variation of the free energy functional is

$$\delta^2 \mathcal{F} = \int_0^\infty dx \left[\frac{1}{\kappa^2} \tilde{f}'^2 + (3f^2 + q^2 - 1) \tilde{f}^2 + 4fq\tilde{f}\tilde{q} + f^2\tilde{q}^2 + \tilde{q}'^2 \right]. \quad (2.96)$$

The boundary conditions on \tilde{f} and \tilde{q} should be chosen so as to not perturb f and h at the surface, so that

$$\tilde{f}'(0) = \tilde{q}'(0) = 0, \quad \tilde{f}(\infty) = \tilde{q}(\infty) = 0. \quad (2.97)$$

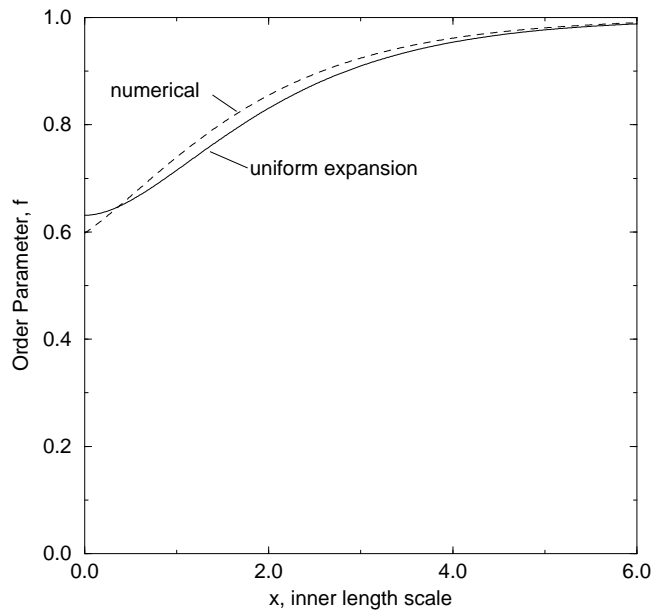


Figure 2.9: A comparison of the two-term uniform solution for the order parameter, $f_{\text{unif},2}(x)$ (dashed line), with the numerical solution (solid line) at $\kappa = 0.5$. The disagreement of the uniform solution with the boundary condition at $x = 0$ is of order κ^2 .

We can then integrate Eq. (2.96) by parts to obtain

$$\delta^2 \mathcal{F} = \int_0^\infty dx \left[\tilde{f} \left(-\frac{1}{\kappa^2} \frac{d^2}{dx^2} + q^2 + 3f^2 - 1 \right) \tilde{f} + \tilde{q} \left(-\frac{d^2}{dx^2} + f^2 \right) \tilde{q} + 4qf\tilde{q}\tilde{f} \right]. \quad (2.98)$$

This quadratic form can be conveniently written as

$$\delta^2 \mathcal{F} = \int_0^\infty dx (\tilde{f}, \tilde{q}) \hat{L}_1 \begin{pmatrix} \tilde{f} \\ \tilde{q} \end{pmatrix} \quad (2.99)$$

where \hat{L}_1 is the self-adjoint linear operator

$$\hat{L}_1 \begin{pmatrix} \tilde{f} \\ \tilde{q} \end{pmatrix} = \begin{pmatrix} -\frac{1}{\kappa^2} \frac{d^2}{dx^2} + q^2 + 3f^2 - 1 & 2fq \\ 2fq & -\frac{d^2}{dx^2} + f^2 \end{pmatrix} \begin{pmatrix} \tilde{f} \\ \tilde{q} \end{pmatrix}. \quad (2.100)$$

In order to analyze the stability, expand \tilde{f} and \tilde{q} as

$$\begin{pmatrix} \tilde{f} \\ \tilde{q} \end{pmatrix} = \sum_n c_n \begin{pmatrix} \tilde{f}_n \\ \tilde{q}_n \end{pmatrix}, \quad (2.101)$$

where the c_n 's are real constants, and $(\tilde{f}_n, \tilde{q}_n)$ is a normalized eigenfunction of \hat{L}_1 with eigenvalue E_n :

$$\hat{L}_1 \begin{pmatrix} \tilde{f}_n \\ \tilde{q}_n \end{pmatrix} = E_n \begin{pmatrix} \tilde{f}_n \\ \tilde{q}_n \end{pmatrix}. \quad (2.102)$$

Then

$$\delta^2 \mathcal{F} = \sum_n E_n c_n^2. \quad (2.103)$$

The second variation $\delta^2 \mathcal{F}$ ceases to be positive-definite when the lowest eigenvalue first becomes negative, indicating that the corresponding solutions (f, q) of the GL equations are unstable. Therefore the entire issue of the stability of the solutions has been reduced to finding the eigenvalue spectrum of the linear stability operator \hat{L}_1 , which in the $\kappa \rightarrow 0$ limit can be studied using matched asymptotic expansions.

The condition that the second variation be positive definite is identical to the traditional requirements of stability calculations using Calculus of Variations. It measures stability of the system with respect to infinitesimal perturbations. We also know, either from theorems of Calculus of Variations or from equivalence with the Schrödinger equation, that the solutions with lowest eigenvalues will never cross zero—they will be lowest energy bound states.

Another way to analyze the stability of solutions to the GL equations is to substitute perturbations into the time-dependent GL equations and find whether they remain bounded over time. This is often presented as a second way to measure the same stability as that of the Calculus of Variations, but it is essentially different. Time-dependent stability analysis is dynamical. Let's look at the derivation of equations to see the difference.

In many systems, one can determine the stability of the solutions by substituting time-dependent perturbations

$$f(x) \rightarrow f(x) + \tilde{f}(x)e^{-Et} \quad (2.104)$$

$$q(x) \rightarrow q(x) + \tilde{q}(x)e^{-Et} \quad (2.105)$$

into the time-dependent equations. Here (f, q) are the exact solutions. Then linearize the resulting equations in order to find linear stability. As above, positive eigenvalue, E , indicates a stable system.

In the gauge where ψ is real, the set of time-dependent differential equations which would yield the exact same results as the Calculus of Variations approach are

$$\frac{\partial f}{\partial t} - \frac{1}{\kappa^2} \nabla^2 f + f \mathbf{Q}^2 - f + f^3 = 0 \quad (2.106)$$

$$\frac{\partial \mathbf{Q}}{\partial t} + \nabla \times \nabla \times \mathbf{Q} + f^2 \mathbf{Q} = 0. \quad (2.107)$$

We just inserted time-dependence of the correct sign to look like a diffusion equation. If we put the perturbations into the above equations (Eqns. 2.104 and 2.105), the resulting equations are

$$-\frac{1}{\kappa^2} \tilde{f}'' + (3f^2 + q^2 - 1)\tilde{f} + 2fq\tilde{q} = E\tilde{f} \quad (2.108)$$

$$-\tilde{q}'' + f^2\tilde{q} + 2fq\tilde{f} = E\tilde{q}. \quad (2.109)$$

You see that the time dependence cancels when we linearize in \tilde{f} and \tilde{q} leaving the eigenvalue E . When $E > 0$, the solutions (f, q) are stable with respect to infinitesimal perturbations. These equations are formally identical to Eqns. 2.102.

The Eqs. 2.107 are almost, but not quite, the full time-dependent Landau-Ginzburg equations. We haven't yet seen the TDGL in the gauge where ψ is real, so let's write them now. If we make a gauge transformation to Eqs. 1.35 and 1.36 of the form

$$\zeta = \psi e^{i\kappa\chi} \quad \mathbf{Q} = \mathbf{A} + \nabla\chi \quad \Theta = \phi - \frac{\partial\chi}{\partial t} \quad (2.110)$$

where we specify

$$\kappa\chi = -\theta \quad \text{for} \quad \psi = f e^{i\theta}, \quad (2.111)$$

we find the TDGL in the gauge where ψ is real

$$\gamma \frac{\partial f}{\partial t} - \frac{1}{\kappa^2} \nabla^2 f + \mathbf{A}^2 f - f + f^3 = 0 \quad (2.112)$$

$$\gamma\kappa^2\phi f + \nabla \cdot (\mathbf{Q}^2 \psi) = 0 \quad (2.113)$$

$$\frac{\partial \mathbf{Q}}{\partial t} + \nabla\phi + \nabla \times \nabla \times \mathbf{Q} + f^2 \mathbf{Q} - \nabla \times \mathbf{H} = 0. \quad (2.114)$$

Given our initial solution in one dimension is of the form

$$\mathbf{Q} = (0, q_y(x), 0) \quad (2.115)$$

$$f = f(x) \quad (2.116)$$

we know the divergence on the right of the second equation, Eq. 2.113, is zero,

$$2f\nabla \cdot \mathbf{Q} = \mathbf{Q} \cdot \nabla f = 0 \quad (2.117)$$

which makes $\phi = 0$. The full TDGL then reduce to Eqs. 2.107. This is true of our initial solution, but not true for general one-dimensional systems.

In two dimensions, however, Eqns. 2.112–2.114 cannot be reduced to Eqn. 2.107. They include an extra degree of freedom in ϕ . This extra degree of freedom allows them to include normal currents, which are dissipative. Recall that the Calculus of Variations perturbations do not include dissipation. Because the equations in one dimension are the same as the TDGL, they do describe dynamic perturbations for this system in one dimension. In two dimensions, however, the Calculus of Variations perturbations describe only non-dissipative perturbations.

The physical perturbations relevant to this system are incident charged particles and thermal fluctuations. They are not infinitesimal and certainly are dissipative. It would be more appropriate to allow perturbations in the normal current for infinitesimal calculations, and any finite perturbations calculated for two dimensions must use the TDGL in order to be relevant. This is the heart of the debate by Kramer et al. about whether perturbations on superheating can describe the first introduction of vortices into a superconductor. Just using the Landau-Ginzburg Hamiltonian is not appropriate to what would seem an immediately relevant problem.

Perturbations using the equations of the Calculus of Variations approach should at least be close to the correct results. It is possible that the least stable subspace of dissipative perturbations is the space of stable perturbations. More ardent numerical work is required to test the dissipative perturbation equations which are of higher order than the conservative ones. We proceed with the conservative Landau-Ginzburg perturbations and their boundary conditions.

The boundary conditions on the differential equations for the perturbations have to leave the applied fields unchanged. Given GL solutions like those shown in Figure 2.7, the applied field, $\mathbf{h}(o) = q'(0) = \mathbf{H}_{\text{applied}}$ and $f'(0) = 0$ must not change. Since the perturbation equations are linear, only the relative magnitude of the solutions is important.

The eigenvalue, E , however, is nonlinearly coupled into the equation. However we scale the perturbations, the size of the eigenvalue will remain the same. It will depend only on the parameters (κ, H_a) of the GL equation. In fact, the magnitude of the stability eigenvalue is another of the new results of this work. Knowledge of the eigenvalues as a function of perturbation wavelengths are useful in calculating higher-order stability. We begin as before with matched asymptotic analysis in inner and outer regions.

2.3.2 One-dimensional Perturbations

Outer solution. The outer equations for (\tilde{f}, \tilde{q}) are rescaled with $x' = \kappa x$ as before to yield (we will drop the subscript n for notational convenience)

$$-\tilde{f}'' + (3f^2 + q^2 - 1)\tilde{f} + 2fq\tilde{q} = E\tilde{f}, \quad (2.118)$$

$$-\kappa^2\tilde{q}'' + f^2\tilde{q} + 2fq\tilde{f} = E\tilde{q}. \quad (2.119)$$

Expanding \tilde{f} , \tilde{q} , and E in powers of κ , and recalling that $q = 0$ to all orders in κ in the outer region, we have at leading order

$$-\tilde{f}_0'' + (3f_0^2 - 1)\tilde{f}_0 = E_0\tilde{f}_0, \quad (2.120)$$

where $f_0 = \tanh\left(\frac{x'+x_0}{\sqrt{2}}\right)$. By changing variables to $y = \tanh\left(\frac{x'+x_0}{\sqrt{2}}\right)$ we see that the solution of Eq. (2.120) is the associated Legendre function of the first kind:

$$\tilde{f}_0(x') = c_0 P_2^\mu \left[\tanh\left(\frac{x'+x_0}{\sqrt{2}}\right) \right], \quad (2.121)$$

where $\mu = -\sqrt{2(2 - E_0)}$ and c_0 is a constant. The leading order solution for \tilde{q} is $\tilde{q}_0 = 0$.

Inner solution. To obtain the inner equations, we rescale as in Eq. (2.66), with the perturbations rescaled as

$$\tilde{f}(x') = \tilde{F}(X), \quad \tilde{q}(x') = \kappa^{-1/2}\tilde{Q}(X), \quad (2.122)$$

such that

$$-\frac{1}{\kappa^2} \tilde{F}'' + (3F^2 + \frac{1}{\kappa} Q^2 - 1)\tilde{F} + \frac{1}{\kappa} 2FQ\tilde{Q} = E\tilde{F}, \quad (2.123)$$

$$-\tilde{Q}'' + F^2\tilde{Q} + 2FQ\tilde{F} = E\tilde{Q}. \quad (2.124)$$

To leading order, $\tilde{F}_0'' = 0$, so that $\tilde{F}_0 = a_0$, with a_0 a constant. The leading order equation for the variation in Q is

$$-\tilde{Q}_0'' + 2F_0Q_0\tilde{F}_0 + (F_0^2 - E_0)\tilde{Q}_0 = 0. \quad (2.125)$$

The solution which satisfies the boundary condition $\tilde{Q}'(0) = 0$ is

$$\tilde{Q}_0(X) = \frac{2a_0A_0B_0}{E_0} \left(e^{-A_0X} - \frac{A_0}{\sqrt{A_0^2 - E_0}} e^{-\sqrt{A_0^2 - E_0}X} \right). \quad (2.126)$$

At $O(\kappa)$ we find

$$\tilde{F}_1'' = Q_0^2\tilde{F}_0 + 2F_0Q_0\tilde{Q}_0, \quad (2.127)$$

with the solution

$$\begin{aligned} \tilde{F}_1(X) = a_1 + a_0B_0^2 & \left[\frac{E_0 + 4A_0^2}{4A_0^2E_0} e^{-2A_0X} - \frac{4A_0^2}{E_0} \frac{e^{-(A_0 + \sqrt{A_0^2 - E_0})X}}{(A_0 + \sqrt{A_0^2 - E_0})^2\sqrt{A_0^2 - E_0}} \right] \\ & + a_0B_0^2 \left[\frac{E_0 + 4A_0^2}{2A_0E_0} - \frac{4A_0^3/E_0}{(A_0 + \sqrt{A_0^2 - E_0})\sqrt{A_0^2 - E_0}} \right] X. \end{aligned} \quad (2.128)$$

We now have enough terms in the inner and outer region for a nontrivial match.

Matching. We complete the matching of the inner and outer perturbations to obtain the eigenvalue, E_0 . Performing a two term inner expansion of the one term outer solution, we have

$$\tilde{f}_0(\kappa X) \sim c_0 \left[P_2^\mu(A_0) + \frac{1}{\sqrt{2}} \operatorname{sech}^2(x_0/\sqrt{2}) \frac{dP_2^\mu(A_0)}{dA_0} \kappa X \right], \quad (2.129)$$

where we have used $\tanh(x_0/\sqrt{2}) = A_0$. Next, the one term outer expansion of the two term inner solution is

$$\tilde{F}_0(x'/\kappa) + \kappa\tilde{F}_1(x'/\kappa) \sim a_0 + \frac{a_0 2^{1/2}(1 - A_0^2)}{E_0} \left[\frac{E_0 + 4A_0^2}{2A_0} - \frac{4A_0^3}{(A_0 + \sqrt{A_0^2 - E_0})\sqrt{A_0^2 - E_0}} \right] x', \quad (2.130)$$

where we have used $B_0 = -2^{1/4}(1 - A_0^2)^{1/2}$. Matching the two expansions using the van Dyke matching principle yields

$$c_0 = \frac{a_0}{P_2^\mu(A_0)}, \quad (2.131)$$

$$\frac{1}{P_2^\mu(A_0)} \frac{dP_2^\mu(A_0)}{dA_0} = \frac{2}{E_0} \left[\frac{E_0 + 4A_0^2}{2A_0} - \frac{4A_0^3}{(A_0 + \sqrt{A_0^2 - E_0})\sqrt{A_0^2 - E_0}} \right]. \quad (2.132)$$

The last equation is a rather complicated implicit equation for the eigenvalue $E_0(A_0)$, which generally must be solved numerically. However, when $A_0 = 1/\sqrt{2}$ we find $E_0 = 0$, corresponding to the critical case, with

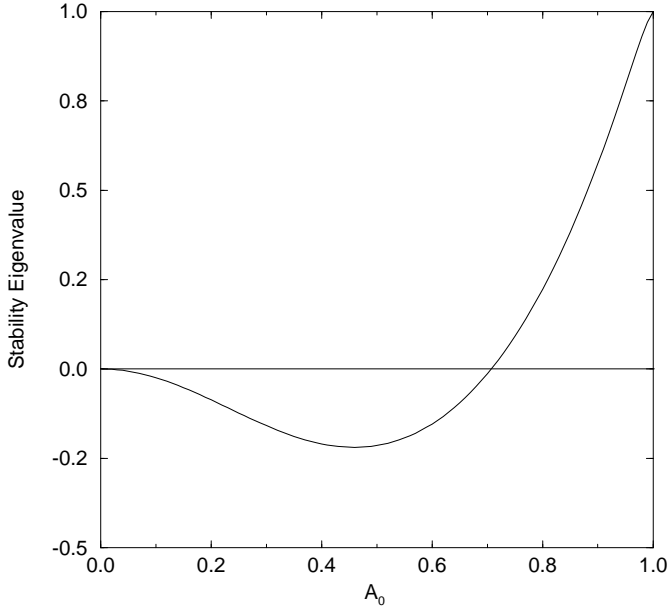


Figure 2.10: The stability eigenvalue $E(A_0)$, with A_0 the value of the order parameter at the surface at leading order. We see that $E > 0$ for $A_0 > 1/\sqrt{2}$, indicating locally stable solutions.

$E > 0$ for $A_0 > 1/\sqrt{2}$. The numerical evaluation of Eq. (2.132) is shown in Fig. 2.10. Therefore, we see that our maximum superheating field (at lowest order) corresponds to the limit of metastability for these one-dimensional perturbations. In Fig. 2.11 we show A_0 as a function of the lowest order magnetic field at the surface, H_0 , from Eq. (2.90). The stability analysis of this section shows that only the upper branch of this double valued function corresponds to solutions which are locally stable, with the field at the “nose” being the superheating field.

2.3.3 Two-dimensional perturbations

We next turn to the stability of the solutions with respect to two dimensional perturbations. It is very likely that there may be solutions stable with respect to one-dimensional perturbations but not two. The GL solutions are minimizers of the free energy and we expect them to usually sit in the well of free energy potential. They will likely always be stable with respect to infinitesimal one-dimensional perturbations. However, we can imagine that if we allow the free energy schematic a second direction, the GL free energy minimizer may be either the minimum or maximum of a parabola in the \hat{y} direction. In other words, we are searching for the applied field at which the GL solution becomes a saddle point in the free energy.

If we perturb the extremal solution (f, \mathbf{q}) of the GL equations by allowing $f \rightarrow f + \delta f$ and $\mathbf{q} \rightarrow \mathbf{q} + \delta \mathbf{q}$, then the second variation of the free energy functional is

$$\delta^2 \mathcal{F} = \int dx dy \left[\frac{1}{\kappa^2} (\nabla \delta f)^2 + 4f(\delta f) \mathbf{q} \cdot \delta \mathbf{q} + f^2(\delta \mathbf{q})^2 + (3f^2 + \mathbf{q}^2 - 1)(\delta f)^2 + (\nabla \times \delta \mathbf{q})^2 \right]. \quad (2.133)$$

We neglect perturbations along the \hat{z} -direction because Fink and Presson [38] showed that terms in \hat{z} are purely positive definite and thus any variation in z only increases the free energy. Expanding in Fourier

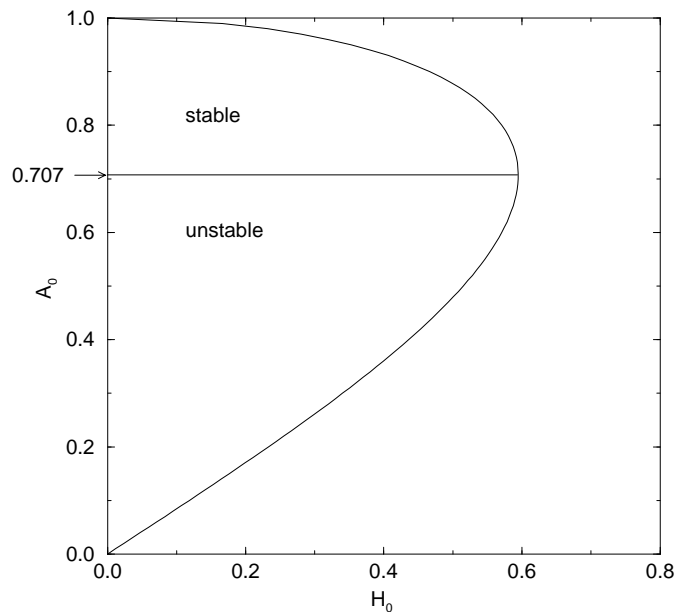


Figure 2.11: The order parameter at the surface, A_0 , as a function of the field at the surface, H_0 , at leading order. The stability analysis shows that only the upper branch corresponds to locally stable solutions. The field at the “nose” is the limit of stability, and corresponds to the superheating field $H_0 = 2^{-3/4} = 0.595$.

modes with respect to y [66],

$$\delta f(x, y) = \tilde{f}(x) \cos ky, \quad \delta q_x(x, y) = \tilde{q}_x(x) \sin ky, \quad \delta q_y(x, y) = \tilde{q}_y(x) \cos ky, \quad (2.134)$$

substituting into Eq. (2.133), recalling that $\mathbf{q} = (0, q(x), 0)$, and integrating over y , we obtain (up to a multiplicative constant)

$$\delta^2 \mathcal{F} = \int_0^\infty dx \left[\frac{1}{\kappa^2} \tilde{f}'^2 + (3f^2 + q^2 + \frac{1}{\kappa^2} k^2 - 1) \tilde{f}^2 + 4fq\tilde{f}\tilde{q}_y + f^2(\tilde{q}_x^2 + \tilde{q}_y^2) + (\tilde{q}_y' - k\tilde{q}_x)^2 \right]. \quad (2.135)$$

By integrating by parts and using the boundary conditions, Eq. (2.97), we can cast this functional into the form

$$\delta^2 \mathcal{F} = \int_0^\infty dx (\tilde{f}, \tilde{q}_y, \tilde{q}_x) \hat{L}_2 \begin{pmatrix} \tilde{f} \\ \tilde{q}_y \\ \tilde{q}_x \end{pmatrix}, \quad (2.136)$$

where the self-adjoint linear operator \hat{L}_2 is given by

$$\hat{L}_2 \begin{pmatrix} \tilde{f} \\ \tilde{q}_y \\ \tilde{q}_x \end{pmatrix} = \begin{pmatrix} -\frac{1}{\kappa^2} \frac{d^2}{dx^2} + q^2 + 3f^2 + k^2/\kappa^2 - 1 & 2fq & 0 \\ 2fq & -\frac{d^2}{dx^2} + f^2 & -k \frac{d}{dx} \\ 0 & k \frac{d}{dx} & f^2 + k^2 \end{pmatrix} \begin{pmatrix} \tilde{f} \\ \tilde{q}_y \\ \tilde{q}_x \end{pmatrix}. \quad (2.137)$$

That the operator is self-adjoint shows that it represents perturbations on a conservative hamiltonian. As in the previous section, we want to determine the eigenvalue spectrum of this operator. We are primarily interested in the effects of long-wavelength perturbations (i.e., $k \rightarrow 0$), so we rescale k as $k = \kappa k'$. Then the eigenvalue equations in terms of the outer coordinate $x' = \kappa x$ are (dropping the prime on k from now on)

$$-\tilde{f}'' + (3f^2 + q^2 - 1 + k^2)\tilde{f} + 2fq\tilde{q} = E\tilde{f}, \quad (2.138)$$

$$-\kappa^2 \tilde{q}_y'' + f^2 \tilde{q}_y + 2fq\tilde{f} - \kappa^2 k \tilde{q}_x' = E\tilde{q}_y, \quad (2.139)$$

$$\kappa^2 k \tilde{q}_x' + (f^2 + \kappa^2 k^2)\tilde{q}_x = E\tilde{q}_x. \quad (2.140)$$

By using the last equation we may eliminate \tilde{q}_x from Eq. (2.139), which becomes

$$-\kappa^2 \frac{d}{dx} \left[\frac{f^2 - E}{f^2 + \kappa^2 k^2 - E} \tilde{q}_y' \right] + f^2 \tilde{q}_y + 2fq\tilde{f} = E\tilde{q}_y. \quad (2.141)$$

For $k = 0$ Eqs. (2.138) and (2.141) reduce to the one-dimensional perturbation equations of the last section, Eqs. (2.118) and (2.119); for $E = 0$ they reduce to the Euler-Lagrange equations derived by Kramer [66].

The perturbation equations (2.138) and (2.141) may be solved by the method of matched asymptotic expansions, just as in the one-dimensional case. The derivation of the eigenvalue condition is essentially identical, with the final result that

$$\frac{1}{P_2^\mu(A_0)} \frac{dP_2^\mu(A_0)}{dA_0} = \frac{2}{E_0} \left[\frac{E_0 + 4A_0^2}{2A_0} - \frac{4A_0^3}{(A_0 + \sqrt{A_0^2 - E_0})\sqrt{A_0^2 - E_0}} \right], \quad (2.142)$$

where now $\mu = -\sqrt{2(2 + E_0 - k^2)}$. The eigenvalue $E_0(k)$ is plotted in Fig. 2.12 for several different values of A_0 . For $A_0 > 1/\sqrt{2}$, $E_0(k) > 0$ for all k , while for $A_0 < 1/\sqrt{2}$ there exists a band of long-wavelength perturbations for which $E_0(k) < 0$. In all cases the most unstable modes are at $k = 0$, i.e., the one-dimensional perturbations are the least stable. This is in contrast to the large- κ limit, where the most unstable mode occurs for $k \neq 0$ [42, 66, 21].

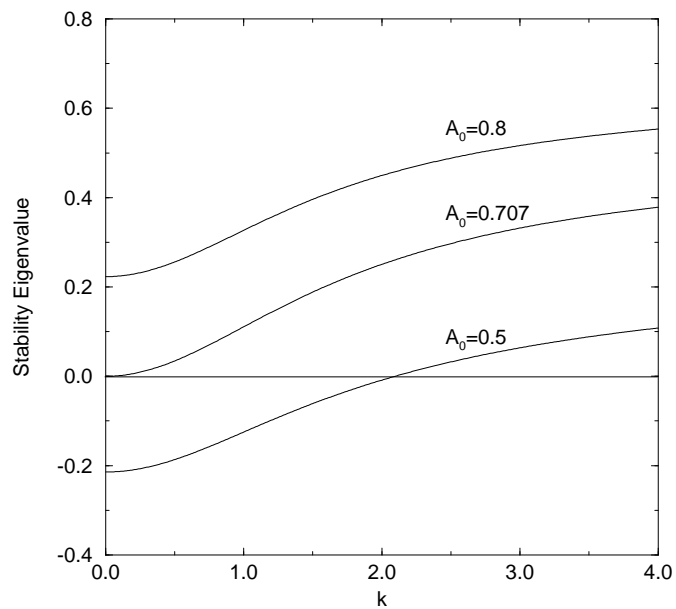


Figure 2.12: The stability eigenvalue $E(k)$ for two-dimensional perturbations of wavenumber k , for several different values of A_0 . For $A_0 > 1/\sqrt{2}$ the eigenvalue is stable for all wavenumbers, while for $A_0 < 1/\sqrt{2}$ there exists a band of wavenumbers for which the solution is unstable.

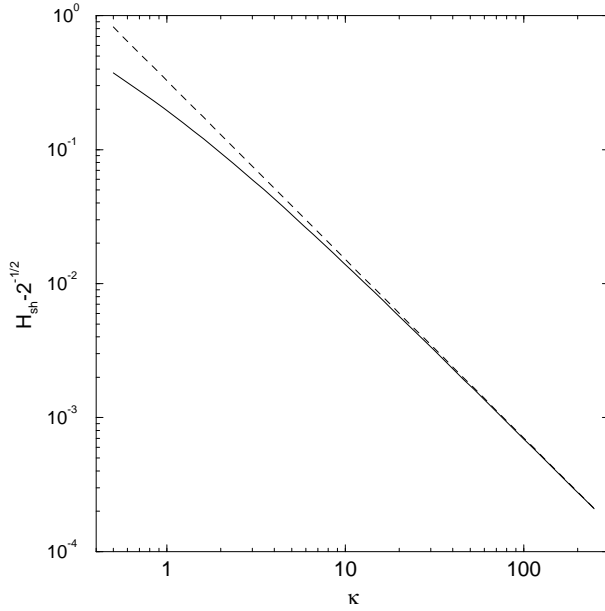


Figure 2.13: This figure shows the numerically calculated superheating field for large κ (solid line) compared with the two-term asymptotic expansion derived by Chapman (dashed line). The slope of the dashed line is $-4/3$.

2.3.4 Large- κ two-dimensional Stability

The exact numerical solution of the Landau-Ginzburg equations shows that the system is unstable with respect to two-dimensional perturbations at an applied field, $H_{2D} < H_{sh}$. Fink and Presson [38] estimate that the H_{2D} separates from H_{sh} at $\kappa \approx 1.10$ or $\kappa \approx 1.13$. Our calculations show the crossover occurs at $1.16 < \kappa < 1.17$. At the bifurcation, the least stable mode lifts from $k = 0$ to steadily higher wavenumbers.

Chapman [21] recently used matched asymptotics to examine the Landau-Ginzburg equations in the high- κ limit. His final result for the superheating field is

$$H_{sh} = \frac{1}{\sqrt{2}} + C\kappa^{-4/3} + O(\kappa^{-6/3}) \quad (2.143)$$

where the constant C is determined from the solution of the second Painlevé transcendent; a numerical evaluation yields $C=0.326$ [26]. The first term was originally derived by Ginzburg [48], and the second term with the unusual dependence on κ is new. We verify the second term in Fig. 2.13. The dependence is correct but does not converge as rapidly as the small- κ solution.

2.4 Numerical methods

We used two separate algorithms to evaluate our solutions of the superheating field. First, we calculated solutions to the Landau-Ginzburg equations for the half-space as a function of $(\kappa, H_{\text{applied}})$. Second, we calculated perturbations to those solutions as a function of wavenumber, k .

Finding solutions to the Landau-Ginzburg equations themselves was straightforward. To ensure that no current passes through the boundary at $x = 0$ and that the sample is totally superconducting infinitely far

from the surface, we impose the boundary conditions

$$f'(0) = 0, \quad f(x) \rightarrow 1 \text{ as } x \rightarrow \infty. \quad (2.144)$$

Since the field at the surface must equal the applied field H_a , and there must be no field infinitely far from the surface, we impose the boundary conditions

$$h(0) = H_a, \quad q(x) \rightarrow 0 \text{ as } x \rightarrow \infty. \quad (2.145)$$

The discretization used a finite domain, so the boundary conditions at infinity were generally enforced at a coordinate large enough not to change the shape of the solutions of the independent variables (f, q) as measured by the norm of the difference between successive solutions,

$$\int (|f_1(x) - f_2(x)| + |q_1(x) + q_2(x)|) dx. \quad (2.146)$$

Later investigations instead used boundary conditions which were the analytically derived asymptotics of the Landau-Ginzburg equations. They had no measurable affect on the independent variables.

For $\kappa \rightarrow 0$, we rescale the equations as $x' = \kappa x$ making the new unit of length the correlation length ξ . Since $\xi \gg \lambda$ in this limit, a numerical solution over a domain much larger than ξ would ensure that the regions of rapid change for f and h would be included. (For small κ , we find that solving for $x' < 500$ is sufficient.) In the large κ limit, we use the rescaled equations again, but we increase the size of the domain depending on the value of κ . (The equations must be solved for domains as large as $x' < 10^4$ for values of $\kappa \sim 10^3$.)

The equations can be solved using the relaxation method [93]. By replacing these ordinary differential equations with finite difference equations, one can start with a guess to the solution and iterate using a multi-dimensional Newton's method until it relaxes to the true solution. In order to more accurately pick up the detail near the boundary, we choose a grid of discrete points with a higher density near $x = 0$. In particular we choose a density which roughly varies as the inverse of the distance from the boundary. (For low κ our density, in units of mesh points per coherence length, varies approximately from 10^7 near the boundary to 10^3 at the farthest point from the boundary, while for high κ it varies from 10^5 to 10^{-2} .)

H_{sh} can be found in the following way. For a given value of κ an initial guess is made where there is no applied field and the sample is completely superconducting ($f \equiv 1, q \equiv 0, h \equiv 0$). The field H_a is then increased in small increments. For each value of H_a a solution is sought using the result from the previous lower field solution as an initial guess. Eventually a maximum value for H_a is reached, above which one of two things happens: our algorithm fails to converge to a solution or it converges to the normal (nonsuperconducting solution). This maximum value of H_a is the numerical result for H_{sh} . Using this algorithm, $H_{\text{sh}}(\kappa)$ can be found for a wide range of κ 's.

It is possible to imagine a situation in which this algorithm might not work. Suppose that you have a solution at H_{a1} and fail to converge on a solution at $H_{a2} = H_{a1} + 0.01$. It is possible that your initial guess was just not close enough. For instance, a smaller stepsize would permit one to find a solution first at $H_{a1} + 0.05$, and then that solution would be close enough to find the solution at $H_{a2} = H_{a1} + 0.01$. The superheating solution could creep away as quickly as you could approach it. Using a variation on the Contracting Mapping Theorem, Herbert Keller [63] showed that Euler's Method, in particular, guarantees that there exists a finite neighborhood of the solution which will always converge for well-behaved systems such as ours.

Each run (for a given κ) takes about 10 seconds on a Pentium II 300. We find it sufficient to deal with superheating field values for $10^{-3} < \kappa < 10^3$.

More interesting is the study of the perturbations. These require a third parameter, the wavenumber k . The solutions are in a three-parameter space (κ, H_a, k) and the solution of each perturbation requires calculation of the initial Landau-Ginzburg solution. Because the two-dimensional perturbations were of interest for large κ where there are not readily available analytic solutions, even asymptotics, the initial

conditions for each run (of wavenumbers) are finicky at best.

The primary objective of solving the two-dimensional perturbations is to find the H_{2D} line, but solutions to our equations yield, in addition, the dependence of the stability eigenvalue on the wavenumber. That is more information than is relevant to the superheating field, so it is not included here.

Calculations of the two-dimensional stability required significantly more computer resources, both in CPU time and storage space. The algorithms were written to function on a cluster of a dozen systems and save only relevant data in indexed, binary files on a central server. Time-critical sections were re-written as Fortran90 subroutines to C⁺⁺ control structures. Finding the bifurcation point at $\kappa \approx 1.17$ required about a week on our Pentium II cluster or three months of computer time on a single machine.

2.5 Discussion

We have solved the Landau-Ginzburg equations both analytically and numerically for a superconducting half-space. The asymptotic methods depend on disparity between coherence length and penetration depth, but the solutions remain relevant even where they are equal. The resulting expansions for the superheating field should be immediately useful for the reverse operation—calculating the Landau-Ginzburg parameter from the superheating field.

The same techniques were also effective for deriving perturbations on the superheating field. These were previously deemed complicated enough to be beyond analysis by most authors. We not only calculated the exact two-dimensional perturbations but also elucidated a vexing question last posed by Kramer [69] about whether perturbation solutions can represent vortex nucleation.

Chapter 3

Phase Transition in a Current-carrying Wire

3.1 Introduction

When a superconductor is placed in a magnetic field equal to its critical field H_c , the normal and superconducting phases can coexist in a state of equilibrium with the two phases separated by normal-superconducting (NS) interfaces. The dynamics of such interfaces is important for various nonequilibrium phenomena. For instance, if the applied magnetic field is quenched below H_c , these interfaces move through the sample, expelling the magnetic flux so as to establish the Meissner phase [41, 76, 6, 29, 82, 18, 91, 19, 50]. Just as superconductivity can be destroyed by applying a magnetic field exceeding H_c , it can also be destroyed by applying a current exceeding the critical depairing current J_c . Thus by analogy with the magnetic field case, one might expect the competition between the superconducting sample and the applied field to stabilize an NS interface in a current-driven system [74]. In contrast to the magnetic field induced NS interfaces, these current-induced NS interfaces are intrinsically nonequilibrium entities, and their structure depends upon the *dynamics* of the order parameter and magnetic field. The evolution and dynamics of these nonequilibrium interfaces is the subject of this chapter.

The current-induced NS interfaces arise in several contexts. First, they are known to be important in understanding the dynamics of the “resistive state” in superconducting wires and films (for a review see [57] or [101]), and in determining the global stability of the normal and superconducting phases in the presence of a current [67]. Second, Aranson *et al.* [1] have recently used simulations to study the nucleation of the normal phase in thin type-II superconducting strips in the presence of both a magnetic field and a transport current. They found that a sufficient current produced large normal droplets containing multiple flux quanta. Without a current one finds stationary, singly quantized vortices, with a larger amount of NS interface per flux quantum than a multiply quantized droplet. They conclude that the current produces an effective surface tension for the NS interface which is positive, stabilizing the interface and producing larger droplets with smaller surface area. In their simulations, topological singularities of multiple flux lasted for the duration of simulations of flux entry from demagnetizing fields. Motivated in part by its role in this phenomenon we wanted to re-examine the nonequilibrium stabilizing effects of current.

Even when the superconducting phase is ostensibly the equilibrium phase, a current makes the normal phase metastable, i.e., linearly stable to infinitesimal superconducting perturbations. A localized superconducting perturbation of finite amplitude, on the other hand, has one of two fates: (1) its amplitude may ultimately shrink to zero restoring the normal phase (undercritical) or (2) it may grow eventually establishing the superconducting state (overcritical). Separating these two possibilities are the *critical nuclei* or *threshold perturbations*, for present purposes stationary solutions of the time-dependent Ginzburg-Landau (TDGL) equations localized around the normal state. As one raises the current, the amplitude of the

	normal	superconducting
J	globally stable	metastable
J^*	metastable	globally stable
$J = 0$		

Table 3.1: We examine transitions between the two homogeneous states of a current-carrying superconductor. While the system does not conserve energy, we can define metastability with respect to small perturbations.

threshold solution grows, implying that the normal phase becomes increasingly stable.

At very low currents, the widths of the critical nuclei shrink as the current is increased, but eventually this trend is reversed and the width grows as the current is increased further. In fact, as the current approaches a particular value, J^* (the “stall current” [1]), the width diverges resulting in two well-separated, stationary NS interfaces. Above J^* , no nucleus solutions exist in the TDGL. The absence of a critical nucleus for the superconducting state defines the normal state above J^* to be globally stable [67, 33].

When a thermal fluctuation is larger than the critical nucleus for a particular critical current, that perturbation will grow first to locally saturate the order parameter, then form separated NS interfaces which move at constant velocities controlled by the applied current. The transformation of random thermal fluctuations into NS interfaces of fixed form is phase ordering. Once an interface forms, it will travel towards the normal phase if $J < J^*$ and towards the superconducting phase if $J > J^*$.

The interface solutions have been studied numerically by Likharev [74], who found that the interfaces were stationary at $J^* \approx 0.335$ for $u = 5.79$, where u characterizes the material and is 5.79 for nonmagnetic impurities [96]. They were also studied by Kramer and Baratoff [67], who found $J^* \approx 0.291$ for $u = 12$ (corresponding to paramagnetic impurities [51]). However, we know of no systematic study of the dependence of J^* upon u . In this work we remedy this situation by using a combination of numerical methods and analysis including matched asymptotic expansions [10, 105]. We show that $J^* \sim u^{-1/4}$ for large u in contrast to a previous conjecture [74], and we find how J^* approaches J_c in the small- u limit.

At currents close to J^* , we can treat the interface velocity as proportional to $(J - J^*)$ and calculate a kind of susceptibility. Likharev [74] defined the constant of proportionality, $\eta = (dc/dJ)^{-1}|_{J=J^*}$, where c is the interface speed; he found $\eta \approx 0.7$ for $u = 5.79$. In the extreme limits, $J \rightarrow 0$ and $J \rightarrow J_c$ Likharev predicted that the speed c diverges. We find c to be bounded in both cases and provide an analytic expression for it as $J \rightarrow 0$.

The results of this work are summarized in Table 3.2. The rest of the chapter is organized as follows. After briefly reviewing the TDGL equations and the approximations used in this work (section 3.3.1), we study the critical nuclei focusing on their size and shape in the limit $J \rightarrow 0$ (section 3.4). We then move on to consider the stationary interface solutions; in particular we map out the dependence of the stall current J^* on u and supplement the numerical work with analysis of the $u \rightarrow \infty$ and $u \rightarrow 0$ limits (section 3.5). Next, we examine moving interfaces first in the linear response regime and then in the limits $J \rightarrow 0$ and $J \rightarrow J_c$ (section 3.6). Appendix C contains a calculation of the amplitudes of the critical nuclei in the $J \rightarrow 0$ limit.

3.2 The Physical System

Our simplified picture of a one-dimensional superconductor carrying a current clarifies some of the essential physics of more complex phenomena in experiments on thin whiskers or strips of superconducting material. A general review of current-induced phenomena in one-dimensional superconductors can be found in Tidecks [101]. In this section, we will discuss properties of samples (dimensions, materials, contacts) and give a brief taxonomy of behaviors.

Table 3.2: Summary of the primary results.

I. Critical nucleus		
Small- J width	$W \sim (uJ)^{-1/2}$	Sec. 3.4.2
Small- J amplitude	$\psi_0 \sim \exp\{-A/uJ\}$	Sec. 3.4.2
II. Stall current J^*		
Large- u	$J^* = 0.584491 u^{-1/4}$	Sec. 3.5.3
Small- u	$J^* = J_c \frac{(1-u/8)^{1/2}}{(1-u/24)^{3/2}}$	Sec. 3.5.4
III. Kinetic coeff. η		
Large- u	$\eta = 0.797 u^{3/4}$	Sec. 3.6
Small- u	$\eta \sim u^{3/2}$	Sec. 3.6
IV. Interface speed		
$J \rightarrow 0$	$c \rightarrow 2/u$	Sec. 3.6
$J \rightarrow J_c$	$c \sim u^{1/2} \quad (u \rightarrow 0)$ $c \sim u^{-0.85} \quad (u \rightarrow \infty)$	Sec. 3.6

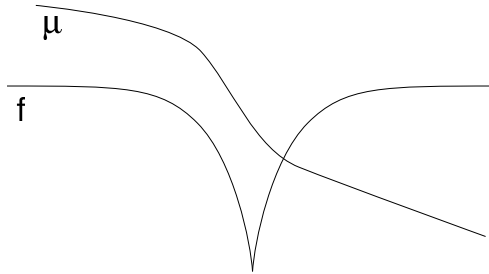


Figure 3.1: A phase-slip center is formed when a local perturbation of the current causes the order parameter to drop to zero. When the order parameter is small, the phase of the order parameter twists another 2π . The order parameter then heals slightly leaving a localized area with higher normal current and a supercurrent decreased to about 25 % of the total current.

Systems are quasi-one-dimensional because the coherence length is larger than the lateral dimensions of the superconducting material. Both whiskers of single crystal and etched film depositions can meet this criterion easily. The point is that the material is thin and skinny enough that variations in the order parameter and its phase are not significant across the width of the superconductor. A sample of YBCO from Jelila et al. [61] was $200 \mu\text{m}$ long, $20 \mu\text{m}$ wide, and $90 \mu\text{m}$ thick. This precludes the formation of vortices in the sample by self-induced magnetization from applied currents.

We have discussed already the metastability of the two uniform states, the normal and superconducting states. Measurements in steady state rarely show a transition from normal to superconducting or vice versa. Instead, the system passes into an intermediate state called the resistive state where the sample is mostly superconducting but there are occasional slips in the order parameter. These slips are oscillatory regions where the order parameter decreases and more of the current is carried by both an increase in the change of phase of the order parameter ($J_s \propto \psi^* \nabla \psi - \psi \nabla \psi^*$) and by a localized normal current. Figure 3.1 shows a single phase slip. At currents above J^* , the resistive state consists of a periodic array of these oscillatory regions, called phase slip centers, PSC. The PSC state allows the strip to remain superconducting above its critical current, J_c .

When the current rises above the critical current, a single PSC will enter. More PSC enter at successively higher applied currents. The result is a series of steps in the I-V curve called a “forked ascension,” shown in Fig. 3.2. Experiments on tin [98, 99] and YBCO [61] demonstrate similar voltage characteristics. Each

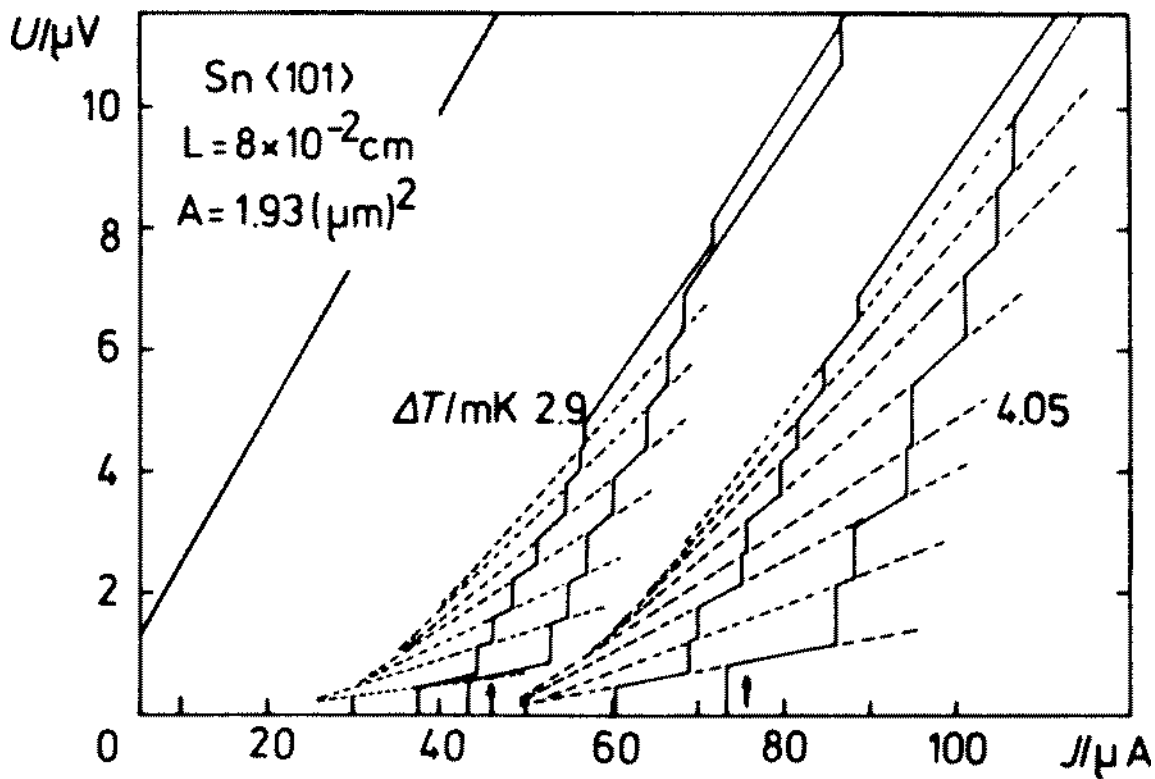


Figure 3.2: These are the dc current-voltage characteristics of a YBCO bridge from Jelila et al. [61]. The dotted lines show hysteresis for rising and falling currents. This I-V is typical of pure superconductors not too far from transition temperatures.

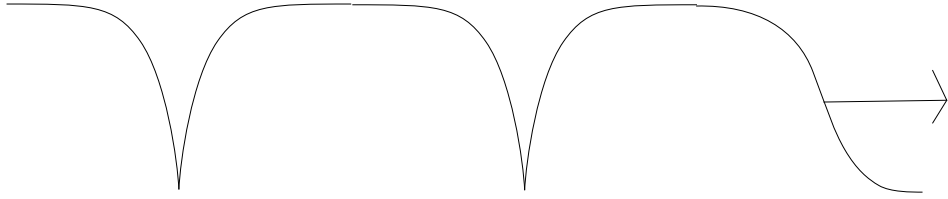


Figure 3.3: Even when the system switches from the normal to the resistive state, the process should occur by means of a moving phase front.

step represents the addition of a PSC. The first solid analysis of PSC by Skocpol, Beasley and Tinkham [98] attributed the stability of the centers to thermal effects. Because the middle of the phase slip is normal, it heats, possibly above the transition temperature. Averaging the additional resistance of each PSC, they used the normal state resistivity to find that the length scale of a PSC is the quasiparticle diffusion length. They mention, however, that in very clean systems near T_c , steps are still observed “due to some intrinsic inability of the uniform state to nucleate in the presence of the phase-slip process.” There is debate over when the normal or superconducting systems are unstable with respect to the formation of phase slip centers, but they appear to be intrinsic to the isothermal behavior of the order parameter and a necessary state in the adiabatic transition from normal to superconducting.

This does not mean, however, that a transition from normal directly to superconducting is not possible. There are two ways to see the transition directly. As is shown in in Pals and Wolter [83] and Jelila et al. [62], the order parameter can take up to 200 ns to respond to a 3 ns change in the applied current. It is possible to drop the current below the PSC nucleation current before the system can respond. Secondly, applied currents in a system near T_c can be so small a PSC cannot form. Each phase slip center has a kind of activation energy, the amount of excess current required to depress the order parameter enough that it reaches zero so a phase slip can occur. If the critical current is less than the amount of current required to form a PSC, then the transition will be direct from normal to superconducting.

Also, if a sample has superconducting contacts, it will be more likely to become superconducting at higher temperatures and higher applied currents [57]. While most experiments etch bridges into uniform substrates, some have applied normal contacts to thin strips [25]. These would be more amenable to measuring direct phase transitions.¹

The transition from normal to the PSC state is not so different from the transition from normal to superconducting. While, in decreasing currents, the PSC state forms much the same way the Abrikosov lattice forms in a type-ii superconductor, the system’s reaction to a sudden decrease in applied current would be nucleation. The supercurrent at the contacts nucleates a local phase change which spreads across the superconductor switching it from normal to the resistive state. The initial wavefront is probably just a switching wave and is exactly what we study here. The subsequent relaxation to the resistive state is not examined here, however. A simple picture is shown in Figure 3.3. In any case, there seems to be little experimental data on this region of the phase diagram.

Even if one can avoid forming PSC, heating of the normal metal masks some of the intrinsic superconducting properties of thin superconductors. Critical currents of cold superconductors can be large enough that resistive heating in normal regions can control the stability of stationary structures [98] and the velocity of NS boundaries [15]. Because we are interested in the coexistence of superconducting and dissipative normal regions, heat flux can be a significant factor in thermally isolated systems.

There is a large literature devoted to heat flux in current-driven superconductors. Hot spots can form stable autosolitons or drive phase transitions for the entire system. We are more interested in the behavior of isothermal systems because they describe fundamental behavior of superconductivity. The velocity of a normal-superconducting interface, for instance, will be limited by some combination of heat flux radiation,

¹Superconducting contacts measure only the pair chemical potential while normal contacts measure the full potential of the electric current [106]. If the edges are in steady state, however, the difference should be negligible.

diffusion of the order parameter, and relaxation times of superconducting pairs into quasiparticles. The experiments and analysis presented here will be related to systems shown to be highly isothermal so that the rate of heat flux will be of minimal importance.

There two ways commonly mentioned to combat heating effects. In the second of their set of articles on nonuniform states in thin strips in 1974 [99], Skocpol et al. point out that near T_c critical currents are small so that applied voltages will heat the sample less. More often, experimenters hope that a superconducting strip on a substrate with good thermal capacitance will dissipate heat efficiently.

More enlightening are time-resolved studies of voltage as an applied current pulse is modulated from above the critical current to currents below J^* and J_{\min} . One experiment which seems a clear attempt to measure phase changes at applied currents below the critical current is Jelila et al. [62]. The measurements are so appropriate they must be discussed despite inconclusive results. They applied a varying current pulse to a thin strip of $\text{YBa}_2\text{C}_3\text{O}_x$ in order first to drive it normal then to reduce the current and watch it return to the superconducting or PSC states. While their main focus was an initial time delay of the material in responding to applied currents, this delay was much better explained in a later PRL by the same group [61]. The earlier paper shows two graphs of voltage versus time with resolution in nanoseconds.

The film itself was grown on a MgO substrate which was verified to have very efficient heat conductivity [78]. The film was a 30 nm thick, 200 μm long, and 29 μm wide microbridge. The normal state resistance of the bridge seems to be around 5 Ω . Experiments were conducted at 4.2 K. We discussed earlier that temperatures close to T_c are better suited to isothermal measurements, but the signal to noise ratio was limited by shunt resistors.

The paper shows two experiments on slightly different samples. The first applies a supercritical 67 mA pulse which drops to 20 mA. Here, the voltage falls within the fall time of the pulse generator, 3 ns. If we try to explain the phase change as the progress of wave fronts, we can conclude the wave fronts traveled faster than 3.3×10^4 m/s.

The second experiment is shown in Figure 3.4. While the initial current of 70 mA drives the system normal we see a broad inductive rise in the voltage. Then the applied current is lowered to less than the critical current, and the system shows one of two behaviors. If the applied current is greater than 57 mA, the system relaxes into a PSC state with a voltage of 92 mV. If the applied current is less than 57 mA, the system returns to the superconducting state. The authors say only that “the resistance drops to zero in about 65 ns.” The shape of the curve is interesting. At early times, we expect the shape to be dominated by rapid phonon removal. Later times, however, show a curious shape of the curve which is not inductive.

It is unclear whether the system has had enough time to form the PSC state before undergoing a transition into the pure superconducting state. Suppose that the last downturn of the voltage, from 207 ns to 224 ns, is related to the movement of normal-superconducting phase fronts in the material. The shape of that part is roughly linear. The change of resistance with time of 0.0742 Ω/ns suggests phase front velocities of about 1600 m/s which is in the general range of the calculations in this chapter.

What exactly is occurring during the phase change is not at all clear. There doesn’t seem to be much data on phase changes at nonzero currents. Rather, most experiments examine the rate of phase transition at zero bias or currents greater than the critical current.

3.3 Models for Phase Transition in a Wire

3.3.1 The TDGL Equations

The starting point for our study is the set of TDGL equations for the order parameter ψ , the scalar potential Φ , and the vector potential \mathbf{A} :

$$\begin{aligned} \hbar\gamma \left(\partial_t + \frac{ie^*\Phi}{\hbar} \right) \psi &= \frac{\hbar^2}{2m} \left(\nabla - \frac{ie^*\mathbf{A}}{\hbar c} \right)^2 \psi \\ &+ |a|\psi - b|\psi|^2\psi, \end{aligned} \tag{3.1}$$

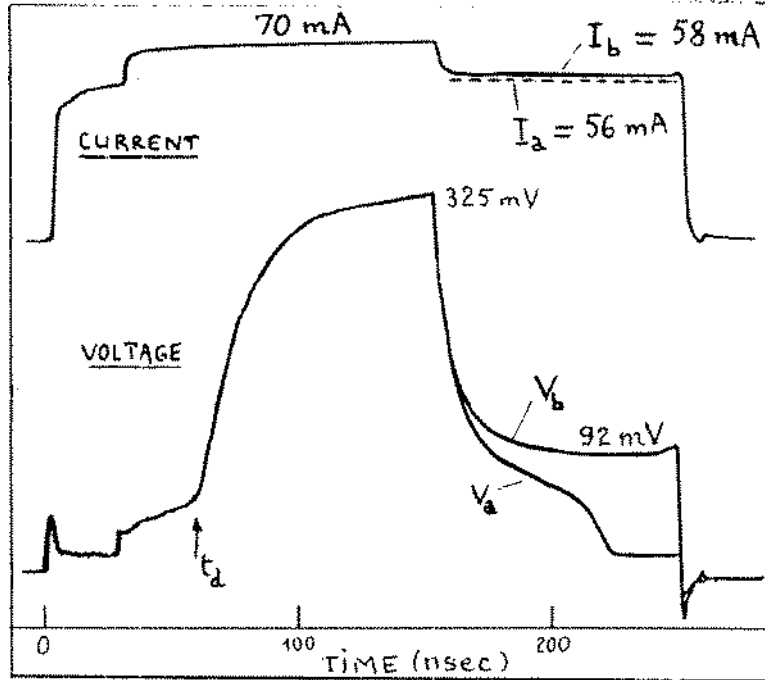


Figure 3.4: This shows the voltage response as a function of time for a YBCO microbridge from Jelila et al. [62]. The higher voltage drives the system normal. The system then returns either to the superconducting state, V_a , or the PSC state, V_b .

$$\nabla \times \nabla \times \mathbf{A} = \frac{4\pi}{c} (\mathbf{J}_n + \mathbf{J}_s), \quad (3.2)$$

where the normal current \mathbf{J}_n and the supercurrent \mathbf{J}_s are given by

$$\mathbf{J}_n = \sigma^{(n)} (-\partial_t \mathbf{A}/c - \nabla \Phi), \quad (3.3)$$

$$\mathbf{J}_s = \frac{\hbar e^*}{2mi} (\psi^* \nabla \psi - \psi \nabla \psi^*) - \frac{e^{*2}}{mc} |\psi|^2 \mathbf{A}, \quad (3.4)$$

and where γ (which is assumed to be real) is a dimensionless quantity characterizing the relaxation time of the order parameter, $\sigma^{(n)}$ is the normal conductivity, and $a = a_0(1 - T/T_{c0})$. From these parameters we can form two important length scales, the coherence length $\xi = \hbar/(2m|a|)^{1/2}$ and the penetration depth $\lambda = [mbc^2/4\pi(e^*)^2|a|]^{1/2}$.

These equations assume relaxational dynamics for the order parameter as well as a two-fluid description for the current. With somewhat restrictive assumptions, they can be derived from the microscopic BCS theory [96, 51]. Further simplification is possible in the limit of a thin, narrow film, that is, when the thickness is less than the coherence length, $d < \xi$, and the width is less than the effective penetration depth [89], $w \ll \lambda^2/d$. In this case the current carried by the film or wire is small, and we needn't worry about the fields it produces. Therefore, Eq. (3.2) may be dropped, and we need only specify the total current $\mathbf{J} = \mathbf{J}_n + \mathbf{J}_s$ (subject to $\nabla \cdot \mathbf{J} = 0$), along with the order-parameter dynamics, Eq. (3.1). This approximation is commonly used for superconducting wires [57] and can be justified mathematically for superconducting films [20]. In addition, we will be considering processes in the absence of an applied magnetic field, so that we may set $\mathbf{A} = \mathbf{0}$. With these simplifications, we can now rewrite the equations in terms of dimensionless

(primed) quantities,

$$\begin{aligned}\psi &= \sqrt{\frac{|a|}{b}}\psi', & \Phi &= \frac{\hbar e^*|a|}{mb\sigma^{(n)}}\mu', \\ x &= \xi x', & t &= \frac{mb\sigma^{(n)}}{e^{*2}|a|}t', \\ J &= \sqrt{\frac{2}{m}\frac{e^*|a|^{3/2}}{b}}J',\end{aligned}\tag{3.5}$$

which leads to

$$u(\partial_{t'} + i\mu')\psi' = (\nabla'^2 + 1 - |\psi'|^2)\psi',\tag{3.6}$$

$$\mathbf{J}' = \text{Im}(\psi'^*\nabla'\psi') - \nabla'\mu', \quad \nabla' \cdot \mathbf{J}' = 0.\tag{3.7}$$

Note that length is measured in units of coherence length². We will drop the primes hereafter. The only parameters remaining in the problem are the scaled current J and a dimensionless material parameter $u = \tau_\psi/\tau_J$, where $\tau_\psi = \hbar\gamma/|a|$ is the order-parameter relaxation time and $\tau_J = \sigma^{(n)}mb/e^{*2}|a|$ is the current relaxation time. We will treat u as a phenomenological parameter and study the nucleation and growth process as a function of u . The microscopic derivations of the TDGL equations predict that $u = 5.79$ (nonmagnetic impurities) [96], and $u = 12$ (paramagnetic impurities) [51], but small u is also useful for modeling gapped superconductors [60].

3.3.2 Generalized TDGL Equations

There have been fruitful generalizations of the TDGL applied to superconducting wires. The simplest recognized that the change in the magnitude of the order parameter is more closely related to the relaxation time of the superconducting pairs while the change in the phase of the order parameter is more closely related to relaxations of the quasiparticle excitations. These authors substituted two relaxation constants, u_ψ and u_ϕ .

More fruitful were several competing derivations of TDGL which account for superconductivity with a finite gap. The first was Kramer and Watts-Tobin [68], but alternative derivations and discussions are available in Ivlev and Kopnin [57] and Tidecks [101]. All derived from microscopic theory, each accounting for somewhat different pair-breaking mechanisms which lead to different contributions to a gap parameter, Γ . The general form of the equations is

$$-u\left(\frac{|\psi|^2}{\Gamma^2} + 1\right)^{-1/2}\left(\frac{\partial\psi}{\partial t} + i\phi\psi + 2\Gamma\frac{\partial|\psi|^2}{\partial t}\right) + \nabla^2\psi + \psi - |\psi|^2\psi = 0\tag{3.8}$$

$$\mathbf{j} = -\nabla\phi + \frac{1}{2i}(\psi^*\nabla\psi - \psi\nabla\psi^*).\tag{3.9}$$

When the gap parameter is zero, these equations reduce to the standard TDGL.

Having more parameters clearly promises greater specificity to particular metals, but the gap parameter explains significant shortcomings in the how the TDGL describe the PSC state. Whereas we show below that the basic TDGL do not allow a normal to superconducting transition above J^* , the equations with a gap do demonstrate such a transition. They also better explain the experimentally observed stability ranges of the resistive state.

The most creative and appropriate generalization of the TDGL for this system is in a paper by Eckern, Schmid, Schmutz, and Schön [33]. They derive a nonlinear Langevin equation similar to the TDGL which is appropriate to dissipative superconducting systems. More interesting is that they are able to develop a

²We warn the reader that this choice is different than in many applications of the TDGL equations, where the penetration depth is chosen as the length scale. In the thin film limit the penetration depth drops out of the calculation, leaving ξ as the length scale.

measure on this system that allows them to work with the Langevin equation much like one treats a typical conservative free energy. They then proceed to describe the basic system stability in terms of metastable and stable configurations and calculate threshold solutions from critical nuclei, much as is done here. It is a fascinating attempt to coax sensible physics out of a nonlinear dissipative system.

3.3.3 Heat Equations

As mentioned earlier, there is a large literature devoted to the analysis of normal-superconducting boundaries driven by heat flux. This analysis is entirely appropriate to a large class of thermally isolated systems. It seems most appropriate, for instance, to current flow through a wire. The analysis of these systems also leads to coupled nonlinear equations, usually parabolic diffusion equations. They also display traveling autosolitons as well as a wealth of other solitons common to reaction-diffusion equations.

The first work on thermal effects in domain boundaries was done by Skocpol, Beasley, and Tinkham [98, 99]. They did steady-state calculations for heat flow in thin bridges where they assumed the normal-superconducting boundary was sharp. They predicted stable solitons where the center of the bridge remained normal while the edges were superconducting.

Recently, Rudyi has both re-examined the stationary thermal solitons [95] and switching waves [94], which we study here for isothermal systems. When looking at thermal variations, one uses the temperature as an independent variable rather than the order parameter. Using the notation, $\Theta(\theta) = (T(\theta) - T_0)/T_c$, where $T(\theta)$ is the film temperature, $\theta = x - vt$ a self-similar variable, T_0 the coolant temperature, and T_c the critical temperature, Rudyi models the system as

$$\Theta_s''(\theta) + \frac{v}{a_s} \Theta_s'(\theta) - b_s \Theta_s(\theta) = 0 \quad (3.10)$$

$$\Theta_n''(\theta) + \frac{v}{a_n} \Theta_n'(\theta) - b_n \Theta_n(\theta) + W = 0. \quad (3.11)$$

The constants concern heat transfer and thermal conductivity. These equations predict a bistable, hysteretic system which collapses through critical nuclei which become phase fronts. While thermal propagation is a different mechanism from isothermal phase propagation, the behavior of the system is almost identical. Most thermal models are well understood as classic reaction-diffusion systems [55] and, as such, they can be analyzed with the standard autosoliton theory [103, 104]. As shown in Appendix B, the TDGL do not quite conform.

While thermal flux can constrain the velocity of a normal-superconducting interface or create nuclei in a filament, its effects can be minimized by good thermal coupling of the superconductor to a substrate. The order parameter relaxation and current relaxation are then the dominant factors in the stabilization of the normal-superconducting interface or the growth of nuclei.

3.4 Nucleation of the Superconducting Phase from the Normal Phase

In the presence of an applied current the normal phase in a wire is linearly stable with respect to superconducting perturbations for *any* value of the current [52, 70]. The reason for this stability is that any quiescent superconducting fluctuation will be accelerated by the electric field, its velocity eventually exceeding the critical depairing velocity, resulting in the decay of the fluctuation. The growth of the superconducting phase therefore requires a nucleus of sufficient size that will locally screen the electric field and allow the superconducting phase to continue growing; smaller nuclei will simply decay back to the normal phase. The amplitude of the “critical” nucleus should decrease as the current approaches zero, reaching zero only at $J = 0$. We expect the *critical* nuclei to be unstable, stationary (but nonequilibrium) solutions of the TDGL equations, which asymptotically approach the normal solution as $x \rightarrow \pm\infty$. These “bump” solutions of

the TDGL equations are the subject of this section. We include here an extensive numerical study of the amplitudes and widths of the critical nuclei, as well as some analytical estimates for these quantities.

3.4.1 Numerical Results

Let us start by discussing the numerical work on the critical nuclei. For the analytic work, we often find it convenient to use the amplitude and phase variables, i.e. $\psi = fe^{i\theta}$; but they are ill-suited for the numerical work, since the calculation of the phase becomes difficult when the amplitude is small. Following Likharev [74] we use instead $\psi = R + iI$, with R and I real, and in one dimension Eqs. (3.3.1) become

$$uR_t = R_{xx} + u\mu I + R - (R^2 + I^2)R, \quad (3.12)$$

$$uI_t = I_{xx} - u\mu R + I - (R^2 + I^2)I, \quad (3.13)$$

$$J = RI_x - IR_x - \mu_x. \quad (3.14)$$

Since the nuclei are unstable stationary states, they are investigated only by time-independent means. Such solutions require a particular gauge choice—in this case $\mu(x) = 0$ where $\psi(x)$ has its maximum amplitude; they are then sought using a relaxation algorithm [92]. Figure 3.5 shows a typical bump's amplitude, $f = \sqrt{R^2 + I^2}$, the associated superfluid velocity $q = (RI_x - IR_x)/f^2$ and the electric field $E(x) = -\mu_x(x)$. The figure shows only half of the solution; $f(x)$, $q(x)$ and $E(x)$ are even about $x = 0$. In Fig. 3.6 we plot the bump's maximum amplitude, ψ_0 , as a function of J ; it grows as the current rises, indicating the increasing stability of the normal phase. In the data presented by Watts-Tobin *et al.* [106] ψ_0 appears to vary linearly with J for small J . However, in our numerical calculations at very small currents the dependence deviates from linearity (see the inset of Fig. 3.6), and ψ_0 drops rapidly to zero as $J \rightarrow 0$, consistent with the exponential behavior suggested in Refs. [57, 59]. More precisely our small- J data ($0.008 \leq J \leq 0.015$) at $u = 5.79$ is fit by

$$\psi_0(J) = B \exp(-A/uJ), \quad (3.15)$$

with $A = 0.042$ and $B = 0.19$. A somewhat similar dependence (with $A = 2/3$) was suggested by Ivlev *et al.* [57, 59]; they were considering a distinct quantity but one also related to critical fluctuations about the normal phase (see the Appendix for more details).

The width of the bump diverges in the small- J limit like $(uJ)^{-1/2}$, as can be seen from the analysis below. So as J is increased from zero, the width initially shrinks, but eventually the width begins to grow again, diverging as the current approaches the stall current J^* . In this limit the bump transforms into two well separated interfaces (see Fig. 3.7).

3.4.2 Analysis in the $J \rightarrow 0$ Limit

The equations for nuclei centered at the origin are

$$\psi_{xx} - iu\mu\psi + \psi - |\psi|^2\psi = 0, \quad (3.16)$$

$$\mu = -Jx + \int_0^x \text{Im}(\psi^*\psi_{x'}) dx', \quad (3.17)$$

where we have dropped the term ψ_t and selected the gauge $\mu(0) = 0$. We saw in Fig. 3.6 that ψ_0 becomes very tiny in the small- J limit, thus the nonlinear terms can be neglected, leading to

$$\psi_{xx} + iuJx\psi + \psi = 0, \quad (3.18)$$

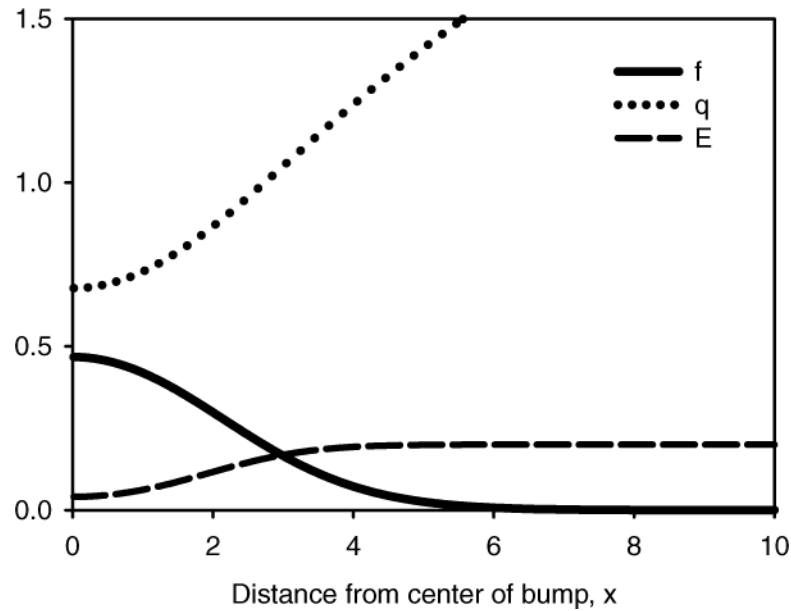


Figure 3.5: The bump's amplitude, $f(x)$, its superfluid velocity, $q(x)$, and the electric field, $E(x)$, for $u = 5.79$ and $J = 0.2$.

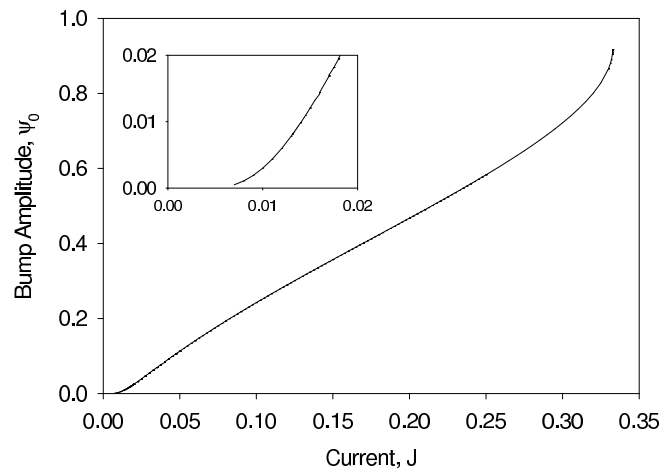


Figure 3.6: The maximum amplitude of the bumps ψ_0 as a function of J for $u = 5.79$. The inset shows the exponential dependence of the small- J data, see Eq. (3.15).

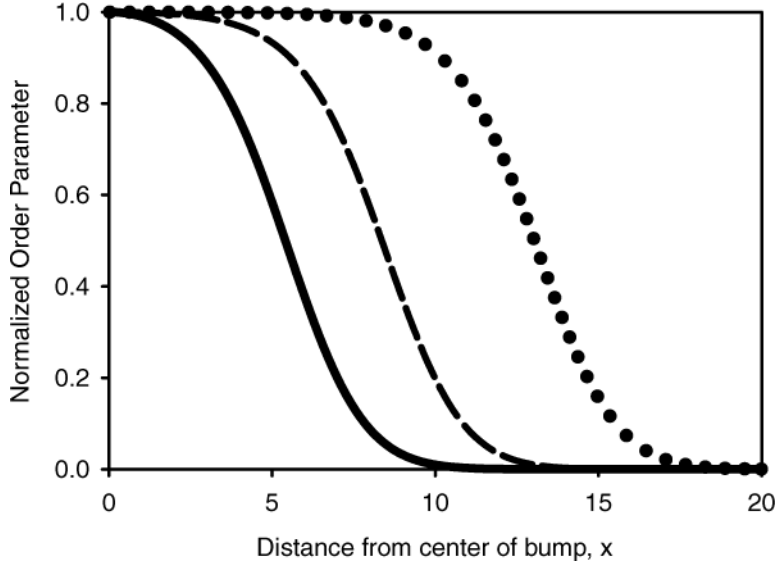


Figure 3.7: The bump profiles for $J^* - J = 10^{-3}$ (solid), $J^* - J = 10^{-5}$ (dashed) and $J^* - J = 10^{-7}$ (dotted) at $u = 5.79$.

a complex version of the Airy equation. Applying the WKB method results in the approximate solution

$$\begin{aligned} \psi \sim & [1 + (uJx)^2]^{-1/8} \\ & \times \exp \left\{ \frac{2}{3uJ} \left[[1 + (uJx)^2]^{3/4} \cos \frac{3\alpha}{2} - 1 \right] \right\} \\ & \times \exp \left\{ i \left[\frac{2}{3uJ} [1 + (uJx)^2]^{3/4} \sin \frac{3\alpha}{2} - \frac{\alpha}{4} \right] \right\}, \end{aligned} \quad (3.19)$$

where $\alpha = \tan^{-1}(uJx)$. The numerical data agrees quite well with this predicted shape in the small- J limit. For small x the expression can be approximated by

$$\psi \sim \exp [i(1 - uJ/4)x - uJx^2/4]. \quad (3.20)$$

We see here that the width of the bump varies like $(uJ)^{-1/2}$ in this limit and that the superfluid velocity $q \approx (1 - uJ/4)$. For large x , on the other hand, where $\alpha \approx \pi/2$, the expression becomes

$$\psi \sim (uJx)^{-1/4} \exp \left[-\frac{\sqrt{2uJ}}{3} |x|^{3/2} (1 - i) \right], \quad (3.21)$$

as one expects for the Airy function. Note that deep in the tail of the solution, we see a different length scale $\lambda_{\text{Airy}} \sim (uJ)^{-1/3}$ arising.

Since the above analysis is of a linear equation, it can not determine the amplitude of the nucleus; for this purpose the nonlinearities must be considered. In the appendix we outline an *ad hoc* calculation of the small- J limit of the bump amplitude. We take a ψ of an unknown amplitude but of a fixed shape inspired by the above analysis and assume that it is a stationary solution of the full TDGL. We then determine its

amplitude self-consistently. The resulting amplitude is

$$|\psi| \approx \left(\frac{2J}{\pi u} \right)^{1/4} \left(\frac{9}{8} - \frac{1}{u} \right)^{-1/2} \exp \left(-\frac{16}{81 u J} \right). \quad (3.22)$$

The factor $A = 16/81$ is within a few percent of that extracted from the numerical data.

3.5 Stationary Interfaces

As the current is raised, the width of the critical nucleus grows and ultimately diverges as the stall current is reached, resulting in well separated, stationary interfaces. These interface solutions will be the subject of the rest of this work.

3.5.1 Numerical Methods and Results

Let us first discuss the numerical work on the interface solutions. For given values of u and J we evolved the TDGL equations from an initial guess which is purely superconducting on the left, $\psi(x) = f_\infty e^{iq_\infty x}$ and $\mu_x(x) = 0$, and purely normal on the right, $\psi(x) = 0$ and $\mu_x(x) = -J$. The values f_∞ and q_∞ are related to the applied current through

$$J = f_\infty^2 \sqrt{1 - f_\infty^2}, \quad (3.23)$$

$$q_\infty = \sqrt{1 - f_\infty^2}. \quad (3.24)$$

Stability requires taking the larger positive root of the former equation [73] which places the following bounds on J , f_∞ and q_∞ :

$$0 \leq J \leq J_c = \sqrt{4/27} \approx 0.3849, \quad (3.25)$$

$$1 \geq f_\infty \geq \sqrt{2/3} \approx 0.8165, \quad (3.26)$$

$$0 \leq q_\infty \leq \sqrt{1/3} \approx 0.5774. \quad (3.27)$$

We employed several schemes to integrate the equations in time including both explicit (Euler) and implicit (Crank-Nicholson) [92].

Initially the front moves and changes shape but eventually it reaches a steady state in which the interface moves at a constant velocity without further deformation. By the time-dependent means we found locally stable, constant-velocity solutions for currents less than J_c . To examine these solutions more accurately, we adopted a time-independent method. First, we transformed coordinates to a moving frame, $x' = x - ct$; next, we chose $\mu = cq_\infty$ as $x \rightarrow -\infty$ which allows for a truly time-independent solution (i.e. one with both amplitude and phase time-independent). Then we searched for stationary solutions using a relaxation algorithm [92] where (u, J) are input parameters and c is treated as an eigenvalue. This approach requires an additional boundary condition to fix translational invariance; we elected to fix μ on the rightmost site. To find the stall currents J^* we can set $c = 0$ and take J or u as the eigenvalue.

Figures 3.8 and 3.9 show the order-parameter amplitude f and the electric-field distribution $E = -\mu_x$ of the stalled interface determined for $u = 500$ and $u = 1.04$ respectively. Note that while f is very flat in the superconducting region, the real and imaginary parts, R and I , oscillate with a wavelength $2\pi/q_\infty$. Because of this additional length scale inherent in R and I , there is little to be gained from varying the mesh size. In fact, this length scale is compressed as we move to the right, and we are only saved from the difficulties of handling rapidly oscillating functions by the fact that the amplitudes decay so quickly.

In the large- u case (see Fig. 3.8), $E(x)$ remains flat throughout most of the space; it changes abruptly from one constant to another only after $f(x)$ has become small. The variations of $f(x)$ are more gradual; however, the greatest changes in f_x occur in that same small area. This region of rapid change is known as a *boundary*

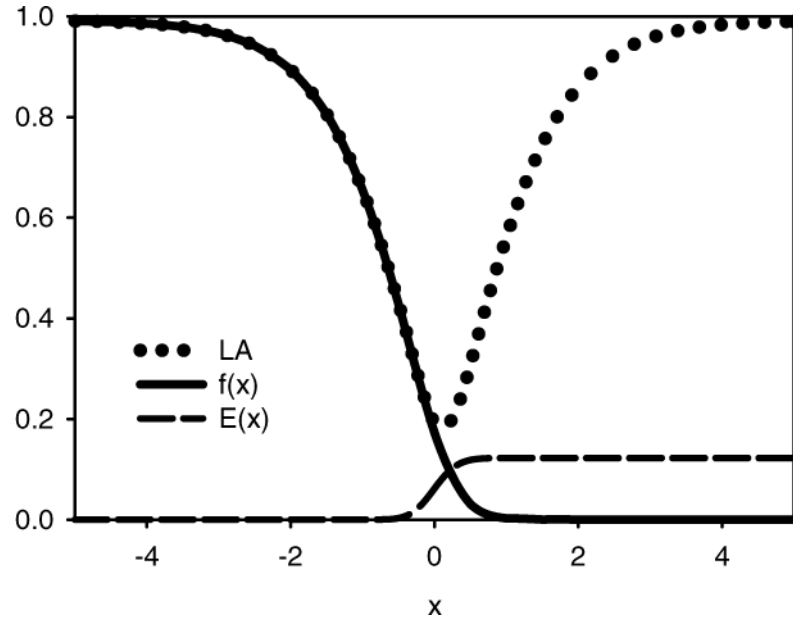


Figure 3.8: The stationary NS interface solution when $u = 500$ for which the stall current $J^* = 0.12252$. Shown here are the numerically determined $f(x)$ and $E(x)$, as well as the Langer-Ambegaokar (LA) solution (Eq. (3.43)), the solution with no electric field corresponding to the same current.

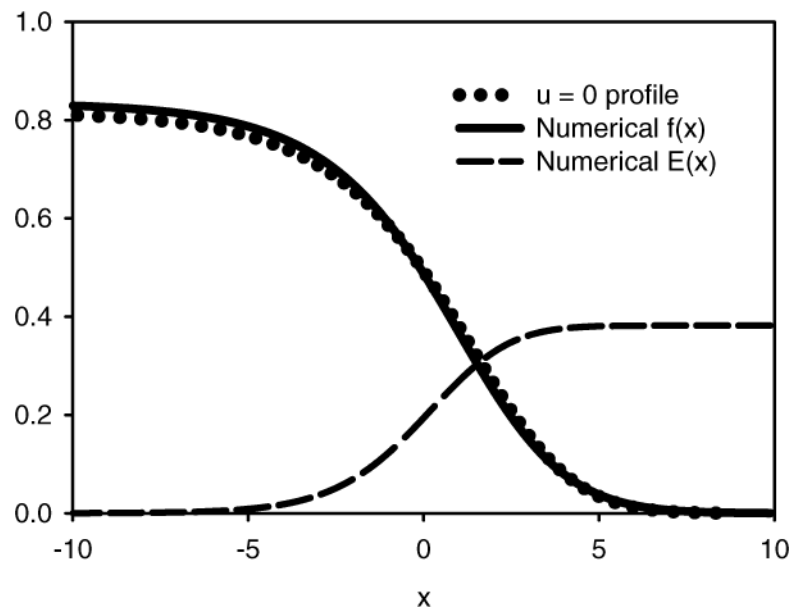


Figure 3.9: The stationary NS interface solution when $u = 1.04$ for which the stall current $J^* = 0.3836$. Shown here are the numerically determined $f(x)$ and $E(x)$, as well as the function $f_0(\hat{x})$, the $u \rightarrow 0$ profile, derived from Eq. (3.70) where $\hat{x} = u^{1/2}x$.

layer; it marks where the current suddenly changes from superconducting to normal, i.e., the position of the NS interface. As u increases, the longer length scale over which f varies on the superconducting side remains essentially fixed, while the boundary-layer thickness shrinks to zero. In the opposite limit, the small- u case (see Fig. 3.9), $f(x)$ and $E(x)$ appear to vary together even in the superconducting region; moreover, the length scale over which they vary grows as u is decreased. We will postpone providing more of the numerical results on the interfaces until some of the analytic arguments are available for comparison.

3.5.2 Asymptotic Analysis of the Interface Solutions: preliminaries

Before addressing the large- u and small- u limits separately, let us put the TDGL equations into a form convenient for analysis and derive expressions for the length scales deep in the superconducting and normal regions. The disparity of these length scales in the large- u limit will motivate the boundary-layer analysis in that regime; while an inequality they satisfy will lead to the conclusion that $J^* \rightarrow J_c$ in the small- u limit.

We make the substitution $\psi = fe^{i\theta}$, which yields

$$uf_t = f_{xx} - f(\theta_x)^2 + f - f^3, \quad (3.28)$$

$$u(\theta_t + \mu)f = 2f_x\theta_x + f\theta_{xx}, \quad (3.29)$$

$$J = f^2\theta_x - \mu_x. \quad (3.30)$$

Next we restrict our attention to stationary solutions. Note that only spatial derivatives of θ appear now, allowing us to work with the superfluid velocity $q = \theta_x$ instead of θ . The equations become

$$f_{xx} - q^2f + f - f^3 = 0, \quad (3.31)$$

$$u\mu f = 2f_xq + fq_x, \quad (3.32)$$

$$J^* = f^2q - \mu_x, \quad (3.33)$$

where J^* replaces J as these equations apply to the stall situation. Next multiply Eq. (3.32) by f and note that the right hand side is now $(f^2q)_x$ which we can express in terms of μ by differentiating Eq. (3.33); these steps lead to

$$\mu_{xx} = uf^2\mu. \quad (3.34)$$

Now let us assume the following asymptotic forms as $x \rightarrow -\infty$:

$$\lim_{x \rightarrow -\infty} f(x) = f_\infty - f_1 e^{x/\lambda_f} + \dots, \quad (3.35)$$

$$\lim_{x \rightarrow -\infty} q(x) = q_\infty + q_1 e^{x/\lambda_q} + \dots, \quad (3.36)$$

$$\lim_{x \rightarrow -\infty} \mu(x) = \mu_\infty - \mu_1 e^{x/\lambda_\mu} + \dots. \quad (3.37)$$

Substituting these expressions into Eqs. (3.31), (3.33) and (3.34) and recalling the boundary conditions yields (is label “approach” correct?)

$$\left(2f_\infty^2 - \lambda_f^{-2}\right) f_1 e^{x/\lambda_f} - 2f_\infty q_\infty q_1 e^{x/\lambda_q} = 0, \quad (3.38)$$

$$-2f_\infty q_\infty f_1 e^{x/\lambda_f} + f_\infty^2 q_1 e^{x/\lambda_q} + \lambda_\mu^{-1} \mu_1 e^{x/\lambda_\mu} = 0, \quad (3.39)$$

$$\lambda_\mu^{-2} - uf_\infty^2 = 0. \quad (3.40)$$

Eq. (3.40) provides an expression for λ_μ , the electric-field screening length. Since f_∞ is always of $O(1)$, we see that λ_μ shrinks as $u \rightarrow \infty$ and diverges as $u \rightarrow 0$, which is consistent with the behavior seen in Figs. 3.8 and 3.9.

More than one decay length appears in Eqs. (3.38) and (3.39). If they are not equal, the term with the

shorter length is exponentially small compared to the other(s) and will not contribute to the $x \rightarrow -\infty$ limit. Since none of the terms in Eq. (3.39) can equal zero individually, we conclude that the longer two of λ_f , λ_q and λ_μ must be equal. Next, because the term multiplying e^{x/λ_q} in Eq. (3.38) cannot equal zero on its own, we determine that $\lambda_q \leq \lambda_f$, making λ_f one of the longer lengths. Finally, if we assume that $\lambda_f = \lambda_\mu > \lambda_q$ we find that $\lambda_f = 2^{-1/2} f_\infty^{-1}$ and $\lambda_\mu = u^{-1/2} f_\infty^{-1}$ and reach a contradiction (except at $u = 2$). Thus provided the original assumption of an exponential approach is valid, we conclude that

$$\lambda_f = \lambda_q \geq \lambda_\mu. \quad (3.41)$$

This equality of λ_f and λ_q is reasonable given that both f and q are related to the complex order parameter ψ . Also, having $\lambda_f > \lambda_\mu$ is consistent with the large- u data seen in Fig. 3.8. If $\lambda_\mu \neq \lambda_f$ then

$$\lambda_f^{-2} = 6f_\infty^2 - 4 = \lambda_{LA}^{-2}. \quad (3.42)$$

We identify this length scale as λ_{LA} since it coincides with that occurring in the solution of Eqs. (3.5.2) without any electric field ($\mu(x) = 0$),

$$f^2(x) = f_\infty^2 - (3f_\infty^2 - 2) \operatorname{sech}^2 \left(\sqrt{\frac{3f_\infty^2 - 2}{2}} x \right), \quad (3.43)$$

which was found by Langer and Ambegaokar [73] in their study of phase slippage. The asymptotic form of Eq. (3.43) looks like Eq. (3.35) with λ_f given by Eq. (3.42). As a matter of fact because $\lambda_f \gg \lambda_\mu$ in the large- u limit, the profile of $f(x)$ is only imperceptibly different from the Langer-Ambegaokar (LA) solution in the superconducting region and deviates from it only in the boundary layer, as is shown in Fig. 3.8.

Recall that λ_μ diverges as $u \rightarrow 0$; the inequality $\lambda_f \geq \lambda_\mu$ implies that λ_f must diverge as fast or faster in this limit. This scenario is consistent with the small- u data shown in Fig. 3.9 in which $f(x)$ and $E(x)$ vary on long length scales. Eq. (3.42) suggests that a diverging λ_f implies that $f_\infty \rightarrow \sqrt{2/3}$ and in turn that $J \rightarrow J_c$ as $u \rightarrow 0$, which is also consistent with what is found numerically.

In the other asymptotic limit, deep in the normal regime, ψ is very small and hence the nonlinear terms in Eqs. (3.3.1) can be dropped as was done for the bumps in the small- J limit. The result is a complex Airy equation, the asymptotic analysis of which was supplied in Eq. (3.21), where we saw the length scale $\lambda_{Airy} \sim (uJ^*)^{-1/3}$. Somewhat like λ_μ , λ_{Airy} shrinks as $u \rightarrow \infty$ and expands as $u \rightarrow 0$ but with different powers of u . The presence of the disparate length scales, λ_f , λ_μ and λ_{Airy} , in the large- u limit motivates the use of the boundary-layer analysis that comes next. We will see that λ_{Airy} scales in the same way as the boundary-layer thickness.

3.5.3 Asymptotic Behavior of the Stall Current as $u \rightarrow \infty$

We have already seen in Fig. 3.8 that the large- u profile can be divided into two regions—one slowly varying, one rapidly varying, also known as the *outer* and *inner* regions, respectively. Furthermore, it has been suggested that the ratio of the length scales characterizing these regions decreases as $u \rightarrow \infty$. These features make the problem ideally suited for boundary-layer analysis, in which one identifies the terms that dominate the differential equation in each region, analyzes the reduced equations consisting of dominant terms and then matches the behavior in some intermediate region.

We start by eliminating the superfluid velocity q from Eqs. (3.5.2), resulting in

$$f_{xx} - (J^* + \mu_x)^2 f^{-3} + f - f^3 = 0, \quad (3.44)$$

$$\mu_{xx} - u f^2 \mu = 0. \quad (3.45)$$

Let us consider first the slowly varying, superconducting region. We saw in the preliminary analysis that for large u , $\mu(x)$ is exponentially small, so we drop it. Next, let us assume that J^* is small and drop it; we can

verify in the end that this is self-consistent. The reduced equation is

$$f_{xx} + f - f^3 \approx 0, \quad (3.46)$$

with solution $f(x) = -\tanh(x/\sqrt{2})$.

Moving in from the left toward the interface (into the boundary-layer region), f becomes small, and the second term in Eq. (3.44) which was subdominant becomes dominant. In this inner region f is small but rapidly varying, thus the dominant terms are

$$f_{xx} \approx \frac{(J^* + \mu_x)^2}{f^3}, \quad (3.47)$$

along with Eq. (3.45). Having identified the dominant terms, now we must make certain they balance. We assume that in the boundary layer, all the quantities scale as powers of u :

$$f \sim u^{-\alpha}, \quad \mu \sim u^{-\beta}, \quad J^* \sim u^{-\gamma}, \quad x \sim u^{-\delta}. \quad (3.48)$$

Balancing terms in Eq. (3.47), we find $2\alpha = \gamma + \delta$, while balancing terms in Eq. (3.45) yields $2(\alpha + \delta) = 1$. Next, we need to ensure that the solutions in the boundary layer match onto the solutions in the superconducting and normal regions. By expanding the superconducting solution near the interface, we see that $f(x) \sim -x/\sqrt{2}$ as the boundary layer is approached; matching to the boundary layer requires $f_x \sim 1$, so that $\alpha = \gamma$. In the normal region, $\mu \approx -J^*x$, so that matching to the boundary layer requires $\mu_x \sim J^*$, and $\beta = \gamma + \delta$. Solving this set of equations, we conclude that $\alpha = \gamma = \delta = 1/4$ and $\beta = 1/2$, i.e., the stall current $J^* \sim u^{-1/4}$ for large u . Note that $J^* \rightarrow 0$ as $u \rightarrow \infty$, so that we were justified in dropping J^{*2}/f^3 from Eq. (3.46). Substituting $J^* \sim u^{-1/4}$ into λ_{Airy} gives $\lambda_{\text{Airy}} \sim u^{-1/4}$, indicating that it may be identified as the boundary-layer thickness.

In order to determine the coefficient of the $u^{-1/4}$ in the stall current we need to solve the boundary layer problem. Let us rescale in the way suggested above:

$$\begin{aligned} f &= u^{-1/4}F, & \mu &= u^{-1/2}M(X), \\ J &= u^{-1/4}\tilde{J}, & x &= u^{-1/4}X. \end{aligned} \quad (3.49)$$

Substituting these rescaled variables into Eqs. (3.44) and (3.45), and then expanding F , M and \tilde{J} in powers of $u^{-1/2}$, we obtain at the lowest order

$$F_{0,XX} - \frac{(\tilde{J}_0 + M_{0,X})^2}{F_0^3} = 0, \quad (3.50)$$

$$M_{0,XX} - F_0^2 M_0 = 0, \quad (3.51)$$

with the boundary conditions (from the outer regions)

$$F_{0,X}(-\infty) = -1/\sqrt{2}, \quad M_0(-\infty) = 0, \quad (3.52)$$

$$F_0(+\infty) = 0, \quad M_{0,X}(+\infty) = -\tilde{J}_0. \quad (3.53)$$

(As before we need an extra boundary condition to fix the translational invariance.) For an arbitrary \tilde{J}_0 the solutions of Eqs. (3.50) and (3.51) cannot satisfy the boundary conditions; \tilde{J}_0 must be tuned to a particular value before all of the boundary conditions are satisfied, leading to a *nonlinear eigenvalue problem* for \tilde{J}_0 . We have solved this eigenvalue problem numerically and find that $\tilde{J}_0 = 0.584491$. Therefore, to leading order we have for the stall current

$$J^* \approx 0.584491 u^{-1/4}. \quad (3.54)$$

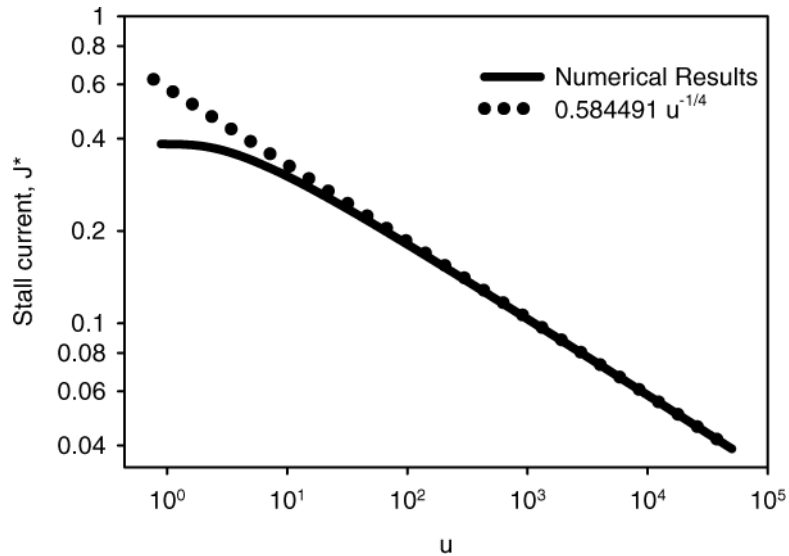


Figure 3.10: A log-log plot of the stall current J^* vs. u . The solid line shows the numerically determined J^* 's as a function of u and the dotted line is $0.584491 u^{-1/4}$ (the large- u behavior predicted by matched asymptotic analysis).

u	J^*	$J^* u^{1/4}$	η	$\eta u^{-3/4}$
1	0.3838	0.3838	0.01871	0.01871
5	0.3407	0.5094	0.6400	0.1914
10	0.3013	0.5359	1.573	0.2797
50	0.2127	0.5655	8.258	0.4315
100	0.1807	0.5715	15.59	0.4931
500	0.1224	0.5788	62.51	0.5875
1000	0.1033	0.5807	111.3	0.6259
5000	0.0693	0.5828	407.9	0.6847
10000	0.0583	0.5833	708.4	0.7084
50000	0.0391	0.5840	2487	0.7440

Table 3.3: Representative numerical results for the stall current J^* and kinetic coefficient η .

This prediction agrees well with the numerical results and disagrees with Likharev's conjecture of a $u^{-1/3}$ dependence [74], as can be seen in Fig. 3.10 and in Table 3.3. It is in principle possible to carry out this procedure to successively higher orders, but the equations become cumbersome. Instead we have simply opted to fit our numerical data to a form inspired by the asymptotic analysis,

$$\begin{aligned} J^* = & 0.584491 u^{-1/4} - 0.117461 u^{-3/4} - 0.12498 u^{-5/4} \\ & + 0.163043 u^{-7/4} + O(u^{-9/4}). \end{aligned} \quad (3.55)$$

Even with the higher order terms, the asymptotics are appropriate only for physically large values of u .

3.5.4 Asymptotic Behavior of the Stall Current as $u \rightarrow 0$

Now let us examine the opposite limit of $u \rightarrow 0$. In this case the electric-field screening length becomes long, and Ivlev *et al.* [60] have proposed that this makes the small- u limit useful for modeling gapped superconductors. As already suggested the inequality of length scales, $\lambda_f \geq \lambda_\mu$ implies that $J^* \rightarrow J_c$. We will begin our small- u analysis by putting this result on firmer ground and extracting as a byproduct the $u \rightarrow 0$ limit of the interface profile.

The rescaled equations. Recall that deep in the superconducting region $\lambda_\mu \sim u^{-1/2}$. This observation suggests that we rescale distance: $x = u^{-1/2}\hat{x}$; furthermore, to ensure that the normal current ($-\mu_x$) scales in the same way as the total current we rescale $\mu = u^{-1/2}\hat{\mu}$ as well. These rescalings yield

$$u\hat{f}_{\hat{x}\hat{x}} - \hat{q}^2\hat{f} + \hat{f} - \hat{f}^3 = 0, \quad (3.56)$$

$$\hat{\mu}\hat{f} = 2\hat{q}\hat{f}_{\hat{x}} + \hat{f}\hat{q}_{\hat{x}}, \quad (3.57)$$

$$J^* = \hat{f}^2\hat{q} - \hat{\mu}_{\hat{x}}, \quad (3.58)$$

placing the small parameter u in front of $\hat{f}_{\hat{x}\hat{x}}$. If we expand these functions as series in powers of u

$$\hat{f} = \hat{f}_0 + u\hat{f}_1 + \dots, \quad (3.59)$$

$$\hat{q} = \hat{q}_0 + u\hat{q}_1 + \dots, \quad (3.60)$$

$$\hat{\mu} = \hat{\mu}_0 + u\hat{\mu}_1 + \dots, \quad (3.61)$$

$$J^* = J_0^* + uJ_1^* + \dots, \quad (3.62)$$

then we find at the lowest order

$$-\hat{q}_0^2\hat{f}_0 + \hat{f}_0 - \hat{f}_0^3 = 0, \quad (3.63)$$

$$\hat{\mu}_0\hat{f}_0 = 2\hat{q}_0\hat{f}_{0,x} + \hat{f}_0\hat{q}_{0,x}, \quad (3.64)$$

$$J_0^* = \hat{f}_0^2\hat{q}_0 - \hat{\mu}_{0,\hat{x}}. \quad (3.65)$$

The solution of Eq. (3.63) is either $\hat{f}_0 = 0$ (the normal phase) or $\hat{f}_0 = (1 - \hat{q}_0^2)^{1/2}$ (the superconducting phase). Let us focus on the superconducting solutions. By eliminating \hat{q}_0 , we obtain the first order equations

$$\hat{f}_{0,\hat{x}} = \frac{\hat{f}_0\sqrt{1 - \hat{f}_0^2}\hat{\mu}_0}{2 - 3\hat{f}_0^2}, \quad (3.66)$$

$$\hat{\mu}_{0,\hat{x}} = \hat{f}_0^2\sqrt{1 - \hat{f}_0^2} - J_0^*. \quad (3.67)$$

Because \hat{f}_0 ranges from f_∞ to 0 and $f_\infty \geq \sqrt{2/3}$, we know that \hat{f}_0 either starts at or passes through $\sqrt{2/3}$. (Strictly speaking we should be writing here $f_{\infty,0}$, the lowest order term in the expansion of f_∞ .) Thus, the effect of the pole in Eq. (3.66) must be considered. If it is not canceled by a zero in $\hat{\mu}_0$, $\hat{f}_{0,\hat{x}}$ diverges at

$$\hat{f}_0 = \sqrt{2/3}.$$

We can obtain an expression for $\hat{\mu}_0(\hat{f}_0)$ by dividing Eq. (3.67) by Eq. (3.66), which leads to

$$\hat{\mu}_0 d\hat{\mu}_0 = \frac{\left[\hat{f}_0^2 \sqrt{1 - \hat{f}_0^2} - J_0^* \right] (2 - 3\hat{f}_0^2)}{\hat{f}_0 \sqrt{1 - \hat{f}_0^2}} d\hat{f}_0. \quad (3.68)$$

Integrating both sides and recalling the boundary condition $\mu_\infty = 0$, we find

$$\begin{aligned} \frac{\hat{\mu}_0^2}{2} &= \hat{f}_0^2 - \frac{3}{4} \hat{f}_0^4 - f_\infty^2 + \frac{3}{4} f_\infty^4 \\ &\quad + 2 J_0^* \ln \left[\frac{1 + \sqrt{1 - \hat{f}_0^2}}{\hat{f}_0} \right] - 3 J_0^* \sqrt{1 - \hat{f}_0^2} \\ &\quad - 2 J_0^* \ln \left[\frac{1 + \sqrt{1 - f_\infty^2}}{f_\infty} \right] + 3 J_0^* \sqrt{1 - f_\infty^2}, \end{aligned} \quad (3.69)$$

where $J_0^* = f_\infty^2 \sqrt{1 - f_\infty^2}$. To keep $\hat{f}_{0,x}$ from diverging, we insist that $\hat{\mu}_0(\hat{f}_0 = \sqrt{2/3}) = 0$ which can be shown from Eq. (3.69) to imply $f_\infty = \sqrt{2/3}$, i.e. the small- u limit of the stall current is the critical depairing current. Note that the pole in Eq. (3.66) and the compensating zero in $\hat{\mu}_0(\hat{f}_0)$ occur at the boundary ($x \rightarrow -\infty$).

We can rearrange Eq. (3.66) as follows

$$\int_{\hat{f}_0(0)}^{\hat{f}_0(\hat{x})} \frac{(2 - 3f^2) df}{f \sqrt{1 - f^2} \hat{\mu}_0(f)} = \hat{x}. \quad (3.70)$$

Then we can substitute in Eq. (3.69) for $\hat{\mu}_0(f)$, numerically integrate the resulting expression and finally invert it in order to calculate $\hat{f}_0(\hat{x})$, the $u \rightarrow 0$ profile. Figure 3.9 includes a comparison of $\hat{f}_0(\hat{x})$ and the profile of a small- u numerical solution.

To find the asymptotic behavior of \hat{f}_0 and $\hat{\mu}_0$ in the superconducting region, Taylor expand $\hat{\mu}_0(\hat{f}_0)$ around f_∞

$$\hat{\mu}_0(\hat{f}_0) = -3\sqrt{2} \left(\hat{f}_0 - \sqrt{2/3} \right)^2 + \dots \quad (3.71)$$

Notice that $\hat{\mu}_0(\hat{f}_0)$ is a second order zero, so that $\hat{f}_{0,\hat{x}} = 0$, as it should at the boundary. As a consequence, the integral supplying the inverse profile, Eq. (3.70), has a pole; integrating the expression in its neighborhood yields $\sqrt{6} \ln(\sqrt{2/3} - \hat{f}_0)$, leading to

$$\hat{f}_0(\hat{x}) \sim \sqrt{2/3} - A_0 \exp\left(\hat{x}/\sqrt{6}\right), \quad (3.72)$$

where A_0 is an integration constant undetermined because of the translational invariance. Note $\hat{f}_0(\hat{x})$ has the form assumed in the preliminary analysis with $\lambda_{f,0} = \sqrt{u/6}$. Putting this result into Eq. (3.66) leads to

$$\hat{\mu}_0(\hat{x}) \sim -3\sqrt{2} A_0^2 \exp\left(2\hat{x}/\sqrt{6}\right), \quad (3.73)$$

where $\lambda_{\mu,0} = u^{1/2} f_\infty$ in agreement with the expression found previously.

Let us examine Eqs. (3.66) and (3.67), which are strictly speaking superconducting solutions, in the normal (small- \hat{f}_0) limit. Eq. (3.67) leads to $\hat{\mu}_0(\hat{x}) \approx -J_c \hat{x}$, and inserting this into Eq. (3.66) reveals that

$\hat{f}_0 \rightarrow 0$ in the following way

$$\hat{f}_0(\hat{x}) \sim \exp(-J_c \hat{x}^2/4). \quad (3.74)$$

This same dependence was seen earlier in the analysis of the bump shapes in the small- J limit, Eq. (3.20).

What is surprising here is that what are ostensibly the “outer” equations for the superconducting region also satisfy the boundary conditions in the normal region and interpolate in between. This is consistent with the numerical observation that there does not seem to be a boundary layer at small u , that the uf_{xx} term is apparently *not* a singular perturbation. With this in mind, we pursue the perturbative expansion to higher orders.

The $O(u)$ equations. The eigenvalue J_0^* was determined by examining the behavior deep in the superconducting region and did not require imposing the boundary conditions on the normal side. Furthermore, the spatial dependence of the solution in this region is of the form assumed in Eqs. (3.5.2). We exploit these features to obtain higher order terms. The $O(u)$ equations are

$$\hat{f}_{0,\hat{x}\hat{x}} - 2\hat{q}_0\hat{f}_0\hat{q}_1 - \hat{q}_0^2\hat{f}_1 - 3\hat{f}_0^2\hat{f}_1 = 0, \quad (3.75)$$

$$\hat{\mu}_0\hat{f}_1 + \hat{f}_0\hat{\mu}_1 = 2\hat{q}_0\hat{f}_{1,\hat{x}} + 2\hat{f}_{0,\hat{x}}\hat{q}_1 + \hat{f}_0\hat{q}_{1,\hat{x}} + \hat{q}_{0,\hat{x}}\hat{f}_1 \quad (3.76)$$

$$J_1^* = 2\hat{f}_0\hat{q}_0\hat{f}_1 + \hat{f}_0^2\hat{q}_1 - \hat{\mu}_{1,\hat{x}}. \quad (3.77)$$

The asymptotic form of $\hat{f}_0(x)$ is

$$\hat{f}_0(x) = \hat{f}_0^{(0)} + \hat{f}_0^{(1)} e^{x/\sqrt{6}} + \hat{f}_0^{(2)} e^{2x/\sqrt{6}} + \dots \quad (3.78)$$

and similarly for $\hat{q}_0(x)$ and $\hat{\mu}_0(x)$. Eqs. (3.5.4) can be satisfied if the asymptotic form of $\hat{f}_1(x)$ is

$$\begin{aligned} \hat{f}_1(x) = \hat{f}_1^{(0)} + & \left(\hat{f}_1^{(1)} + \hat{g}_1^{(1)}\hat{x} \right) e^{x/\sqrt{6}} \\ & + \left(\hat{f}_1^{(2)} + \hat{g}_1^{(2)}\hat{x} \right) e^{2x/\sqrt{6}} + \dots, \end{aligned} \quad (3.79)$$

and similarly for $\hat{q}_1(x)$ and $\hat{\mu}_1(x)$. At $O(u^2)$, $\hat{f}_2(x)$ would have second-order polynomials multiplying the exponentials, and so on. Substituting these expressions into the differential equations allows us to determine the unknown constants (except for those associated with the translational invariance). For f_∞ it yields the series

$$f_\infty = \sqrt{\frac{2}{3}} + \frac{u}{24\sqrt{6}} + \frac{u^2}{768\sqrt{6}} + \dots, \quad (3.80)$$

which corresponds to

$$J^* = \frac{2}{3\sqrt{3}} - \frac{u^2}{576\sqrt{3}} - \frac{u^3}{5184\sqrt{3}} + \dots. \quad (3.81)$$

Note that the first correction to the $u \rightarrow 0$ limit of J^* is of $O(u^2)$, since the lowest term J_c is at the maximum of $J^*(f_\infty) = f_\infty^2 \sqrt{1 - f_\infty^2}$.

The series found through the asymptotic perturbative expansion above can be obtained by another method. Looking back at Eqs. (3.72) and (3.73), we note that the ratio of decay lengths $\lambda_f/\lambda_\mu = 2$. If we insert the expressions we have for these length scales, Eqs. (3.40) and (3.42), we find as $u \rightarrow 0$

$$\frac{\lambda_f}{\lambda_\mu} = \left[\frac{uf_\infty^2}{6f_\infty^2 - 4} \right]^{1/2} = 2. \quad (3.82)$$

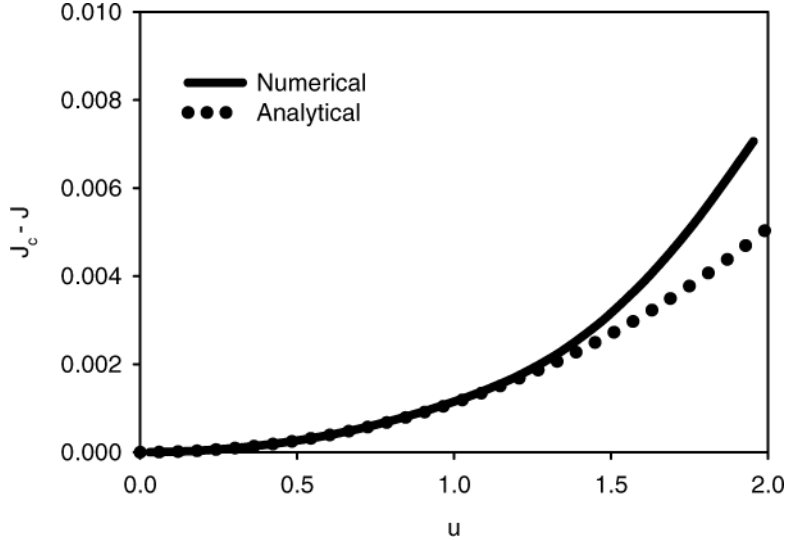


Figure 3.11: $(J_c - J)$ for the numerical data (solid line) and for the result of the small- u analysis, Eq. (3.83) (dashed line).

Solving for f_∞ , and then calculating J^* , we find

$$J^* = J_c(1 - u/8)^{1/2}(1 - u/24)^{-3/2}, \quad (3.83)$$

with $J_c = \sqrt{4/27}$, which when expanded for small- u agrees with the series (3.81) found above. We plot the small- u numerical data and this expression together in Fig. 3.11. The fit is surprisingly good at small u , suggesting to us that the corrections to Eq. (3.83) are exponentially small as $u \rightarrow 0$.

3.6 Moving Interfaces

At currents other than J^* , the NS interfaces move with a constant velocity. For such solutions the operator ∂_t can be replaced by $-c\partial_x$, so that Eqs. (3.5.2) become

$$-cu f_x = f_{xx} - f q^2 + f - f^3, \quad (3.84)$$

$$u(-cq + \mu)f = 2f_x q + f q_x, \quad (3.85)$$

$$J = f^2 q - \mu_x. \quad (3.86)$$

While the boundary conditions on f and q remain the same, that on the scalar potential becomes $\mu_\infty = cq_\infty$. Actually, it is more convenient to use instead $\tilde{\mu} = \mu - cq$, which is the gauge-invariant potential in the constant-velocity case.

The superconducting phase invades the normal phase if $J < J^*$ and vice versa if $J > J^*$. For currents near J^* , the interface speed is proportional to $(J - J^*)$. In this linear response regime, one can define a kinetic coefficient (which Likharev [74] refers to as a “viscosity”)

$$\eta = \left(\frac{dc}{dJ} \right)_{J=J^*}^{-1}. \quad (3.87)$$

Figure 3.12 shows the numerically determined kinetic coefficient as a function of u . For large- u , we find $\eta \sim u^{3/4}$ for which we provide an argument below.

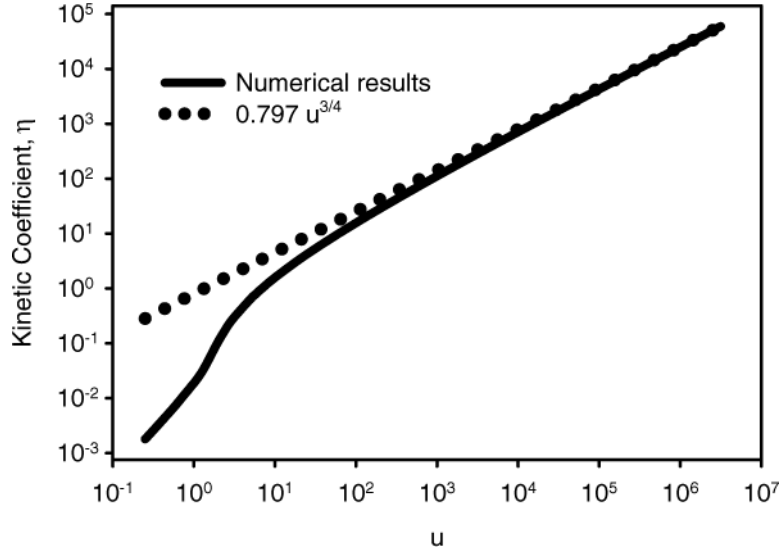


Figure 3.12: A log-log plot of the numerically determined kinetic coefficient as a function of u (the solid line) along with an asymptotic fit of $0.797u^{3/4}$ (the dotted line).

The velocity of the interface does not depend on the direction of the applied current. This can be seen from the symmetry of the current in the equations we use, but it seems not to make physical sense. In fact an article by Gurevich and Mints [54] addresses effects of the collision of quasiparticles with the NS boundary, and they do cause a small asymmetry in the normal zone propagation. The TDGL do not, however, account for kinetics across a phase boundary, so the effect is not included in Likharev's equations.

Farther from the stall current, the velocities deviate from this linear behavior, as seen in Fig. 3.13. The greatest departure occurs in the limits $J \rightarrow 0$ and $J \rightarrow J_c$. In fact, Likharev [74] conjectured that the interface speed diverges in both of these limits; we find that it is bounded.

The $J \rightarrow 0$ limit. The moving interface equations, Eqs. (3.6), simplify in the $J \rightarrow 0$ limit, since that limit implies that both $q \rightarrow 0$ and $\mu \rightarrow 0$, leaving only

$$f_{xx} + ucf_x + f - f^3 = 0. \quad (3.88)$$

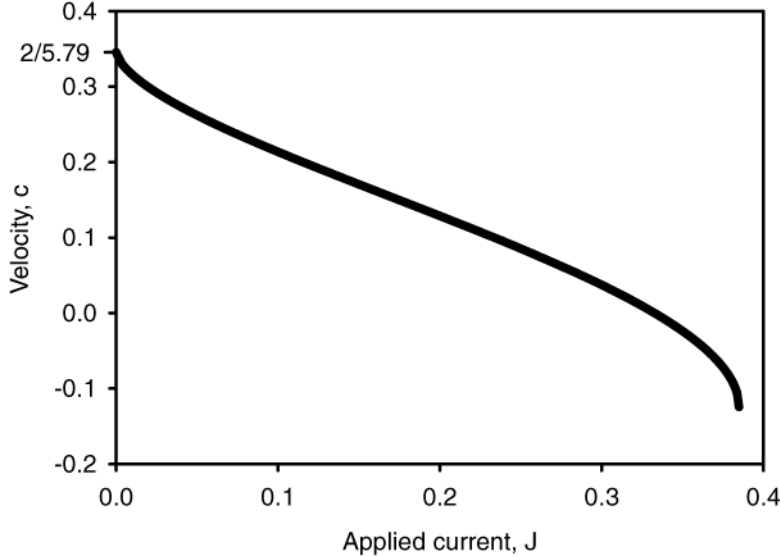
If we replace uc in the above equation by a speed v , then we have the steady-state version of Fisher's equation [39], which is known to have propagating front solutions with $v = 2$ [2]. In our case this implies that as $J \rightarrow 0$, $c = 2/u$, which is in good agreement with the numerical data shown in Fig. 3.13.

We can combine the above result with an earlier one to suggest that $\eta \sim u^{3/4}$ as $u \rightarrow \infty$. In the large- u limit, we have information on the following two points: (1) the stalled interface ($J = J^* \sim u^{-1/4}$, $c = 0$); and (2) the interface in the absence of current ($J = 0$, $c = 2/u$). In going from (1) to (2), the changes in current and velocity are $\Delta J \sim u^{-1/4}$ and $\Delta c \sim u^{-1}$. As $u \rightarrow \infty$, both of these changes are small so that η might be approximated by

$$\eta \approx \frac{\Delta J}{\Delta c} \sim u^{3/4}, \quad (3.89)$$

yielding the behavior seen in the numerical data (see Fig. 3.12 and Table 3.3).

The $J \rightarrow J_c$ limit. The numerical work indicates that the velocity is finite as $J \rightarrow J_c$; the limiting velocity is shown in Fig. 3.14 as a function u . We can find an analytic bound on this velocity as follows. First, take Eqs. (3.6), use the gauge-invariant potential $\tilde{\mu}$, and find the constant-velocity analog of Eq. (3.34). Then

Figure 3.13: The velocity of the front versus the current J for $u = 5.79$.

substitute the asymptotic forms, Eqs. (3.5.2), into the resulting equations, leading to

$$\left(cu\lambda_f^{-1} + \lambda_f^{-2} - 2f_\infty^2 \right) f_1 e^{x/\lambda_f} = 2f_\infty q_\infty q_1 e^{x/\lambda_q}, \quad (3.90)$$

$$(uf_\infty^2 - \lambda_\mu^{-2}) \tilde{\mu}_1 e^{x/\lambda_\mu} = cq_1 \lambda_q^{-2} e^{x/\lambda_q}, \quad (3.91)$$

$$\begin{aligned} 2f_\infty q_\infty f_1 e^{x/\lambda_f} + (f_\infty^2 - c\lambda_q^{-1}) q_1 e^{x/\lambda_q} \\ - \tilde{\mu}_1 \lambda_\mu^{-1} e^{x/\lambda_\mu} = 0. \end{aligned} \quad (3.92)$$

Arguments similar to those following Eqs. (3.38–3.40) lead one to the conclusion that in this case $\lambda_f = \lambda_q = \lambda_\mu$. The above equations can then be shown to yield the following relation

$$\begin{aligned} u^2 c^2 + (2u\lambda^{-1} - 2uf_\infty^2 \lambda - u^2 f_\infty^2 \lambda) c \\ + [2(uf_\infty^2 \lambda^2 - 1)(3f_\infty^2 - 2) - uf_\infty^2 + \lambda^{-2}] = 0, \end{aligned} \quad (3.93)$$

where we have used $q_\infty^2 = 1 - f_\infty^2$. We find the bound by: (1) solving Eq. (3.93) for c ; (2) substituting in $f_\infty = \sqrt{2/3}$ (which corresponds to $J = J_c$); and (3) extremizing that result with respect to the decay length λ . The small- u limit of the resulting bound is $-\sqrt{2u}/9$, and the large- u limit is $-1/2\sqrt{3}$. The square-root dependence of the velocity in the small- u limit agrees with the data. Now we can consider going from the stall current ($J^*, c = 0$) to the critical depairing current ($J_c, c \sim u^{1/2}$) which results in changes $\Delta J \sim u^2$ and $\Delta c \sim u^{1/2}$, suggesting that the small- u kinetic coefficient $\eta \sim u^{3/2}$, which is in rough agreement with the numerical data. We have also observed that as a function of J the speed appears to approach its bound via a square root dependence

$$c(J) = A + B(J_c - J)^{1/2} \quad (3.94)$$

for all u .

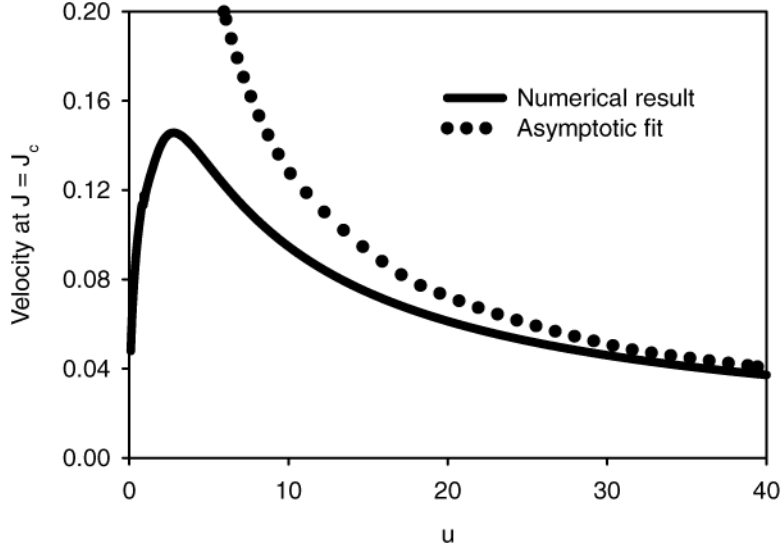


Figure 3.14: The velocity as $J \rightarrow J_c$ as a function of u . For large u , the velocity asymptotically approaches $0.92u^{-0.85}$.

3.7 Summary and Remarks

In this chapter we have studied in detail the nucleation and growth of the superconducting phase in the presence of a current. The finite amplitude critical nuclei grow as the current is increased, with the amplitude eventually saturating as the stall current J^* is approached, leading to the formation of interfaces separating the normal and superconducting phases. The stall current can be calculated in the limit of large u using matched asymptotic expansions, demonstrating once again the utility of this technique for problems in inhomogeneous superconductivity. We have also derived an analytic expression for the stall current for small u , which we believe to be correct up to exponentially small corrections. Deviations from the stall current cause the interfaces to move, and we have calculated the mobility of these moving interfaces for a wide range of u . Finally we have shown that the interface velocity $c = 2/u$ as $J \rightarrow 0$ and that c is bounded as $J \rightarrow J_c$, in contrast to some conjectures in the literature.

As in the magnetic-field analogy, the issue of stability and dynamics of the current-induced NS interfaces will be more complicated and interesting in the two-dimensional case. Some preliminary work in this direction has been reported by Aranson *et al.*[1], who find that the current has a stabilizing effect on the NS interface. This can be interpreted as a positive surface tension for the interface, due entirely to *nonequilibrium* effects. They provide a heuristic derivation of an interesting free-boundary problem for the interfacial dynamics (a variant of the Laplacian growth problem); however, this free-boundary problem is sufficiently complicated that they were unable to solve it to compare with their numerical results. Clearly, further work in this direction would be helpful in understanding the nucleation and growth of the superconducting phase in two-dimensional superconducting films.

Appendix A

Detailed Derivation of the TDGL

A.1 Derive TDGL from Landau-Ginzburg Free Energy

This note shows the details of deriving the time-dependent GL equations from the GL free energy.

$$\frac{\partial \psi}{\partial t} = -\Gamma \frac{\delta G}{\delta \psi^*} = -\Gamma \left(\frac{\partial}{\partial \psi^*} - \frac{\partial}{\partial x_i} \frac{\partial}{\partial \frac{\partial \psi^*}{\partial x_i}} \right) G \quad (\text{A.1})$$

Start with the GL free energy

$$f = f_n + \alpha |\psi|^2 + \frac{\beta}{2} |\psi|^4 + \frac{|\mathbf{h}|^2}{8\pi} + \frac{1}{2m_s} \left| \left(-i\hbar \nabla - \frac{e_s \mathbf{A}}{c} \right) \psi \right|^2. \quad (\text{A.2})$$

Now work out the functional derivative with respect to ψ^*

$$\frac{\partial}{\partial \psi^*} (\psi^* \psi) = \psi \quad (\text{A.3})$$

$$\frac{\partial}{\partial \psi^*} (\psi^{*2} \psi^2) = |\psi|^2 \psi \quad (\text{A.4})$$

$$\frac{\partial}{\partial \psi^*} \left[(i\hbar \nabla + \frac{e}{c} \mathbf{A}) \psi \cdot (-i\hbar \nabla + \frac{e}{c} \mathbf{A}) \psi^* \right] = \frac{e}{c} \mathbf{A} \cdot (i\hbar \nabla + \frac{e}{c} \mathbf{A}) \psi \quad (\text{A.5})$$

$$\frac{\partial}{\partial x_i} \frac{\partial}{\partial \frac{\partial \psi^*}{\partial x_i}} \left[(i\hbar \nabla + \frac{e}{c} \mathbf{A}) \psi \cdot (-i\hbar \nabla + \frac{e}{c} \mathbf{A}) \psi^* \right] = -i\hbar \nabla \cdot (i\hbar \nabla + \frac{e}{c} \mathbf{A}) \psi \quad (\text{A.6})$$

Put it together to find

$$\frac{\delta G}{\delta \psi^*} = \alpha \psi + \beta |\psi|^2 \psi + \frac{1}{2m} \left(\frac{2ie\hbar}{c} \mathbf{A} \cdot \nabla \psi + \left(\frac{e}{c} \mathbf{A} \right)^2 \psi - \hbar^2 \nabla^2 \psi \right) \quad (\text{A.7})$$

$$= \alpha \psi + \beta |\psi|^2 \psi + \frac{1}{2m} \left(i\hbar \nabla + \frac{e}{c} \mathbf{A} \right)^2 \psi \quad (\text{A.8})$$

Now do the next independent variable, \mathbf{A} . First we write out some simple definitions for reference.

$$\nabla \times \mathbf{A} = \left(\frac{\partial A_z}{\partial y} - \frac{\partial A_y}{\partial z} \right) \hat{i} - \left(\frac{\partial A_z}{\partial x} - \frac{\partial A_x}{\partial z} \right) \hat{j} + \left(\frac{\partial A_y}{\partial x} - \frac{\partial A_x}{\partial y} \right) \hat{k} \quad (\text{A.9})$$

$$\nabla \times \nabla \times \mathbf{A} = \left[\frac{\partial}{\partial y} \left(\frac{\partial A_y}{\partial x} - \frac{\partial A_x}{\partial y} \right) + \frac{\partial}{\partial z} \left(\frac{\partial A_z}{\partial x} - \frac{\partial A_x}{\partial z} \right) \right] \hat{i} \quad (\text{A.10})$$

$$- \left[\frac{\partial}{\partial x} \left(\frac{\partial A_y}{\partial z} - \frac{\partial A_z}{\partial y} \right) - \frac{\partial}{\partial z} \left(\frac{\partial A_z}{\partial y} - \frac{\partial A_y}{\partial z} \right) \right] \hat{j} \quad (\text{A.11})$$

$$+ \left[- \frac{\partial}{\partial x} \left(\frac{\partial A_z}{\partial y} - \frac{\partial A_y}{\partial z} \right) - \frac{\partial}{\partial y} \left(\frac{\partial A_z}{\partial x} - \frac{\partial A_x}{\partial z} \right) \right] \hat{k} \quad (\text{A.12})$$

Now let's look at the functional derivative of $(\nabla \times \mathbf{A})^2$. When we look at a single component, it becomes a little clearer.

$$\frac{\partial}{\partial x} \frac{\partial(\nabla \times \mathbf{A})^2}{\partial \frac{\partial A_x}{\partial x}} = 0 \quad (\text{A.13})$$

$$\frac{\partial}{\partial y} \frac{\partial(\nabla \times \mathbf{A})^2}{\partial \frac{\partial A_x}{\partial y}} = \frac{\partial}{\partial y} 2(\nabla \times \mathbf{A}) \cdot (-\hat{k}) \quad (\text{A.14})$$

$$\frac{\partial}{\partial z} \frac{\partial(\nabla \times \mathbf{A})^2}{\partial \frac{\partial A_x}{\partial z}} = \frac{\partial}{\partial z} 2(\nabla \times \mathbf{A}) \cdot \hat{j} \quad (\text{A.15})$$

You can see we are reconstructing a cross product

$$\frac{\delta(\nabla \times \mathbf{A})^2}{\delta A_x} = 2 \left[\frac{\partial(\nabla \times \mathbf{A})_z}{\partial y} - \frac{\partial(\nabla \times \mathbf{A})_y}{\partial z} \right] \quad (\text{A.16})$$

to get

$$\frac{\delta}{\delta \mathbf{A}} (\nabla \times \mathbf{A})^2 = 2 \nabla \times \nabla \times \mathbf{A} \quad (\text{A.17})$$

Similarly,

$$\frac{\delta}{\delta \mathbf{A}} (\nabla \times \mathbf{A}) \cdot \mathbf{H} = \nabla \times \mathbf{H} \quad (\text{A.18})$$

Now figure out the rest of the derivative for \mathbf{A} .

$$\frac{\partial}{\partial \mathbf{A}} \left[(i\hbar \nabla + \frac{e}{c} \mathbf{A}) \psi \cdot (-i\hbar \nabla + \frac{e}{c} \mathbf{A}) \psi^* \right] = \frac{e}{c} \psi (-i\hbar \nabla + \frac{e}{c} \mathbf{A}) \psi^* + \text{c.c.} \quad (\text{A.19})$$

We can add the two pieces together to find the current

$$- \frac{ie\hbar}{2mc} (\psi \nabla \psi^* - \psi^* \nabla \psi) + \frac{e^2}{mc^2} \mathbf{A} |\psi|^2 \quad (\text{A.20})$$

Putting the second equation together, we find

$$\frac{\delta G}{\delta \mathbf{A}} = \frac{1}{4\pi} \nabla \times (\nabla \times \mathbf{A} - \mathbf{H}) - \frac{ie\hbar}{2mc} (\psi \nabla \psi^* - \psi^* \nabla \psi) + \frac{e^2}{mc^2} \mathbf{A} |\psi|^2 \quad (\text{A.21})$$

A.2 Find Dimensionless Variables

We start now with the known form of the TDGL,

$$\frac{1}{\Gamma} \left(\frac{\partial \psi}{\partial t} + \frac{ie}{\hbar} \phi \psi \right) + \alpha \psi + \beta |\psi|^2 \psi + \frac{1}{2m} (i\hbar \nabla + \frac{e}{c} \mathbf{A})^2 \psi = 0 \quad (\text{A.22})$$

$$\frac{\sigma}{c} \frac{\partial \mathbf{A}}{\partial t} + \sigma \nabla \phi + \frac{c}{4\pi} \nabla \times \nabla \times \mathbf{A} - \frac{ie\hbar}{2m} (\psi \nabla \psi^* - \psi^* \nabla \psi) + \frac{e^2}{mc} \mathbf{A} |\psi|^2 = 0 \quad (\text{A.23})$$

We begin by requiring ψ vary between zero and one so that $\psi = \psi_0 \psi'$ where $\psi_0 = \sqrt{-\alpha/\beta}$. That determines the overall factor on the first equation.

$$\frac{\alpha}{\alpha \Gamma} \left(\frac{\partial \psi'}{\partial t} + \frac{ie}{\hbar} \phi \psi' \right) + \alpha \psi' - \alpha |\psi'|^2 \psi' - \alpha \left(\frac{i\hbar}{\sqrt{-2m\alpha}} \nabla + \frac{e}{\sqrt{-2m\alpha c^2}} \mathbf{A} \right)^2 \psi' = 0 \quad (\text{A.24})$$

We can immediately determine $\mathbf{A} = A_0 \mathbf{A}'$ to be

$$A_0 = \sqrt{\frac{-2m\alpha c^2}{e^2}}. \quad (\text{A.25})$$

We also see that the gradient's factor is of the form

$$\frac{\hbar}{\sqrt{-2m\alpha}} \frac{1}{\lambda} = \frac{1}{\kappa} = \frac{\xi}{\lambda} \quad (\text{A.26})$$

where $x = \lambda x'$.

$$-\frac{1}{-\alpha \Gamma} \left(\frac{\partial \psi'}{\partial t} + \frac{ie}{\hbar} \phi \psi' \right) + \psi' - |\psi'|^2 \psi' - \left(\frac{i}{\kappa} \nabla' + \mathbf{A}' \right)^2 \psi' = 0 \quad (\text{A.27})$$

Looking now to the second equation, we can divide through by A_0 to see

$$\frac{\sigma}{ct_0} \frac{\partial \mathbf{A}'}{\partial t'} + \sqrt{\frac{-e^2}{2m\alpha c^2}} \frac{\sigma \phi_0}{\lambda} \nabla' \phi' + \frac{c}{4\pi \lambda^2} \nabla' \times \nabla' \times \mathbf{A}' + \frac{ie\hbar\alpha}{2m\lambda\beta} \sqrt{\frac{-e^2}{2m\alpha c^2}} (\psi' \nabla' \psi'^* - \psi'^* \nabla' \psi') - \frac{e^2 \alpha}{mc\beta} \mathbf{A}' |\psi'|^2 = 0 \quad (\text{A.28})$$

The last term is the only one we already know. Multiplying all terms by the inverse of its prefactor gives

$$-\frac{\sigma}{ct_0} \frac{mc\beta}{e^2 \alpha} \frac{\partial \mathbf{A}'}{\partial t'} + \frac{m\sigma\phi_0}{\kappa\hbar e |\psi_0|^2} \nabla' \phi' - \frac{mc^2 \beta}{4\pi e^2 \alpha \lambda^2} \nabla' \times \nabla' \times \mathbf{A}' - \frac{i}{2\lambda} \sqrt{\frac{-\hbar^2}{2m\alpha}} (\psi' \nabla' \psi'^* - \psi'^* \nabla' \psi') + \mathbf{A}' |\psi'|^2 = 0 \quad (\text{A.29})$$

Now we know from the third term that we must define

$$x_0 = \lambda = \sqrt{\frac{-mc^2 \beta}{4\pi e^2 \alpha}}. \quad (\text{A.30})$$

With that, the third term simplifies dramatically to yield

$$\frac{4\pi\sigma\lambda^2}{c^2 t_0} \frac{\partial \mathbf{A}'}{\partial t'} + \frac{m\sigma\phi_0}{\kappa\hbar e |\psi_0|^2} \nabla' \phi' + \nabla' \times \nabla' \times \mathbf{A}' - \frac{i}{2\kappa} (\psi' \nabla' \psi'^* - \psi'^* \nabla' \psi') + \mathbf{A}' |\psi'|^2 = 0 \quad (\text{A.31})$$

The last definitions look clear.

$$t_0 = \frac{4\pi\sigma\lambda^2}{c^2} \quad \text{and} \quad \phi_0 = \kappa|\psi_0|^2 \frac{\hbar e}{\sigma m} \quad (\text{A.32})$$

If we return to the equation for ψ to finish changing its variables, we find

$$\frac{\alpha}{\alpha\Gamma} \left(\frac{\partial\psi'}{\partial t} + \frac{ie}{\hbar} \phi\psi' \right) = \frac{1}{\alpha t_0\Gamma} \left(\frac{\partial\psi'}{\partial t'} + \frac{ie\phi_0 t_0}{\hbar} \phi'\psi' \right). \quad (\text{A.33})$$

We are hoping to find that

$$\frac{ie\phi_0 t_0}{\hbar} = i\kappa = i\frac{\lambda}{\xi}, \quad (\text{A.34})$$

which it is. Our final equations, when this becomes clearer, will be (dropping primes)

$$\gamma \left(\frac{\partial\psi}{\partial t} + i\kappa\phi\psi \right) - \psi + |\psi|^2\psi + \left(\frac{i}{\kappa} \nabla + \mathbf{A} \right)^2\psi = 0 \quad (\text{A.35})$$

$$\frac{\partial\mathbf{A}}{\partial t} + \nabla\phi + \nabla \times \nabla \times \mathbf{A} - \frac{i}{2\kappa} (\psi \nabla\psi^* - \psi^* \nabla\psi) + \mathbf{A}|\psi|^2 = 0 \quad (\text{A.36})$$

Appendix B

Likharev's Equations as an Active Kinetic Equation

Likharev's equations behave like nonlinear diffusion equations. They don't appear to be the same at first glance, however. We would like to see whether they could resemble more traditional diffusion equations, so we begin with Likharev's equations

$$uf_t = f_{xx} - f\theta_x^2 + f - f^3 \quad (B.1)$$

$$u(\theta_t + \mu)f^2 = (f^2\theta_x)_x \quad (B.2)$$

$$J = f^2\theta_x - \mu_x. \quad (B.3)$$

and try to coax them into a form like that discussed in Gurevich and Mints [55]

$$\tau_\psi \frac{\partial \psi}{\partial t} = l_\psi^2 \frac{\partial^2 \psi}{\partial x^2} - F(\psi, \phi, \beta) \quad (B.4)$$

$$\tau_\phi \frac{\partial \phi}{\partial t} = l_\phi^2 \frac{\partial^2 \phi}{\partial x^2} - R(\psi, \phi, \beta) \quad (B.5)$$

where β is a parameter representing our (u, J) . We may be able to put our equations in this form if we change variables from (f, θ) to (f, j_s) where $j_s = f^2\theta_x$ is the supercurrent. Equation B.1 is already in the correct form if we substitute $\theta_x = j/f^2$.

$$uf_t = f_{xx} + f \left(1 - f^2 - \frac{j^2}{f^4} \right) \quad (B.6)$$

If we take the derivative of B.2, we get

$$u(\theta_{xt} + \mu_x)f^2 + 2\frac{f_x}{f}(f^2\theta_x) = (f^2\theta_x)_{xx} \quad (B.7)$$

We can get rid of θ by constructing the derivative of the supercurrent

$$(f^2\theta_x)_t = 2ff_t\theta_x + f^2\theta_{xt}. \quad (B.8)$$

We substitute f_t from B.1

$$2uff_t\theta_x = 2f\theta_x(uf_t) = 2f\theta_x(f_{xx} - f\theta_x^2 + f - f^3) \quad (B.9)$$

into the derivative of the supercurrent to find

$$u(f^2\theta_x)_t = (f^2\theta_x)_{xx} - 2\frac{f_x}{f}(f^2\theta_x)_x + u(J - f^2\theta_x)f^2 + 2f\theta_x f_{xx} - 2f^2\theta_x^3 + 2(1 - f^2)f^2\theta_x. \quad (\text{B.10})$$

It is time to substitute $f^2\theta_x = j$ to find

$$uj_t = j_{xx} - 2\frac{f_x}{f}(f_x j_x - f_{xx} j) - (2 + u)f^2 j + 2j + uJf^2 - \frac{2j^3}{f^4}. \quad (\text{B.11})$$

We could condense this a little to

$$uj_t = j_{xx} - 2\frac{j^2}{f} \left(\frac{f_x}{j} \right)_x + u(J - j)f^2 + 2j \left(1 - f^2 - \frac{j^2}{f^4} \right). \quad (\text{B.12})$$

What remains is of the form of an active kinetic system

$$\frac{\partial x_i}{\partial t} = F_i(x_1, x_2, \dots, x_n) + \frac{\partial}{\partial r} \left(\sum_{j=1}^n D_{ij} \frac{\partial x_j}{\partial r} \right) \quad (i = 1, 2, \dots, n) \quad (\text{B.13})$$

as described in Vasil'ev, Romanovskii, and Yakhno [103], but the numerous spatial derivatives complicate the first integrals typically used to examine such equations.

Appendix C

Amplitude of the Critical Nuclei in the $J \rightarrow 0$ Limit

In this appendix we provide a self-consistent calculation of the amplitude of the critical nuclei in the $J \rightarrow 0$ limit. Choosing the gauge appropriate for bumps centered at $x = 0$ and combining Eqs. (3.3.1) into one equation yields

$$\begin{aligned} & [-u\partial_t + iuJx + \partial_x^2 + 1] \psi(x, t) = |\psi(x, t)|^2 \psi(x, t) \\ & + iu \left[\int_0^x dy \operatorname{Im}(\psi^*(y, t)\partial_y\psi(y, t)) \right] \psi(x, t). \end{aligned} \quad (\text{C.1})$$

The propagator for the linear operator appearing on the left hand side of Eq. (C.1) satisfies the condition

$$\begin{aligned} & [-u\partial_t + iuJx + \partial_x^2 + 1] \quad G(x, x'; t - t')\Theta(t - t') \\ & = \quad -u \delta(x - x')\delta(t - t') \end{aligned} \quad (\text{C.2})$$

and is given by

$$\begin{aligned} G(x, x'; \tau) = & \left(\frac{u}{4\pi\tau} \right)^{1/2} \exp \left[\frac{\tau}{u} - \frac{J^2\tau^3}{12u} \right] \\ & \times \exp \left[\frac{iJ\tau(x + x')}{2} - \frac{u(x - x')^2}{4\tau} \right]. \end{aligned} \quad (\text{C.3})$$

Ivlev *et al.* [59, 57] used this linear propagator to evolve perturbations having widths of $O(1)$ and carrying no current. Without the nonlinear terms such perturbations initially grow but ultimately reach a maximum size and then decay away. Ivlev *et al.* suggested that the amplitudes of the critical nuclei are exponentially small in the $J \rightarrow 0$ limit by asking what sized initial perturbations are of $O(1)$ at their maxima. Their arguments motivated us to use the propagator in a more careful estimate of the amplitude that includes the nonlinear terms as an essential ingredient.

We can convert Eq. (C.1) into an integral equation by multiplying both sides of Eq. (C.1) (with $x \rightarrow x'$ and $t \rightarrow t'$) by $G(x, x'; t - t')$ and integrating over all x' and integrating t' from 0 to t . After some manipulation

these steps lead to

$$\begin{aligned} \psi(x, t) &= \int_0^t dt' \int_{-\infty}^{\infty} dx' G(x, x', t - t') \\ &\times \left\{ \psi(x', t') \delta(t - t') - \frac{1}{u} |\psi(x', t')|^2 \psi(x', t') \right. \\ &\left. - i \left[\int_0^{x'} dy \operatorname{Im}(\psi^*(y, t') \partial_y \psi(y, t')) \right] \psi(x', t') \right\}, \end{aligned} \quad (\text{C.4})$$

where $t > 0$.

In order to estimate the amplitude of the threshold solutions, we will substitute into Eq. (C.4) the following form

$$\psi(x, t) = \psi_0 \exp \left\{ -\frac{uJx^2}{4} + ix \right\}. \quad (\text{C.5})$$

Note that this form is stationary and has a fixed Gaussian shape (which is inspired by our WKB approximation, see Eq. (3.20)) but it has an arbitrary amplitude which we will determine self-consistently.

Let us take the $t \rightarrow \infty$ limit and focus on $x = 0$ since our interest is in the amplitude. After substituting Eq. (C.5) into Eq. (C.4), we can do both integrals for the first term on the right hand side exactly, and it can be seen to decay to zero in the $t \rightarrow \infty$ limit. Next, we perform the x' integration of the second term on the right hand side (II), which yields

$$II = -\frac{\psi_0^3}{uJ} \int_0^\infty \frac{d\tau}{\sqrt{1+3\tau}} \exp \left\{ \frac{24\tau^2 - 4\tau^3 - 3\tau^4}{12uJ(1+3\tau)} \right\}, \quad (\text{C.6})$$

where $\tau = Jt$. We now apply the method of steepest descent to obtain

$$II \approx -\frac{\sqrt{\pi}\psi_0^3}{\sqrt{2uJ}} \exp \left\{ \frac{32}{81} \frac{uJ}{\tau} \right\}. \quad (\text{C.7})$$

In the third term on the right hand side (III) of Eq. (C.4), we make the substitution $y = vx'$ and then perform the x' integration giving

$$\begin{aligned} III &= \frac{\psi_0^3}{uJ^2} \int_0^\infty d\tau \int_0^1 dv \frac{(2\tau + \tau^2)}{\sqrt{[1 + \tau(1 + 2v^2)]^3}} \\ &\times \exp \left\{ \frac{24v^2\tau^2 - 4\tau^3 - (1 + 2v^2)\tau^4}{12uJ[1 + (1 + 2v^2)\tau]} \right\}. \end{aligned} \quad (\text{C.8})$$

The maximum of the term in the exponential of III occurs at $v = 1$ (which is an endpoint). Linearizing about that maximum provides

$$\begin{aligned} III &\approx \frac{\psi_0^3}{uJ^2} \int_0^\infty \frac{d\tau \tau(2 + \tau)}{\sqrt{(1 + 3\tau)^3}} \exp \left\{ \frac{24\tau^2 - 4\tau^3 - 3\tau^4}{12uJ(1 + 3\tau)} \right\} \\ &\times \int_0^1 dw \exp \left\{ -\frac{\tau^2(2 + \tau)^2 w}{uJ(1 + 3\tau)^2} \right\}, \end{aligned} \quad (\text{C.9})$$

where $w = 1 - v$. After the w integration, we apply the method of steepest descent to the τ integration to

obtain

$$III \approx \frac{\sqrt{\pi u} \psi_0^3}{\sqrt{2J}} \frac{9}{8} \exp \left\{ \frac{32}{81 uJ} \right\}. \quad (\text{C.10})$$

Putting all of these results back into Eq. (C.4) gives

$$\psi_0 \approx \frac{\sqrt{\pi u} \psi_0^3}{\sqrt{2J}} \exp \left\{ \frac{32}{81 uJ} \right\} \left[\frac{9}{8} - \frac{1}{u} \right], \quad (\text{C.11})$$

which provides the expression given in the text, Eq. (3.22). This calculation clearly runs into trouble when $u < 8/9$; however, the numerical coefficients in front of these integrals are sub-leading terms, and they can be varied by adding sub-leading terms to the initial Gaussian guess.

Bibliography

- [1] I. Aranson, B. Ya. Shapiro, and V. Vinokur. Nucleation and growth of the normal phase in thin superconducting strips. *Physical Review Letters*, 76(1):142–5, 1996.
- [2] D. G. Aronson and H. F. Weinberger. Multidimensional nonlinear diffusion arising in population genetics. *Advances in Mathematics*, 30(1):33–76, 1978.
- [3] Bardeen and Schrieffer. In C. J. Gorter, editor, *Low Temperature Physics*, volume III. North-Holland, Amsterdam, 1961.
- [4] Grigory Isaakovich Barenblatt. *Scaling, self-similarity, and intermediate asymptotics*, chapter 8. Cambridge University Press, New York, 1996. Barenblatt explains a fine detail of the stability of invariant solutions to time-dependent equations.
- [5] Antonia Barone, editor. *Superconductive Particle Detectors*. World Scientific, Teaneck, NJ, 1988.
- [6] S. J. Di Bartolo and A. T. Dorsey. Velocity selection for propagating fronts in superconductors. *Physical Review Letters*, 77(21):4442–5, 1996.
- [7] S. John Di Bartolo. *Superheating Fields and Interface Motion in One-dimensional Models of Superconductors*. PhD thesis, University of Virginia, 205 McCormick Road, Charlottesville, VA 22901, Aug. 1997.
- [8] C. P. Bean and J. D. Livingston. Surface barrier in type-ii superconductors. *Physical Review Letters*, 12(1), Jan. 1964.
- [9] Richard Ernest Bellman. *Stability Theory of Differential Equations*. McGraw-Hill, New York, 1953. Richard Bellman has written many works relevant to the numerical and analytical analysis of wave propagation.
- [10] C. M. Bender and S. A. Orszag. *Advanced mathematical Methods for Scientists and Engineers*. McGraw-Hill, New York, 1978.
- [11] G. Boato, G. Gallinaro, and C. Rizzuto. *Solid State Communications*, 3:173, 1965.
- [12] C. Bolley and B. Helffer. Superheating in a film in the weak κ limit: numerical results and approximate models. Preprint, 1994.
- [13] C. Bolley and B. Helffer. *RAIRO Modél. Math. Anal. Numér.*, 31:121, 1997.
- [14] C. J. Boulter and J. O. Indekeu. Accurate analytic expression for the surface tension of a type-i superconductor. *Physical Review B*, 54(17):12407–12, 1996.
- [15] R. F. Broom and E. H. Rhoderick. *Br. J. Appl. Phys.*, 11, 1960.

- [16] J. P. Burger. Superheating and supercooling in first kind superconductors. In P. R. Wallace, editor, *Superconductivity: Proceedings of the Advanced Summer Study Institute, McGill University, Montreal*, volume 1, pages 461–488, 1969.
- [17] L. Burlachkov. Magnetic relaxation over the bean-livingston surface barrier. *Physical Review B*, 47(13):8056–64, 1993.
- [18] S. J. Chapman. Asymptotic analysis of the ginzburg-landau model of superconductivity: Reduction to a free boundary model. *Quarterly Journal of Applied Mathematics*, 53:601–27, 1995.
- [19] S. J. Chapman. Stability of travelling waves in models of superconductivity. *IMA Journal of Applied Mathematics*, 54(2):159–69, 1995.
- [20] S. J. Chapman, Qiang Du, and M. D. Gunzburger. A model for variable thickness superconducting thin films. *Z angew Math Phys (ZAMP)*, 47:410–431, 1996. All thin superconductors behave as type-ii superconductors.
- [21] S. Jonathan Chapman. Superheating field of type-ii superconductors. *SIAM J. Appl. Math*, 55(5):1233–1258, 1995. Our use of matched asymptotics to find the superheating field for type-i superconductors is analogous to this author’s work on type-ii superconductors.
- [22] P.-G. de Gennes. Vortex nucleation in type ii superconductors. *Solid State Communications*, 3:127–130, Apr. 1965. De Gennes derives the superheating field in the limit $\kappa \gg 1$.
- [23] P.-G. de Gennes. *Superconductivity in Metals and Alloys*. Addison-Wesley, New York, 1966.
- [24] R. W. DeBlois and W. DeSorbo. *Physical Review Letters*, 12:499, 1964.
- [25] G. J. Dolan and L. D. Jackel. *Physical Review Letters*, 39:1628, 1977.
- [26] A. Dolgert and S. J. Di Bartolo. Last integral of Chapman’s Painlevé Equation. Unpublished.
- [27] A. J. Dolgert, S. J. Di Bartolo, and A. T. Dorsey. Superheating fields of superconductors: Asymptotic analysis and numerical results. *Physical Review B*, 53(9):5650–60, Mar. 1996.
- [28] A. J. Dolgert, T. Blum, A. T. Dorsey, and M. Fowler. Nucleation and growth of the superconducting phase in the presence of a current. *Physical Review B*, 57(9):5432–43, Mar. 1998.
- [29] A. T. Dorsey. Dynamics of interfaces in superconductors. *Annals of Physics*, 233(2):248–69, Aug. 1994.
- [30] A. T. Dorsey and R. E. Goldstein. Shapes of flux domains in the intermediate state of type-i superconductors. *Physical Review B*, 57(5):3058–72, Feb. 1998.
- [31] Qiang Du. Global existence and uniqueness of solutions of the time-dependent ginzburg-landau model for superconductivity. *Applicable Analysis*, 53:1–17, 1994. This work begins with a very clear analysis of the Time-dependent Ginzburg-Landau Equations in several gauges.
- [32] Qiang Du, Max D. Gunzburger, and Janet S. Peterson. Analysis and approximation of the ginzburg-landau model of superconductivity. *SIAM Review*, 34(1):54–81, Mar. 1992. This work begins with a fine introduction to the Ginzburg-Landau equations.
- [33] Ulrich Eckern, Albert Schmid, Manfred Schmutz, and Gerd Schön. Stability of superconducting states out of thermal equilibrium. *Journal of Low Temperature Physics*, 36(5/6):643–687, 1979.
- [34] V. F. Elesin. Threshold instability and inhomogenous states in nonequilibrium superconductors with optical and tunnel quasiparticle pumping. *Sov. Phys. JETP*, 49(6):1121–1127, Jun. 1979.

- [35] J. Feder and D. S. McLachlan. Superheating and supercooling in single spheres of tin, indium, and gold-plated indium. *Physics Review*, 177:763–76, 1969.
- [36] H. J. Fink. Delayed flux entry into type II superconductors. *Physics Letters*, 20(4):356–7, 1966.
- [37] H. J. Fink, D. S. McLachlan, and B. Rothberg Bibby. In D. F. Brewer, editor, *Progress in Low Temperature Physics*, volume VII B. North-Holland Publishing, Amsterdam, 1978.
- [38] H. J. Fink and A. G. Presson. Stability limit of the superheated meissner state due to three-dimensional fluctuations of the order parameter and vector potential. *Physics Review*, 182:498–503, Jun. 1969.
- [39] R. A. Fisher. *Ann. Eugen.*, 7:355, 1937.
- [40] Ian Foster. *Designing and Building Parallel Programs*. Addison-Wesley, Reading, Mass., 1994.
- [41] H. Frahm, S. Ullah, and A. T. Dorsey. Flux dynamics and the growth of the superconducting phase. *Physical Review Letters*, 66(23):3067–70, 1991.
- [42] V. P. Galaiko. *Zh. Eksp. Teor. Fiz.*, 50:717, 1966.
- [43] V. P. Galaiko. *Sov. Phys. JETP*, 23:475, 1966. Translation of above to English.
- [44] V. P. Galaiko. *Zh. Eksp. Teor. Fiz.*, 54:318, 1968.
- [45] V. P. Galaiko. *Sov. Phys. JETP*, 27:179, 1968.
- [46] A. K. Geim, I. V. Grigorieva, S. V. Dubonos, J. G. S. Lok, J. C. Maan, A. E. Filippov, and F. M. Peeters. Phase transitions in individual sub-micrometre superconductors. *Nature*, 390, Nov. 1997. These authors seem blithely unaware that superconducting transitions in a magnetic field are first order or that there is a length scale involved.
- [47] I. M. Gelfand and S. V. Fomin. *Calculus of Variations*. Englewood Cliffs, N.J., Prentice-Hall, 1963.
- [48] V. L. Ginzburg. On the destruction and the onset of superconductivity in a magnetic field. *Soviet Physics JETP*, 7(78), Jul. 1958.
- [49] V. L. Ginzburg. On heat-transfer (heat conduction) and the thermoelectric effect in the superconducting state. *Soviet Physics Uspekhi*, 41(3):307–311, 1998.
- [50] R. E. Goldstein, D. P. Jackson, and A. T. Dorsey. Current-loop model for the intermediate state of type-i superconductors. *Physical Review Letters*, 76(20):3818–21, 1996.
- [51] L. Gor'kov and G. Eliashberg. *Soviet Physics JETP*, 27:328–334, 1968.
- [52] L. P. Gor'kov. Singularities of the resistive state with current in thin superconducting films. *JETP Letters*, 11(1):32–5, Jan. 1970. The authors demonstrate qualitatively the essentially nonlinear character of the current-voltage characteristic of a superconducting film. To this end, they confine themselves to the model of a film with paramagnetic impurities (or in a strong magnetic field), for which the role of the anomalous terms is small. (From INSPEC).
- [53] Orsay group on Superconductivity. Strong field effects at the surface of a superconductor. In D. F. Brewer, editor, *Quantum Fluids*, pages 26–67. North Holland, Amsterdam, 1966.
- [54] A. Vl. Gurevich and R. G. Mints. Aysmmetry of the normal zone propagation velocity in superconductors. *Cryogenics*, pages 102–104, Feb. 1981. This article is a direct example of the limitations of Ginzburg-Landau theory to describe time-dependent phenomena.
- [55] A. Vl. Gurevich, R. G. Mints, and A. A. Pukhov. Motion of a kink in a bistable medium with hysteresis. *Physica D*, 35:382–394, 1989.

- [56] Arieh Iserles. *A First Course in the Numerical Analysis of Differential Equations*. Cambridge University Press, New York, NY, 1996.
- [57] B. I. Ivlev and N. B. Kopnin. Electric currents and resistive states in thin superconductors. *Advances in Physics*, 33(1):47–114, 1984. Comprehensive review article.
- [58] B. I. Ivlev and N. B. Kopnin. Theory of current states in narrow superconducting channels. *Soviet Physics Uspekhi*, 27(3):206–27, 1984.
- [59] B. I. Ivlev, N. B. Kopnin, and L. A. Maslova. Dynamics of the resistive state of superconductors. *Soviet Physics JETP*, 51:986, 1980.
- [60] B. I. Ivlev, N. B. Kopnin, and L. A. Maslova. Resistive state of superconductors. *Soviet Physics Solid State*, 22(2):149–50, 1980.
- [61] F. S. Jelila, J-P Maneval, F-R Ladan, F. Chibane, and A. Marie de Ficquelmont. Time of nucleation of phase-slip centers in $\text{Yba}_2\text{Cu}_3\text{O}_7$ superconducting bridges. *Physical Review Letters*, 81(9):1933–36, 1998.
- [62] F. S. Jelila, J-C Villégier, and J-P Maneval. Restoration of the superconducting order parameter after a supercritical current pulse. *Physica C*, 235–240:1983–84, 1994.
- [63] Herbert Keller. *Numerical Methods for Two-Point Boundary-Value Problems*. Dover Publications, Inc., New York, 1992.
- [64] B. S. Kerner and V. V. Osipov. Autosolitons. *Sov. Phys. Usp.*, 32(2), Feb. 1989. Review article.
- [65] A. N. Kolmogorov, I. G. Petrovskii, and N. S. Pishunov. *Bull. Univ. Moscow, Ser. Int. A*, 1, 1937.
- [66] L. Kramer. Spontaneous vortex nucleation in superconductors. *Physics Review*, 170, 1968.
- [67] L. Kramer and A. Baratoff. Lossless and dissipative current-carrying states in quasi-one-dimensional superconductors. *Physical Review Letters*, 38(9):518–521, Feb. 1976. These authors solve Likharev’s equation for a nucleus in the normal metal but discuss more the phase slip regime.
- [68] L. Kramer and R. J. Watts-Tobin. Theory of dissipative current-carrying states in superconducting filaments. *Physical Review Letters*, 40(15):1041–44, 1978. Because the TDGL cannot account for PSC stability above J^* , they derive generalized TDGL which can account for TDGL above J_{\max} .
- [69] Lorenz Kramer. Breakdown of the superheated meissner state and spontaneous vortex nucleation in type ii superconductors. *Z. Physik*, 259:333–346, 1973. Kramer tries to end the debate on the relationship between perturbations to the superheated state and vortex nucleation by calculating global stability of a few configurations.
- [70] I. O. Kulik. *Soviet Physics JETP*, 32:318, 1970.
- [71] L. D. Landau. On the theory of superconductivity. In D. ter Haar, editor, *Collected Papers of L. D. Landau*. Gordon and Breach, New York, 1965.
- [72] L. D. Landau and E. M. Lifshitz. *Fluid Mechanics*, volume 6 of *Course of Theoretical Physics*. Pergamon Press, second english edition, 1987.
- [73] J. S. Langer and Vinay Ambegaokar. Intrinsic resistive transition in narrow superconducting channels. *Physical Review*, 164(2):498–510, 1967.
- [74] K. K. Likharev. Isothermal domains in quasi-one-dimensional superconductors. *JETP Lett.*, 20(11):338–339, 1974.

- [75] K. K. Likharev and L. A. Yakobson. Dynamical properties of superconducting filaments of finite length. *Sov. Phys. JETP*, 41(3):470–575, 1974. Examines the CV characteristics of a current-carrying filament.
- [76] Fong Liu, M. Mondello, and N. Goldenfeld. Kinetics of the superconducting transition. *Physical Review Letters*, 66(23):3071–4, 1991.
- [77] J.-P. Maneval, H. K. Phan, and F. Chibane. The electron-phonon coupling constant lambda (acoustic) of YBaCuO deduced from the photoresistive response. *Proceedings of the SPIE—The International Society for Optical Engineering*, 2159:172–9, 1994.
- [78] J.-P. Maneval, Hong Khoi Phan, and F. Chibane. On the response time of $\text{YBa}_2\text{Cu}_3\text{O}_7$ superconducting bolometer films. *Physica C*, 235–240:3389–90, 1994.
- [79] J. Matricon and D. Saint-James. Superheating fields in superconductors. *Physics Letters*, 24A, 1967. This is the first numerical calculation of the superheating field for many values of κ .
- [80] G. Meagher, D. DiSanto, A. Kotlicki, G. Eska, and B. G. Turrell. Nucleation of the supercooled normal to superconducting phase transition in small indium spheres induced by γ radiation. *Physical Review Letters*, 79(2):285–288, Jul. 1997.
- [81] John Neu. Vortex dynamics in superconductors. This is a photocopy publicly distributed. It presents a unique view of the time-dependent Ginzburg-Landau equations.
- [82] J. C. Osborn and A. T. Dorsey. Surface tension and kinetic coefficient for the normal/superconducting interface: numerical results versus asymptotic analysis. *Physical Review B*, 50(21):15961–6, 1994.
- [83] J. A. Pals and J. Wolter. Measurement of the order-parameter relaxation in superconducting Al-strips. *Physics Letters*, 70A(2):150–152, Feb. 1979.
- [84] H. Parr. Field dependence of the superconductive penetration depth in tin up to the superheating limit. *Physical Review B*, 12(11):4886–98, 1975.
- [85] H. Parr. Field dependence of the superconductive penetration depth in In and dilute InBi alloys. *Physical Review B*, 14(7):2842–8, 1976.
- [86] H. Parr. Ideal superheating and supercooling limits in superconducting In and dilute InBi alloys. *Physical Review B*, 14(7):2849–56, 1976.
- [87] H. Parr. Superconductive superheating field for finite kappa. *Zeitschrift fur Physik B*, 25(4):359–61, 1976.
- [88] H. Parr and J. Feder. Superconductivity in β -phase gallium. *Physical Review B*, 7(1):166–81, 1973.
- [89] J. Pearl. *Applied Physics Letters*, 5:65, 1964.
- [90] G. Pettersen and H. Parr. Ideal metastability fields and field penetration in type-i and type-ii superconducting InBi single spheres. *Physical Review B*, 19(7):3482–99, 1979.
- [91] A. B. Pippard. *Phil. Mag.*, 41:243, 1950.
- [92] W. H. Press, B. P. Flannery, S. A. Teukolsky, and W. T. Vetterling. *Numerical Recipes*. Cambridge University Press, New York, 1986.
- [93] W. H. Press, S. A. Teukolsky, W. T. Vetterling, and B. P. Flannery. *Numerical Recipes in FORTRAN*. Cambridge University Press, Cambridge, UK, second edition, 1992.

- [94] A. S. Rudyč. Normal autosoliton and switching wave in a thin, current-carrying, superconducting film. *Tech. Phys. Lett.*, 22(10), Oct. 1996.
- [95] A. S. Rudyč. Stationary normal zone in a bounded one-dimensional superconductor. *Tech. Phys. Lett.*, 22(5), May 1996.
- [96] A. Schmid. *Phys. Kondens. Mater.*, 5:302, 1966.
- [97] Albert Schmid and Gerd Schön. Linearized kinetic equations and relaxation processes of a superconductor near t_c . *Journal of Low Temperature Physics*, 20(1/2):207–227, 1975. These authors discuss Schön waves, a non-dissipative approach to motion in superconductors.
- [98] W. J. Skocpol, M. R. Beasley, and M. Tinkham. Phase-slip centers and nonequilibrium processes in superconducting tin microbridges. *Journal of Low Temperature Physics*, 16(1/2):145–167, Jan. 1974.
- [99] W. J. Skocpol, M. R. Beasley, and M. Tinkham. Self-heating hotspots in superconducting thin-film microbridges. *Journal of Applied Physics*, 45(9):4054–66, Sep. 1974.
- [100] F. W. Smith, A. Baratoff, and M. Cardona. Superheating, supercooling, surface superconductivity and ginzburg-landau parameters of pure type-i superconductors and their alloys. *Physik der Kondensierten Materie*, 12(2):145–192, 1970.
- [101] Reinhard Tidecks. *Current-Induced Nonequilibrium Phenomena in Quasi-One-Dimensional Superconductors*, volume 121 of *Springer Tracts in Modern Physics*. Springer-Verlag, 1990.
- [102] M. Tinkham. *Introduction to Superconductivity*. McGraw-Hill, New York, 1975.
- [103] Yu. M. Romanovskii V. A. Vasil'ev and V. G. Yakhno. Autowave proceses in distributed kinetic systems. *Usp. Fiz. Nauk*, 128:625–666, Aug. 1979. Review article.
- [104] Yu. M. Romanovskii V. A. Vasil'ev and V. G. Yakhno. Autowave proceses in distributed kinetic systems. *Sov. Phys. Usp.*, 22(8):615–639, Aug. 1979. Review article. English translation.
- [105] M. van Dyke. *Perturbation Methods in Fluid Mechanics*. Parabolic Press, Stanford CA, 1975.
- [106] R. J. Watts-Tobin, Y. Krähenbühl, and L. Kramer. Nonequilibrium theory of dirty, current-carrying superconductors: Phase-slip oscillators in narrow filaments near T_c^* . *Journal of Low Temperature Physics*, 42(5/6):459–501, 1981.